



HAL
open science

Structuration and glass transition temperature of the adsorbed polymer layer : some insights in the property deviations of the ultra-thin polymer film

Aparna Beena Unni

► **To cite this version:**

Aparna Beena Unni. Structuration and glass transition temperature of the adsorbed polymer layer : some insights in the property deviations of the ultra-thin polymer film. Material chemistry. Université de Bretagne Sud; Mahatma Gandhi University, 2016. English. NNT : 2016LORIS416 . tel-01439328

HAL Id: tel-01439328

<https://theses.hal.science/tel-01439328>

Submitted on 18 Jan 2017

HAL is a multi-disciplinary open access archive for the deposit and dissemination of scientific research documents, whether they are published or not. The documents may come from teaching and research institutions in France or abroad, or from public or private research centers.

L'archive ouverte pluridisciplinaire **HAL**, est destinée au dépôt et à la diffusion de documents scientifiques de niveau recherche, publiés ou non, émanant des établissements d'enseignement et de recherche français ou étrangers, des laboratoires publics ou privés.



THÈSE / UNIVERSITÉ DE BRETAGNE-SUD

sous le sceau de l'Université Bretagne Loire

pour obtenir le titre de

DOCTEUR DE L'UNIVERSITÉ DE BRETAGNE-SUD

Mention :

École doctorale SICMA

présentée par : **Aparna BEENA UNNI**

Préparée à l'IRD, FRE CNRS 3744
Institut de Recherche Dupuy de Lôme

Etablissement de rattachement :
Université de Bretagne Sud

Structuration and glass transition temperature of the adsorbed polymer layer: some insights in the property deviations of the ultra-thin polymer film

Thèse soutenue le 24th Octobre 2016

devant le jury composé de :

Prof. Jean Paul CHAPEL

Rapporteur (Université de Bordeaux, France)

Dr. Allison SAITER

Rapporteur (Université de Rouen, France)

Prof. Alain GIBAUD

Examineur (Université du Maine, France)

Prof. Nicolas DELORME

Examineur (Université du Maine, France)

Prof. Yves GROHENS

Directeur de thèse (Université de Bretagne Sud, France)

Dr. Guillaume VIGNAUD

Co- Directeur de thèse (Université de Bretagne Sud, France)

Prof. Sabu THOMAS

Co- Directeur de thèse (Mahatma Gandhi University, India)



Structuration and glass transition temperature of the adsorbed polymer layer: some insights in the property deviations of the ultra-thin polymer film

*A dissertation submitted in the partial fulfilment of the requirement for the degree of
Doctor of Philosophy*

by

Aparna BEENA UNNI

University of South Brittany

Department of Sciences & Engineering Sciences

&

International and Inter University Centre for Nanoscience and Nanotechnology

Mahatma Gandhi University, India

Defended on 24th October, 2016, in front of the following commission:

Prof. Jean Paul CHAPEL

Reviewer (Université de Bordeaux, France)

Dr. Allison SAITER

Reviewer (Université de Rouen, France)

Prof. Alain GIBAUD

Examiner (Université du Maine, France)

Prof. Nicolas DELORME

Examiner (Université du Maine, France)

Prof. Yves GROHENS

Director of Thesis (Université de Bretagne Sud, France)

Dr. Guillaume VIGNAUD

Co-Director of Thesis (Université de Bretagne Sud, France)

Prof. Sabu THOMAS

Co-Director of Thesis (Mahatma Gandhi University, India)

Dedicated to my Grandparents

Late. Smt. Saraswathy Amma

&

Late. Mr. Sreedharan Nair

Acknowledgments

First and foremost I thank Prof. Yves GROHENS and Prof. Sabu THOMAS who have been always there to listen and give their valuable advices. My PhD would not have been possible without their kind help and support.

I express my deepest gratitude to Dr. Guillaume VIGNAUD. I am very fortunate to have an advisor like him who helped me through out with his appropriate suggestions. He has been always there with patience and support, keeping me in the right track for solving problems, leading to the completion of this dissertation.

I thank Dr. Bastien SEANTIER for his kindness and patience for training me with AFM. He was helpful and was always ready for technical discussions. I thank Dr. HELIAS and Dr. CHEBIL for the training during initial days of my work. My hearty thanks to Dr. GIERMANSKA and Prof. CHAPEL for very nice discussions and fruitful experiments we had during the collaboration at *CRPP*. I appreciate very much a number of interesting discussions with Dr. J. K. Bal, who was always willing to help me with my doubts.

I am much obliged to Prof. Christophe BALLEY, Prof. Jean-François FELLER, Dr. Stéphane BRUZAUD, Prof. Pierre-Yves MANACH, Dr. Alain BOURMAUD, Dr. Antoine LE-DUIGOU and Dr. Mickaël CASTRO. I would like to acknowledge Dr. Isabelle PILLIN, Mr. Hervé BELLEGOU, Mr. Anthony MAGUERESSE, Mr. Antoine KERVOELEN and Mrs. Françoise PÉRESSE for their technical supports.

I would also like to express my sincere gratitude towards the reviewers Prof. Jean Paul CHAPEL and Dr. Allison SAITER for their kind time spend for reviewing this dissertation. I convey my gratitude towards the jury members Prof. Alain GIBAUD and Dr. Nicolas DELORME for their valuable support.

Special thanks to Dr. Nandakumar Kalarikkal, Dr. Nisha Kurivilla and Dr. Gargi Raina for guiding me towards research.

I take this opportunity to thank all teachers in my life. I thank all my colleagues at NSS college of Engineering, Palakkad, for their kind support.

It is important to mention that I was lucky to have a group of fun loving intellectual friends around me. I thank Dr. Benjamin Saulnier, Clara Jimenez-Saelices, Morgane Deroine, Marine Lan for creating a wonderful ambience in the lab. I would also like to thank Morgane Tanguy, Antoine Jouin, Antoine Lemartinel, Abhishek Sachan, Tran Manh-Trung, Clement Gourier, Camille Goudenhoft, Justin Merotte, Kevin Henry, Dr. Yves-Marie Corre, Dr. Rajendran Muthuraj, Dr. David Siniscalco, Dr. Pierre Lemechko, Dr. Abdel Kader and Mikael Kedzierski for making a very good atmosphere around me. Even if we had very short time together, I am much obliged to Dr. Neethu Ninan for her kind advice and help. I extend my deepest appreciation for my dearest friends Talal Manzoor and Krishna Priya C V, for their support and patience throughout my PhD.

I am always indebted to my grandparents Mr. Medayil Ramachandran Nair and Late. Ms. Anandavalli Amma. Thanks to all my family members for their kind support. Lot of thanks to Ila devi Unni, for being such a wonderful sister. Special thanks for her concern and prayers for my publications. Finally, but the foremost, I thank my parents M. R. Unni , Ms. Beena Sreedharan Nair and Ettumanoorappan for their unconditional support, blessings and love.

I thank each and every one of those who helped me all along, leading to the attainment of this degree.

CONTENTS

| | |
|---|----|
| Introduction | 1 |
| Chapter 1. Materials and Methods | 19 |
| 1.1 Materials used..... | 20 |
| 1.1.1 Polymers..... | 20 |
| 1.1.2 Ceria Nanoparticles | 21 |
| 1.2 Sample preparation | 21 |
| 1.2.1 Substrate preparation..... | 21 |
| 1.2.2 Thin film formation..... | 25 |
| 1.3 Characterization..... | 29 |
| 1.3.1 Ellipsometry | 29 |
| 1.3.2 Atomic force microscopy | 35 |
| 1.3.3 X-ray Reflectivity..... | 40 |
| 1.3.4 Contact angle goniometry | 43 |
| 1.3.5 Solvent rinsing using dip coater | 45 |
| Chapter 2. Density variations of polymer thin films under confinement; a study based on Ceria nanoparticle adsorption | 49 |
| 2.1 Introduction | 50 |
| 2.2 Ceria NP adsorption for sensing the density variations..... | 52 |
| 2.3 NP deposition on polymer thin films and data acquisition..... | 54 |
| 2.4 Nanoparticle adsorption as a function of refractive index value of polymers..... | 56 |
| 2.5 Density and NP adsorption of PS thin films..... | 58 |

| | | |
|---|---|-----|
| 2.6 | Density and NP adsorption of PMMA thin films | 61 |
| 2.7 | Influence of substrate on NP adsorption..... | 63 |
| 2.8 | Correlation of density with thin film thermal behavior | 68 |
| 2.9 | Conclusion | 71 |
| Chapter 3. Stable ultrathin polymer films (<7nm) made by solvent rinsing | | 79 |
| 3.1 | Introduction | 80 |
| 3.2 | Ultrathin polymer films | 83 |
| 3.2.1 | Formation of ultrathin film (< 7 nm) by direct spin-coating..... | 83 |
| 3.2.2 | Formation of ultrathin films (≤ 7 nm) by solvent rinsing treatment | 85 |
| 3.3 | Correlation between the kinetics of dissolution and annealing | 91 |
| 3.4 | Morphology and verification of residual layer on substrates surface..... | 92 |
| 3.5 | Stability or instability of residual films of tunable thickness | 94 |
| 3.5.1 | The stability of residual films on H-Si wafers | 94 |
| 3.5.2 | The instability/metastability of residual films on SiO _x -Si wafers | 97 |
| 3.6 | Conclusion | 105 |
| Chapter 4. Characteristic features of ultrathin polymer residual layer studied by rinsing with different solvents. | | 111 |
| 4.1 | Introduction | 112 |
| 4.2 | The film prior to solvent rinsing..... | 116 |
| 4.3 | Thickness of polymer residual layer after rinsing with various solvents | 117 |
| 4.4 | The morphology of polymer residual layer after rinsing with various solvents..... | 118 |
| 4.5 | The stability/instability of polymer residual layer analyzed with Van der Waals - intermolecular theory | 123 |

| | | |
|--|---|-----|
| 4.6 | The stability/instability of polymer residual layer analyzed with effective free energy of the system | 127 |
| 4.7 | Conclusion | 131 |
| Chapter 5. Stability and glass transition temperature of residual films on H-Si wafers | | 139 |
| 5.1 | Introduction | 140 |
| 5.2 | Thickness and morphology of polymer residual layer after rinsing with various solvents | 143 |
| 5.3 | The stability/instability of polymer residual layer analyzed with Van der Waals - intermolecular theory | 146 |
| 5.4 | Glass transition properties of polymer residual layer | 149 |
| 5.5 | Conclusion | 153 |
| Conclusion and Perspectives | | 163 |

Introduction

Miniaturization being one of the most sought after criteria in current technological research, the number of studies focusing on the confinement increases day by day. Polymer films that are confined by their thickness (Polymer thin films) obtained great scientific attention due to their wide variety of technological and industrial applications. It found numerous applications in biomedical area, [1], [2] nanoelectronics, [3]–[6] tissue engineering, [7], [8] lithographic resists, [9], [10] coatings, [11] sensors, [12] adhesives, [13] organic solar cells, [14], [15] etc. just to mention a few. The properties of such polymer films, which are confined by their thickness are the combination of its interfacial properties and size effects. Generally these films are found to be in the following forms

1. Free standing: films that have two free surfaces
2. Supported: films with one free surface and supported by a substrate
3. Capped: films without free surface



Figure 0-1. Three forms of polymer thin films: free standing, supported and capped films.

In this thesis, we focus on the confinement effects of supported polymer thin films. The properties of the supported polymer thin films are resulting from the cumulative effect of interplay between the free surface, the substrate interface, size reduction etc. Such films exhibits various anomalous properties compared to their bulk counterparts. It includes the deviations in viscosity, physical aging, stability, density, glass transition temperature etc. just to mention a few. [16]–[20]

The property deviations of polymer films when they are confined by their thickness remain an interesting topic of discussion from long. Since Jackson and McKenna (1991) first discovered a reduced glass transition temperature (T_g) in *ortho*-terphenyl (o-TP) confined in nanometer size pores, there has been a great deal of interest in nano-confinement effects on T_g and on the dynamics of amorphous materials. [21]

The question, “Is the molecular surface of polystyrene really glassy?” was raised by Meyers et al. back in 1992. [22] In 1993, Reiter observed the dewetting of polystyrene thin films at a thickness below 10 nm at temperatures inferior to its bulk glass transition temperature. These findings suggest that T_g was lower for ultrathin films than for thick films. This was the first direct evidence of the thickness dependent chain mobility of polymer films confined at nanoscale. [23] Later a liquid-like layer at the free surface was suggested as the main contributing factor to reduced T_g values in thin films by Keddie *et. al.* [24] This was the first systematic investigation of glass transition in thin polymer films, which involved the ellipsometric measurements of T_g in PS films supported on hydrogen terminated Si wafers. [24] The T_g was correlated to the films thickness by means of an empirical equation as follows:

$$T_g(h) = T_g(\infty) \left[1 - \left(\frac{A}{h} \right)^\delta \right]$$

Here $T_g(\infty)$ refers to the bulk T_g value, h is the film thickness, A and δ are the fitting parameters. They found that the T_g values for films whose thickness is less than 40 nm was reduced below the bulk value. The lowest measured T_g value was 25 K less than the bulk value. Quantitatively similar results were obtained for various molecular weight studied. This means that neither chain entanglements nor bulk radius of gyration, R_g plays a significant role in defining this T_g reduction for supported PS thin films. [25]–[28] This effect was suggested as being dominated by the existence of a liquid-like layer near the free surface with a characteristic size which increased as the temperature was raised.

Focusing more on the influence of free surface on the film properties, an enhanced mobility and thereby reduced T_g was attributed to the chain end segregation to the surface by Mayes. [29] However, if chain ends were the origin of this effect, it would be expected that the thickness dependence of T_g could be significantly altered by varying the surface chain-end concentration by modification of the polymer molecular weight, which is not supported by experimental data. Many studies were done on the free standing polymer films in order to understand more about the influence of free surface. The first measurements of T_g values in free-standing PS films have been done by Forrest *et al.* using Brillouin light scattering for films of 29-70 nm.[30] The T_g of a 20 nm thick film was found to be reduced by more than 70 °C relative to the bulk, whereas for a similar thickness supported PS films, only a variation of 10 °C is observed. [31]

Subsequently a lot of experimental studies supported the notion that mobility is enhanced near the free surface, which includes the contribution from Forrest et al. [32], [33], Ediger et. al. [34]–[36], McKenna et al. [37], [38] and many others. [39]–[41]. Although there is substantial evidence supporting a free-surface effect as the origin of T_g reductions in nanoconfined PS films, there is not yet a detailed understanding of the free-surface effect.

Concerning the substrate interface, further work from Keddie et.al revealed the significant role of specific interactions between polymer and substrate, that can determine the T_g variations. [42] From this study, PMMA on a gold substrate displays depressions in T_g , while the same polymer on a silicon oxide substrate showed a small increase of T_g . The elevated T_g in PMMA-SiO₂ system was attributed to the attractive interaction between PMMA and the Si native oxide due to hydrogen bonding whereas PMMA-gold interaction is much weaker resulting in decreased T_g value. The study of van Zanten *et al.* focused on the effect of polymer substrate interaction using poly-2-vinylpyridine on oxide-coated Si substrates that possess much stronger attractive interaction. [43] In that case, the T_g value was found to increase above the bulk T_g , with a maximum increase of 50 K for 7.7 nm film. Later, a lot of studies reported the significant influence of polymer substrate interaction by the T_g averaged along with the whole film thickness. [31], [38], [44]–[55]

Taking in account the presence of free surface along with the polymer substrate interface, an empirical equation was suggested by Hsu *et al.* which predicted an enhancement of T_g relative to its bulk value, in addition to commonly encountered T_g reduction. [56] In this case, the measures of free surface effect along with the polymer substrate interaction were considered with the film thickness and characteristic length which determine the glass transition temperature. Interface and surface effects on the glass transition in thin polystyrene films were studied by Positron annihilation lifetime spectroscopy (PALS) measurement showing that the entire film may not be characterized as having only one value of T_g . It was later proposed a three-layer model in which, every layer possesses different mobilities and glass transition temperatures. [57] A continuous multilayer model was later developed by Kim *et. al.* [58] which explained the decrease in the T_g with decreasing thickness via ellipsometry where they obtained a depth dependent T_g profile.

The model film consists of many continuous layers and each layer has a different T_g , which increases monotonically to the bulk T_g with increasing distance from the free surface of the film. The first experimental measurements of T_g in different layers of PS films were made by Bliznyuk *et al.* on supported films and Ellison and Torkelson, on both free-standing and supported films using scanning force microscopy and fluorescence-multilayer method respectively. [59], [60] Bliznyuk *et al.* showed that for films of ~ 25 nm, the glass-transition temperature in the surface region decreases by ~ 33 K with decreasing film thickness. Ellison and Torkelson have found that when the thicknesses of all three layers are comparable (~ 12 nm), the T_g decreases by 14, 5, and 4 K for surface, middle, and substrate layers respectively. Experiments with neutron reflectivity measurements on multilayered PS thin films suggested that in supported films T_g is apparently determined by competition between the surface and interfacial T_g . [61] Multiple glass transition temperatures of polymer thin films as probed by multi-wavelength ellipsometry [58], [62]–[65] and by Atomic Force Microscopy spectroscopy [66] gave evidences for the thin films which are organized as multilayers. Strong substrate dependence of stratification properties in the multi layers was also observed during the experiments. However, the layer models remain empirical to some extent and it need to fit to experimental data to obtain the essential parameters that characterize the surface layer and interfacial region. A recent study by the florescence bilayer method could recover the bulk T_g on a time scale reflecting the degree of adsorption, by submerging the adsorbed layer by the deposition of an additional layer above the residual layer. [67] They also found that there exists a substantial reduction in T_g as compared to bulk due to the influence of the free surface. Apart from the surface and interface effects, there are various other factors that are known to influence T_g in confined systems including tacticity, [68]–[70] molecular weight for PMMA thin films, [63], [71]–[73] sample preparation and measurement environment, [74]–[77] annealing conditions, [78] chemical structure [79], [80] etc. It is also important to mention that no shift in T_g is reported by the study on the effect of the substrate on the T_g of PMMA films, due to film confinement and substrate interaction. [81], [82]

Considering the theories used for explaining the anomalous glass transition, Cohen and Turnbull introduced the free volume theory in order to explain the anomalous behavior in glass transition temperature for thin confined films. [83] It is based on the assumption that molecular transport in viscous fluids occurs only when voids, having a volume large enough to accommodate a molecule, form by the redistribution of some “free volume”.

The specific free volume is defined by $V_f = V - V_{occ}$, where V is the total specific volume and V_{occ} is the occupied volume including the interstitial free volume and the van der Waals volume of molecules. In this model, the slowdown of the molecular transport in super cooled was assumed to be occurring to a decrease of free volume rather than to the existence of energy barriers. Later this model was broadened by Macedo and Litovitz taking into account both attractive and repulsive forces. [84] A sliding model was proposed by de Gennes which could explain many of the qualitative features of the T_g reductions in the presence of free surface. [85] The model proposed a competition between two different modes of mobility: (1) the usual small length scale segmental mobility associated with the bulk glass transition and (2) the polymer chain ‘slides’ along the direction of the primitive path, which requires less free volume. [86] Though the preceded experiments could provide a qualitative agreement with this model, quantitative differences still exist. [87], [88] Another explanation was from Ngai who proposed a coupling model to glass transition dynamics. [89], [90] This approach has attempted to couple conventional ideas of glass transition dynamics with polymer chain confinement. Adam and Gibbs developed a theory of the glass transition where the decrease of the configurational entropy with decreasing temperature implies a concomitant increase of the length scale of the glass transition. [91] Apart from this, various other approaches like the thermodynamic models, [92] mode coupling theory, [93] Donth’s approach [94], [95] etc. are also commonly used. More recently, Napolitano et al. showed that an essential parameter in the process of adsorption regulating the magnitude of T_g deviations from bulk behavior is the amount of free interface, that is, the portion of interface exhibiting no adsorbed polymer chains (Interstitial free volume). [96] Later, the free volume holes diffusion (FVHD) model nicely rationalized the connection between the magnitude of T_g deviations and the amount of free interface. [97]–[99] It also provides a way to understand the physical aging. However, modern theory demonstrates that dynamical heterogeneity emerges during the glass transition, [100] indicating that the diffusion of free volume holes in glassy state might also show dynamical heterogeneity, that is, some free volumes diffuse faster and others move slower. [101]

Considering all this available reports, the factors affecting the glass transition properties, the deviations in thin film properties due to confinement etc., needs lot more experiments for a clearer understanding. The main goal of this work is to contribute towards the studies on confinement effects in supported polymer thin films.

Considering various properties that change due to confinement, at the outset we investigate the density variations in polymer thin films. In order to avoid the fitting models that are commonly employed in the measurement techniques which can mislead the density determination, a novel method of ceria nanoparticles adsorption was used for probing the density variations. One of the main difficulties that were faced during our first study was, the polymer films become unstable when they are reduced by their thickness and it dewets. So the next aim was to obtain stable films with very small thickness. For this, a top down solvent rinsing method was employed along with tuning of substrate properties, which gave stable polymer residual layers of thickness ranging from 1.3 - 7nm. It was indeed intriguing to study the influence of solvents that were employed for the rinsing process and hence it is analyzed in detail. Finally the glass transition properties of the residual layers are studied.

The manuscript is organized in the following way:

Chapter 1: This chapter presents the materials and the experimental techniques that have been used in this work. The first part deals with the studied materials, followed by the methods employed for carrying out the experiments and finally the characterization techniques involved in this work are described.

Chapter 2: This chapter begins with a brief introduction to density studies and its significance. The possibility of using ceria nanoparticles for probing the polymer thin films density and the underlying theory is discussed. Then the study of Ceria nanoparticle adsorption on polystyrene and poly (methyl methacrylate) films of varying thickness is detailed, which throws light on the density evolution of these films with respect to their thickness. The influence of substrate on this study is verified and finally a brief note on the correlation of density with thin film thermal behavior is made.

Chapter 3: In this chapter, initially the stability issues observed when the polymer thin films are confined by their thickness are discussed. Then the instabilities observed on ultrathin film by direct spin-coating is discussed which is followed by the discussion about the formation of ultrathin films by solvent rinsing method.

The kinetics of dissolution during solvent rinsing and the effect of annealing are discussed. Then the stability/instability of the residual layer is analyzed experimentally and is compared with the Lifshitz van der Waals intermolecular theory.

Chapter 4: This chapter analyses significance of solvent used in the solvent assisted rinsing experiments. It starts with a brief introduction about the interaction of supported polymer films with the solvent.

Then, the thickness and morphology details of the residual layer after rinsing with various solvents are discussed. Then the stability/instability of the residual layers is analyzed experimentally and is interpreted with the help of Lifshitz van der Waals intermolecular theory.

Chapter 5: This chapter begins with an introduction to the glass transition behavior reported for confined supported polymer thin films. The thickness and morphology details of polymer residual layers obtained after rinsing with various solvents are discussed. The stability of such films is analyzed both experimentally and theoretically. Finally the observations on glass transition properties of such films are studied by means of multi wavelength ellipsometry are discussed in detail.

Finally, some general conclusions and future perspectives are discussed.

REFERENCES

- [1] V. K. Vendra, L. Wu, and S. Krishnan, “Polymer Thin Films for Biomedical Applications,” in *Nanotechnologies for the Life Sciences*, Wiley, 2007.
- [2] A. L. Hook, C.-Y. Chang, J. Yang, J. Luckett, A. Cockayne, S. Atkinson, Y. Mei, R. Bayston, D. J. Irvine, R. Langer, D. G. Anderson, P. Williams, M. C. Davies, and M. R. Alexander, “Combinatorial discovery of polymers resistant to bacterial attachment,” *Nat. Biotechnol.*, vol. 30, no. 9, pp. 868–875, Sep. 2012.
- [3] J. Ouyang, C.-W. Chu, C. R. Szmanda, L. Ma, and Y. Yang, “Programmable polymer thin film and non-volatile memory device,” *Nat Mater*, vol. 3, no. 12, pp. 918–922, Dec. 2004.
- [4] C. D. Dimitrakopoulos and P. R. L. Malenfant, “Organic Thin Film Transistors for Large Area Electronics,” *Adv. Mater.*, vol. 14, no. 2, pp. 99–117, Jan. 2002.
- [5] S. R. Forrest, “The path to ubiquitous and low-cost organic electronic appliances on plastic,” *Nature*, vol. 428, no. 6986, pp. 911–918, Apr. 2004.
- [6] C. Kim, A. Facchetti, and T. J. Marks, “Polymer Gate Dielectric Surface Viscoelasticity Modulates Pentacene Transistor Performance,” *Science (80-.)*, vol. 318, no. 5847, pp. 76–80, Oct. 2007.
- [7] X. Liu and P. X. Ma, “Polymeric Scaffolds for Bone Tissue Engineering,” *Ann. Biomed. Eng.*, vol. 32, no. 3, pp. 477–486, 2004.
- [8] L. Lu, C. A. Garcia, and A. G. Mikos, “In vitro degradation of thin poly(DL-lactic-co-glycolic acid) films,” *J. Biomed. Mater. Res.*, vol. 46, no. 2, pp. 236–244, 1999.
- [9] Y.-C. Tseng, Q. Peng, L. E. Ocola, D. A. Czaplewski, J. W. Elam, and S. B. Darling, “Enhanced polymeric lithography resists via sequential infiltration synthesis,” *J. Mater. Chem.*, vol. 21, no. 32, pp. 11722–11725, 2011.
- [10] H. Duan, J. Zhao, Y. Zhang, E. Xie, and L. Han, “Preparing patterned carbonaceous nanostructures directly by overexposure of PMMA using electron-beam lithography,” *Nanotechnology*, vol. 20, no. 13, p. 135306, 2009.

- [11] X. Li, X. Yu, and Y. Han, "Polymer thin films for antireflection coatings," *J. Mater. Chem. C*, vol. 1, no. 12, pp. 2266–2285, 2013.
- [12] B. Adhikari and S. Majumdar, "Polymers in sensor applications," *Prog. Polym. Sci.*, vol. 29, no. 7, pp. 699–766, Jul. 2004.
- [13] Q. Huang, I. Yoon, J. Villanueva, K. Kim, and D. J. Sirbuly, "Quantitative mechanical analysis of thin compressible polymer monolayers on oxide surfaces," *Soft Matter*, vol. 10, no. 40, pp. 8001–8010, 2014.
- [14] S. Günes, H. Neugebauer, and N. S. Sariciftci, "Conjugated Polymer-Based Organic Solar Cells," *Chem. Rev.*, vol. 107, no. 4, pp. 1324–1338, Apr. 2007.
- [15] G. Li, R. Zhu, and Y. Yang, "Polymer solar cells," *Nat. Photonics*, vol. 6, no. 3, pp. 153–161, Mar. 2012.
- [16] H. Bodiguel and C. Fretigny, "Reduced viscosity in thin polymer films," *Phys. Rev. Lett.*, vol. 97, no. 26, pp. 266105, 1–4, 2006.
- [17] C. J. Ellison, S. D. Kim, D. B. Hall, and J. M. Torkelson, "Confinement and processing effects on glass transition temperature and physical aging in ultrathin polymer films: novel fluorescence measurements.," *Eur. Phys. J. E. Soft Matter*, vol. 8, no. 2, pp. 155–66, May 2002.
- [18] J. E. Pye and C. B. Roth, "Above, below, and in-between the two glass transitions of ultrathin free-standing polystyrene films: Thermal expansion coefficient and physical aging," *J. Polym. Sci. Part B Polym. Phys.*, vol. 53, no. 1, pp. 64–75, Jan. 2015.
- [19] A. Sharma and G. Reiter, "Instability of Thin Polymer Films on Coated Substrates: Rupture, Dewetting, and Drop Formation," *J. Colloid Interface Sci.*, vol. 178, no. 2, pp. 383–399, 1996.
- [20] G. Vignaud, M. S. Chebil, J. K. Bal, N. Delorme, T. Beuvier, Y. Grohens, and A. Gibaud, "Densification and Depression in Glass Transition Temperature in Polystyrene Thin Films," *Langmuir*, vol. 30, no. 39, pp. 11599–11608, 2014.

- [21] C. L. Jackson and G. B. McKenna, “Proceedings of the International Discussion Meeting on Relaxations in Complex Systems The glass transition of organic liquids confined to small pores,” *J. Non. Cryst. Solids*, vol. 131, pp. 221–224, 1991.
- [22] G. F. Meyers, B. M. DeKoven, and J. T. Seitz, “Is the molecular surface of polystyrene really glassy?,” *Langmuir*, vol. 8, no. 9, pp. 2330–2335, Sep. 1992.
- [23] G. Reiter, “Mobility of polymers in films thinner than their unperturbed size,” *Europhys. Lett.*, vol. 23, no. 8, p. 579, 1993.
- [24] J. L. Keddie, R. A. L. Jones, and R. A. Cory, “Size-Dependent Depression of the Glass Transition Temperature in Polymer Films .,” *Europhys. Lett.*, vol. 27, no. July, pp. 59–64, 1994.
- [25] O. K. C. Tsui and H. F. Zhang, “Effects of Chain Ends and Chain Entanglement on the Glass Transition Temperature of Polymer Thin Films,” *Macromolecules*, vol. 34, no. 26, pp. 9139–9142, Dec. 2001.
- [26] C. J. Ellison, M. K. Mundra, and J. M. Torkelson, “Impacts of Polystyrene Molecular Weight and Modification to the Repeat Unit Structure on the Glass Transition–Nanoconfinement Effect and the Cooperativity Length Scale,” *Macromolecules*, vol. 38, no. 5, pp. 1767–1778, Mar. 2005.
- [27] S. Kawana and R. A. L. Jones, “Character of the glass transition in thin supported polymer films,” *Phys. Rev. E*, vol. 63, no. 2, p. 21501, 2001.
- [28] J. Mattsson, J. A. Forrest, and L. Börjesson, “Quantifying glass transition behavior in ultrathin free-standing polymer films,” *Phys. Rev. E*, vol. 62, no. 4, pp. 5187–5200, Oct. 2000.
- [29] A. M. Mayes, “Glass Transition of Amorphous Polymer Surfaces,” *Macromolecules*, vol. 27, no. 11, pp. 3114–3115, May 1994.
- [30] J. A. Forrest, K. Dalnoki-Veress, J. R. Stevens, and J. R. Dutcher, “Effect of Free Surfaces on the Glass Transition Temperature of Thin Polymer Films,” *Phys. Rev. Lett.*, vol. 77, no. 10, pp. 2002–2005, Sep. 1996.

- [31] J. A. Forrest, K. Dalnoki-Veress, and J. R. Dutcher, “Interface and chain confinement effects on the glass transition temperature of thin polymer films,” *Phys. Rev. E*, vol. 56, no. 5, pp. 5705–5716, 1997.
- [32] D. Qi, Z. Fakhraai, and J. A. Forrest, “Substrate and chain size dependence of near surface dynamics of glassy polymers,” *Phys. Rev. Lett.*, vol. 101, no. 9, pp. 1–4, 2008.
- [33] Z. Fakhraai and J. A. Forrest, “Measuring the surface dynamics of glassy polymers,” *Science*, vol. 319, pp. 600–604, 2008.
- [34] K. Paeng, S. F. Swallen, and M. D. Ediger, “Direct Measurement of Molecular Motion in Freestanding Polystyrene Thin Films,” *J. Am. Chem. Soc.*, vol. 133, no. 22, pp. 8444–8447, Jun. 2011.
- [35] K. Paeng, R. Richert, and M. D. Ediger, “Molecular mobility in supported thin films of polystyrene, poly(methyl methacrylate), and poly(2-vinyl pyridine) probed by dye reorientation,” *Soft Matter*, vol. 8, no. 3, pp. 819–826, 2012.
- [36] M. D. Ediger and J. A. Forrest, “Dynamics near Free Surfaces and the Glass Transition in Thin Polymer Films: A View to the Future,” *Macromolecules*, vol. 47, pp. 471–478, 2014.
- [37] M. Alcoutlabi and G. B. McKenna, “Effects of confinement on material behaviour at the nanometre size scale,” *J. Phys. Condens. Matter*, vol. 17, no. 15, pp. R461–R524, 2005.
- [38] H. Yoon and G. B. McKenna, “Substrate Effects on Glass Transition and Free Surface Viscoelasticity of Ultrathin Polystyrene Films,” *Macromolecules*, vol. 47, no. 24, pp. 8808–8818, Dec. 2014.
- [39] B. Zuo, Y. Liu, L. Wang, Y. Zhu, Y. Wang, and X. Wang, “Depth profile of the segmental dynamics at a poly(methyl methacrylate) film surface,” *Soft Matter*, vol. 9, no. 39, pp. 9376–9384, 2013.
- [40] F. Chen, C.-H. Lam, and O. K. C. Tsui, “The Surface Mobility of Glasses,” *Science (80-.)*, vol. 343, no. 6174, pp. 975–976, Feb. 2014.
- [41] J. DeFelice, S. T. Milner, and J. E. G. Lipson, “Simulating Local Tg Reporting Layers in Glassy Thin Films,” *Macromolecules*, vol. 49, no. 5, pp. 1822–1833, Mar. 2016.

- [42] J. L. Keddie, R. A. L. Jones, and R. A. Cory, "Interface and surface effects on the glass-transition temperature in thin polymer films," *Faraday Discuss.*, vol. 98, pp. 219–230, 1994.
- [43] J. van Zanten, W. Wallace, and W. Wu, "Effect of strongly favorable substrate interactions on the thermal properties of ultrathin polymer films," *Physical Review E*, vol. 53, pp. R2053–R2056, 1996.
- [44] O. K. C. Tsui, T. P. Russell, and C. J. Hawker, "Effect of Interfacial Interactions on the Glass Transition of Polymer Thin Films," *Macromolecules*, vol. 34, no. 16, pp. 5535–5539, Jul. 2001.
- [45] R. S. Tate, D. S. Fryer, S. Pasqualini, M. F. Montague, J. J. de Pablo, and P. F. Nealey, "Extraordinary elevation of the glass transition temperature of thin polymer films grafted to silicon oxide substrates," *J. Chem. Phys.*, vol. 115, no. 21, p. 9982, 2001.
- [46] D. S. Fryer, R. D. Peters, E. J. Kim, J. E. Tomaszewski, J. J. de Pablo, P. F. Nealey, C. C. White, and W. Wu, "Dependence of the Glass Transition Temperature of Polymer Films on Interfacial Energy and Thickness," *Macromolecules*, vol. 34, no. 16, pp. 5627–5634, Jul. 2001.
- [47] S. Napolitano, D. Prevosto, M. Lucchesi, P. Pingue, M. D'Acunto, and P. Rolla, "Influence of a reduced mobility layer on the structural relaxation dynamics of aluminum capped ultrathin films of poly(ethylene terephthalate).," *Langmuir*, vol. 23, no. 4, pp. 2103–9, Feb. 2007.
- [48] D. Labahn, R. Mix, and A. Schönhals, "Dielectric relaxation of ultrathin films of supported polysulfone," *Phys. Rev. E*, vol. 79, no. 1, p. 11801, Jan. 2009.
- [49] Y. Shin, H. Lee, W. Lee, and D. Y. Ryu, "Glass Transition and Thermal Expansion Behavior of Polystyrene Films Supported on Polystyrene-Grafted Substrates," *Macromolecules*, 2016.
- [50] H. Yang and J. S. Sharp, "Interfacial Effects and the Glass Transition in Ultrathin Films of Poly(tert-butyl methacrylate)," *Macromolecules*, vol. 41, no. 13, pp. 4811–4816, Jul. 2008.

- [51] W. Ding, R. F. Sanchez, M. R. Ruggles, and P. Bernazzani, “Effect of surface interactions on the glass transition temperature behavior of amorphous polystyrene,” *J. Polym. Res.*, vol. 20, no. 6, p. 146, May 2013.
- [52] R. P. White, C. C. Price, and J. E. G. Lipson, “Effect of Interfaces on the Glass Transition of Supported and Freestanding Polymer Thin Films,” *Macromolecules*, vol. 48, no. 12, pp. 4132–4141, Jun. 2015.
- [53] J. Baschnagel, H. Meyer, F. Varnik, S. Metzger, M. Aichele, M. Müller, and K. Binder, “Computer Simulations of Polymers Close to Solid Interfaces: Some Selected Topics,” *Interface Sci.*, vol. 11, no. 2, pp. 159–173, 2003.
- [54] D. Hudzinsky, A. V. Lyulin, A. R. C. Baljon, N. K. Balabaev, and M. A. J. Michels, “Effects of strong confinement on the glass-transition temperature in simulated atactic polystyrene films,” *Macromolecules*, vol. 44, no. 7, pp. 2299–2310, Apr. 2011.
- [55] J. Xu, L. Ding, J. Chen, S. Gao, L. Li, D. Zhou, X. Li, and G. Xue, “Sensitive Characterization of the Influence of Substrate Interfaces on Supported Thin Films,” *Macromolecules*, vol. 47, no. 18, pp. 6365–6372, 2014.
- [56] D. T. Hsu, F. G. Shi, B. Zhao, and M. Brongo, “Theory for the thickness dependent glass transition temperature of amorphous polymer thin films,” in *Electrochemical Society, Low and High Dielectric Constant Materials, and Thin Film Materials for Advanced Packaging Technologies*, 2000, vol. 99, no. 7, pp. 53–61.
- [57] G. DeMaggio, W. Frieze, D. Gidley, M. Zhu, H. Hristov, and a. Yee, “Interface and Surface Effects on the Glass Transition in Thin Polystyrene Films,” *Phys. Rev. Lett.*, vol. 78, no. 8, pp. 1524–1527, Feb. 1997.
- [58] J. H. Kim, J. Jang, and W.-C. Zin, “Thickness Dependence of the Glass Transition Temperature in Thin Polymer Films,” *Langmuir*, vol. 17, no. 9, pp. 2703–2710, May 2001.
- [59] V. N. Bliznyuk, H. E. Assender, and G. A. D. Briggs, “Surface Glass Transition Temperature of Amorphous Polymers. A New Insight with SFM,” *Macromolecules*, vol. 35, no. 17, pp. 6613–6622, Aug. 2002.

- [60] C. J. Ellison and J. M. Torkelson, “The distribution of glass-transition temperatures in nanoscopically confined glass formers.,” *Nat. Mater.*, vol. 2, no. 10, pp. 695–700, Oct. 2003.
- [61] R. Inoue, K. Kawashima, K. Matsui, T. Kanaya, K. Nishida, G. Matsuba, and M. Hino, “Distributions of glass-transition temperature and thermal expansivity in multilayered polystyrene thin films studied by neutron reflectivity,” *Phys. Rev. E*, vol. 83, no. 2, p. 21801, Feb. 2011.
- [62] A. El Ouakili, G. Vignaud, E. Balnois, J.-F. Bardeau, and Y. Grohens, “Multiple glass transition temperatures of polymer thin films as probed by multi-wavelength ellipsometry,” *Thin Solid Films*, vol. 519, no. 6, pp. 2031–2036, Jan. 2011.
- [63] T. Lan and J. M. Torkelson, “Methacrylate-based polymer films useful in lithographic applications exhibit different glass transition temperature-confinement effects at high and low molecular weight,” *Polymer*, vol. 55, no. 5, pp. 1249–1258, Mar. 2014.
- [64] M. Y. Efremov, A. V. Kiyanova, J. Last, S. S. Soofi, C. Thode, and P. F. Nealey, “Glass transition in thin supported polystyrene films probed by temperature-modulated ellipsometry in vacuum,” *Phys. Rev. E - Stat. Nonlinear, Soft Matter Phys.*, vol. 86, pp. 1–11, 2012.
- [65] A. El Ouakili, G. Vignaud, E. Balnois, J.-F. Bardeau, and Y. Grohens, “Glass transition temperatures of isotactic poly(methylmethacrylate) thin films and individual chains probed by multi wavelength ellipsometry,” *Eur. Phys. J. Appl. Phys.*, vol. 56, p. 13703, 2011.
- [66] N. Delorme, M. S. Chebil, G. Vignaud, V. Le Houerou, J.-F. Bardeau, R. Busselez, A. Gibaud, and Y. Grohens, “Experimental evidence of ultrathin polymer film stratification by AFM force spectroscopy,” *Eur. Phys. J. E*, vol. 38, no. 6, p. 56, 2015.
- [67] M. J. Burroughs, S. Napolitano, D. Cangialosi, and R. D. Priestley, “Direct Measurement of Glass Transition Temperature in Exposed and Buried Adsorbed Polymer Nanolayers,” *Macromolecules*, vol. 49, no. 12, pp. 4647–4655, 2016.

- [68] Y. Grohens, M. Brogly, C. Labbe, M.-O. David, and J. Schultz, “Glass Transition of Stereoregular Poly(methyl methacrylate) at Interfaces,” *Langmuir*, vol. 14, no. 11, pp. 2929–2932, May 1998.
- [69] Y. Grohens, L. Hamon, G. Reiter, a. Soldera, and Y. Holl, “Some relevant parameters affecting the glass transition of supported ultra-thin polymer films,” *Eur. Phys. J. E*, vol. 8, no. 2, pp. 217–224, May 2002.
- [70] B. Frieberg, E. Glynos, G. Sakellariou, and P. F. Green, “Physical aging of star-shaped macromolecules,” *ACS Macro Lett.*, vol. 1, no. 5, pp. 636–640, 2012.
- [71] W. Xia, D. D. Hsu, and S. Keten, “Molecular Weight Effects on the Glass Transition and Confinement Behavior of Polymer Thin Films,” *Macromol. Rapid Commun.*, vol. 36, no. 15, pp. 1422–1427, 2015.
- [72] K. Geng and O. K. C. Tsui, “Effects of Polymer Tacticity and Molecular Weight on the Glass Transition Temperature of Poly(methyl methacrylate) Films on Silica,” *Macromolecules*, p. acs.macromol.6b00108, 2016.
- [73] K. Geng, F. Chen, and O. K. C. Tsui, “Molecular-weight dependent T_g depression of silica-supported poly (α -methyl styrene) films,” *J. Non. Cryst. Solids*, vol. 407, pp. 296–301, 2015.
- [74] A. N. Raegen, M. V Massa, J. A. Forrest, and K. Dalnoki-Veress, “Effect of atmosphere on reductions in the glass transition of thin polystyrene films,” *Eur. Phys. J. E*, vol. 27, no. 4, pp. 375–377, 2008.
- [75] J. D. Ferry, *Viscoelastic properties of polymers*. John Wiley & Sons, 1980.
- [76] G. B. McKenna, “Size and confinement effects in glass forming liquids: Perspectives on bulk and nano-scale behaviours,” in *Le Journal de Physique IV*, 2000, vol. 10, no. PR7, pp. 7–53.
- [77] G. Reiter and S. Napolitano, “Possible origin of thickness-dependent deviations from bulk properties of thin polymer films,” *J. Polym. Sci. Part B Polym. Phys.*, vol. 48, no. 24, pp. 2544–2547, 2010.

- [78] S. Napolitano and M. Wübbenhorst, “The lifetime of the deviations from bulk behaviour in polymers confined at the nanoscale,” *Nat. Commun.*, vol. 2, p. 260, Mar. 2011.
- [79] C. B. Roth and J. R. Dutcher, “Glass transition temperature of freely-standing films of atactic poly (methyl methacrylate),” *Eur. Phys. J. E*, vol. 12, no. 1, pp. 103–107, 2003.
- [80] R. D. Priestley, M. K. Mundra, N. J. Barnett, L. J. Broadbelt, and J. M. Torkelson, “Effects of nanoscale confinement and interfaces on the glass transition temperatures of a series of poly (n-methacrylate) films,” *Aust. J. Chem.*, vol. 60, no. 10, pp. 765–771, 2007.
- [81] M. Erber, M. Tress, E. U. Mapesa, A. Serghei, K.-J. Eichhorn, B. Voit, and F. Kremer, “Glassy Dynamics and Glass Transition in Thin Polymer Layers of PMMA Deposited on Different Substrates,” *Macromolecules*, vol. 43, no. 18, pp. 7729–7733, Sep. 2010.
- [82] F. Kremer, M. Tress, and E. U. Mapesa, “Glassy dynamics and glass transition in nanometric layers and films: A silver lining on the horizon,” *J. Non. Cryst. Solids*, vol. 407, pp. 277–283, 2015.
- [83] M. H. Cohen and D. Turnbull, “Molecular Transport in Liquids and Glasses,” *J. Chem. Phys.*, vol. 31, no. 5, pp. 1164–1169, 1959.
- [84] P. B. Macedo and T. A. Litovitz, “On the Relative Roles of Free Volume and Activation Energy in the Viscosity of Liquids,” *J. Chem. Phys.*, vol. 42, p. 245, 1965.
- [85] P. G. de Gennes, “Glass transitions in thin polymer films,” *Eur. Phys. J. E*, vol. 2, pp. 201–205, 2000.
- [86] M. S. Dehua Liu, “Thermodynamic and glass transition behavior in CO₂ – polymer systems emphasizing the surface region,” The Ohio State University, 2016.
- [87] K. Akabori, K. Tanaka, T. Kajiyama, and A. Takahara, “Anomalous Surface Relaxation Process in Polystyrene Ultrathin Films,” *Macromolecules*, vol. 36, no. 13, pp. 4937–4943, Jul. 2003.
- [88] S. Kim and J. M. Torkelson, “Distribution of glass transition temperatures in free-standing, nanoconfined polystyrene films: a test of de Gennes’ sliding motion mechanism,” *Macromolecules*, vol. 44, no. 11, pp. 4546–4553, 2011.

- [89] K. L. Ngai, A. K. Rzos, and D. J. Plazek, "Reduction of the glass temperature of thin freely standing polymer films caused by the decrease of the coupling parameter in the coupling model," *J. Non. Cryst. Solids*, vol. 235, pp. 435–443, 1998.
- [90] K. L. Ngai, "Mobility in thin polymer films ranging from local segmental motion, Rouse modes to whole chain motion: A coupling model consideration," *Eur. Phys. J. E*, vol. 8, no. 2, pp. 225–235, 2002.
- [91] G. Adam and J. H. Gibbs, "On the temperature dependence of cooperative relaxation properties in glass-forming liquids," *J. Chem. Phys.*, vol. 43, no. 1, pp. 139–146, 1965.
- [92] J. H. Gibbs and E. A. DiMarzio, "Nature of the Glass Transition and the Glassy State," *J. Chem. Phys.*, vol. 28, p. 373, 1958.
- [93] W. Götze, *Complex dynamics of glass-forming liquids: A mode-coupling theory*, vol. 143. OUP Oxford, 2008.
- [94] E. Donth, "Characteristic length of the glass transition," *J. Polym. Sci. Part B Polym. Phys.*, vol. 34, no. 17, pp. 2881–2892, 1996.
- [95] A. Saiter, L. Delbreilh, H. Couderc, K. Arabeche, A. Schönhals, and J.-M. Saiter, "Temperature dependence of the characteristic length scale for glassy dynamics: Combination of dielectric and specific heat spectroscopy," *Phys. Rev. E*, vol. 81, no. 4, p. 41805, 2010.
- [96] S. Napolitano, C. Rotella, and M. Wübbenhorst, "Can Thickness and Interfacial Interactions Univocally Determine the Behavior of Polymers Confined at the Nanoscale?," *ACS Macro Lett.*, vol. 1, no. 10, pp. 1189–1193, Oct. 2012.
- [97] J. G. Curro, R. R. Lagasse, and R. Simha, "Diffusion model for volume recovery in glasses," *Macromolecules*, vol. 15, no. 6, pp. 1621–1626, 1982.
- [98] S. Napolitano and D. Cangialosi, "Interfacial Free Volume and Vitrification: Reduction in Tg," *Macromolecules*, vol. 46, pp. 8051–8053, 2013.

- [99] D. Cangialosi, V. M. Boucher, A. Alegria, and J. Colmenero, “Free volume holes diffusion to describe physical aging in poly (methyl methacrylate)/silica nanocomposites,” *J. Chem. Phys.*, vol. 135, no. 1, p. 14901, 2011.
- [100] L. Berthier and G. Biroli, “Theoretical perspective on the glass transition and amorphous materials,” *Rev. Mod. Phys.*, vol. 83, no. 2, p. 587, 2011.
- [101] S. Napolitano, *Non-equilibrium Phenomena in Confined Soft Matter: Irreversible Adsorption, Physical Aging and Glass Transition at the Nanoscale*. Springer, 2015.

Chapter 1. Materials and Methods

Summary

This chapter provides the details of different materials used in this work, the experimental techniques and protocols employed for developing the samples used etc. It also gives the details of the characterization techniques used along with a brief description to their basic principle.

1.1 Materials used

1.1.1 Polymers

The polymers Polystyrene (PS) and Poly methyl methacrylate (PMMA) have been used for the studies. The details of these polymers are given as the following.

1.1.1.1 Polystyrene

Polystyrene, which is also known as polyvinyl benzene, is a long chain hydrocarbon wherein alternating carbon centers are attached to phenyl groups. Its chemical formula is $(C_8H_8)_n$ and can be structurally represented as follows.

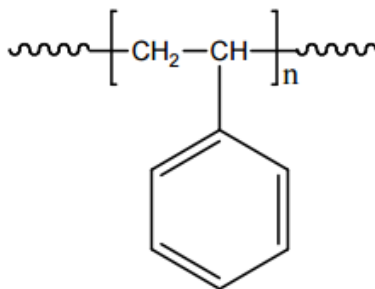


Figure 1-1: Structure of polystyrene.

Polystyrene P10447-S purchased from Polymer Source, which is obtained by living anionic polymerization of styrene was used for the studies. The molecular weight and molecular number are 135.8 and 129.71 kg/mol respectively with a poly dispersity index of 1.05. This PS has an atactic tacticity, which means that the chain on which the phenyl groups are attached does not possess a specific order.

1.1.1.2 Poly (methyl methacrylate)

Poly (methyl methacrylate), PMMA is a polymer with the following chemical structure, which is formed by the polymerization of methyl methacrylate.

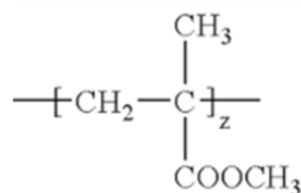


Figure 1-2: Structure of PMMA

We use the PMMA-17 purchased from Polymer experts, with a molecular weight of 152.8 kg/mol, molecular number = 141.6 kg/mol with a poly dispersity index of 1.08. It is syndiotactic in tacticity, which means that the substituents have alternate positions along the chain.

1.1.2 Ceria Nanoparticles

Cerium oxide/ceria nanoparticle (CeO₂ NP) [1], [2] dispersions (10%/w, pH 1.5) were supplied by the Rhodia-Solvay chemical company (Belgium). The size distribution of the NPs was found to be log-normal with median diameter 8.3 nm and a polydispersity 0.26 as measured from dynamic light scattering. The CeO₂ NPs were stabilized at low pH by a combination of long range electrostatic forces and short range hydration interactions.

1.2 Sample preparation

The preparation of the sample is done in two steps: (1) preparation of the substrate (2) thin film deposition.

1.2.1 Substrate preparation

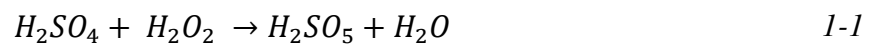
Considering the supported thin films, it is important to set the properties of the substrate by means of various surface treatments. The silicon wafers purchased from SILTRONIX with an orientation 100±0.5° were used as the substrate, which underwent one of the following treatments to obtain the respective property.

1.2.1.1 RCA treatment

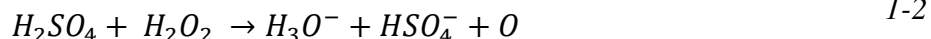
This method was developed by Werner Kern while working for the Radio Corporation of America (RCA) and was named after the institute. A solution of ammonium hydroxide (NH_4OH , 25%), hydrogen peroxide (H_2O_2 , 35%) and MilliQ water is taken in the ratio 2:1:1. The wafer segments are immersed in this solution and heated at 100°C for 10 minutes. The organic contaminants are removed by the solvating action of ammonium hydroxide and the oxidizing action of hydrogen peroxide [3]. The oxidizing agent H_2O_2 forms a continuous, thin silicon oxide layer (SiO_x) layer ($\sim 2\text{nm}$) on the substrate surface. After treatment, the substrates are rinsed thoroughly with MilliQ water. The result of this process is similar to the piranha treatment (which removes the organic contaminants leaving a hydrophilic wafer with an oxide layer) and is used when the wafer is not grossly contaminated. Hence the RCA treated wafers are also represented by $\text{SiO}_x\text{-Si}$. Usually we perform only the manipulations discussed above for RCA cleaning, which provides an organic and particle cleaning. Apart from this, there exist further extensions such as oxide strip, ionic cleaning etc., which can be performed depending on the properties required for the substrate.

1.2.1.2 Piranha treatment

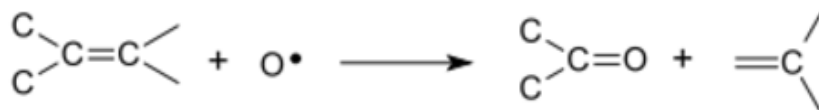
The solution for piranha treatment is made by mixing concentrated sulfuric acid and 30% hydrogen peroxide solution in a ratio of 2:1. This solution is energetic and even potentially explosive. Its preparation is exothermic and hence care should be taken to add the peroxide to acid very slowly. The beaker with the piranha solution is kept in a water bath which is at 80°C . The Si wafer with an initial diameter of 100mm, which are cut to a desired size using a diamond scribe is immersed in this piranha solution and is kept for 30 minutes. The wafers after the treatment are rinsed thoroughly with MilliQ water, which has a resistivity of $18.2\text{M}\Omega$ and is then dried with dry Nitrogen. When the wafers are immersed in the piranha solution two distinct processes occur. The first and faster process is removal of hydrogen and oxygen as units of water by the concentrated sulfuric acid as shown below:



In piranha solution, this dehydration process exhibits itself as the rapid carbonization of common organic materials. Secondly, the hydrogen peroxide degrades to form hydronium ions, bisulfate ions and transiently atomic oxygen. This energetically favored process boosted by the sulfuric acid can be represented as follows:



The atomic oxygen thus formed can even dissolve the elemental carbon, which is immensely stable. A carbonyl group is formed when the piranha solution disrupts the stable carbon-carbon surface bonds and the atomistic oxygen gets attached directly to a surface carbon.



The carbonyl group is formed by the capture of electron bonding pair from the central carbon atom by the oxygen atom, disrupting the bonds of the target carbon atom with one or more of its neighbors. This result is a cascading effect in which a single atomic oxygen reaction initiates significant unraveling of the local bonding structure, which in turn allows a wide range of aqueous reactions to affect previously impervious carbon atoms. The organic contaminants from the silicon surface are thus removed leaving the oxide etched hydroxyl groups on the surface. The thickness of this oxide layer is measured to be 1.7nm by means of ellipsometry. The substrate after piranha treatment is represented as SiO_x -Si considering the silicon wafer which is terminated with hydroxyl groups.



Figure 1-3: Silicon surface before and after the piranha treatment [4]

1.2.1.3 HF treatment

The HF treatment is performed by immersing the clean wafers with a native oxide in 5% Hydrofluoric acid (HF) for 5 minutes. We do the HF treatment of the wafers after its piranha/ RCA treatment. As the acid can corrode the glassware, a Teflon beaker is used for this process.

- In the first step, the wet-chemical oxide is dissolved by HF molecules, forming SiF_6^{2-} ions in solution.
- The second major step is the etching of the last monolayer of Si^{2+} , which is bonded to the bulk material.
- Finally, a hydrogen passivated silicon surface is obtained [5].

Thus with HF treatment, the oxide layer is removed forming H-terminated hydrophobic substrate

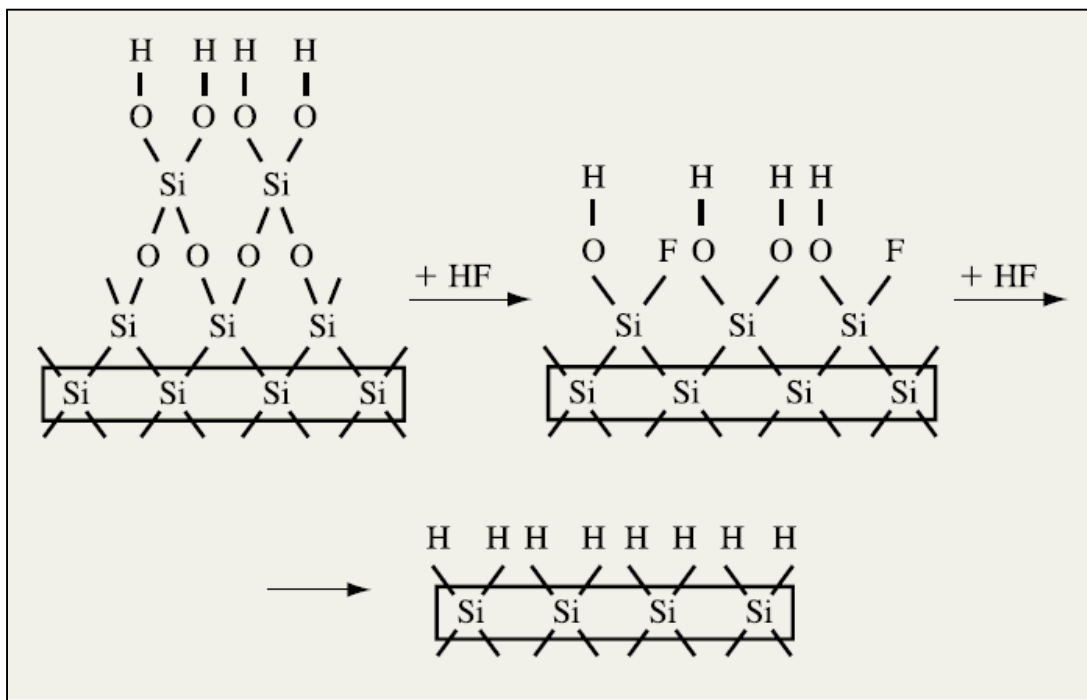


Figure 1-4: Schematic representation showing the changes of oxidized Si (100) wafer when immersed in HF solution [5], [6]

1.2.2 Thin film formation

1.2.2.1 The polymer solution for spin coating

The solutions of PS and PMMA for spin coating are made using 99.8%, anhydrous toluene purchased from Sigma Aldrich. The toluene was chosen considering its solubility parameter. The solubility parameter helps to characterize the solubility and can imply how compactable/good a solvent is, for a particular polymer. We have used Hansen solubility parameters which consider the specific interactions, especially hydrogen bonding for the estimation of solubility [7]. The basic equation governing the assignment of Hansen parameters is that the total cohesion energy, E , is the sum of the individual energies corresponding to the three types of interactions:

$$E = E_D + E_P + E_H \quad 1-3$$

Where E_D is the dispersive component, P : the polar interaction, H : the hydrogen bond interaction. Dividing this by the molar volume gives the square of the total (or Hansen) solubility parameter as the sum of the squares of the Hansen D , P , and H components:

$$E/V = E_D/V + E_P/V + E_H/V \quad 1-4$$

i.e. the cohesive energy density δ^2 between two substances can be expressed based on dispersive force, polar interaction and hydrogen bond interaction as follows

$$\delta^2 = \delta_D^2 + \delta_P^2 + \delta_H^2 \quad 1-5$$

According to equation 1-5, the solubility parameter of a given solvent can be considered as a vector with components δ_D , δ_P and δ_H . This means that each solvent can be located in a three dimensional system as a fixed point with co-ordinates agreeing with equation 1-5. The axes of the system are the dispersion axis δ_D , the polar axis δ_P , and the hydrogen bonding axis δ_H . The Hansen characterization is considered as a sphere whose center has δ_D , δ_P and δ_H values of PS as shown in the Figure 1-5 below.

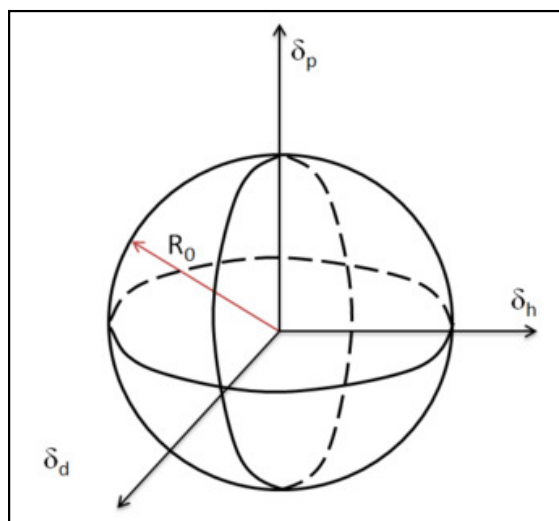


Figure 1-5: Representation of Hansen solubility sphere.

The radius of the sphere R_o is termed as the interaction radius, which is experimentally calculated. The boundary of the spherical characterization is based on the requirement that ‘good’ solvents have a distance from the center of the sphere R_a less than R_o . The distance between the center of solubility sphere and the position the compound can be expressed as:

$$R_a = \sqrt{(2\delta_{D,PS} - 2\delta_{D,S})^2 + (\delta_{P,PS} - \delta_{P,S})^2 + (\delta_{H,PS} - \delta_{H,S})^2} \quad 1-6$$

where S stands for the solvent. The smaller R_a , the more likely they are to be thermodynamically compatible. It is also important to calculate the Relative energy difference (RED) that determines the quality of solubility.

$$RED = \frac{R_a}{R_o} \quad 1-7$$

- $RED < 1$ the molecules are alike and are soluble
- $RED = 1$ the system will partially dissolve
- $RED > 1$ the system will not dissolve

Hence good solvent possess a low relative energy difference value.

Table 1-1: The Hansen solubility parameter values of PS, PMMA and toluene [7], [8]

| Solvent | δ_d (MPa ^{0.5}) | δ_p (MPa ^{0.5}) | δ_h (MPa ^{0.5}) |
|-------------|----------------------------------|----------------------------------|----------------------------------|
| Polystyrene | 21.28 | 5.75 | 4.3 |
| PMMA | 18.6 | 10.5 | 7.5 |
| Toluene | 18 | 1.4 | 2 |

Considering the solubility components of PS, PMMA and toluene as shown in the table 1-1 and using the equations 1-6 and 1-7, the *RED* value is 0.65 considering PS-toluene and 0.84 for PMMA-toluene system. As for both polymers the *RED* with toluene is less than 1, it was selected as the solvent for the polymer solution used for spin coating. The polymer solution was prepared 24 h prior to spin coating, for better polymer dissolution due to this aging time.

1.2.2.2 Spin coating

We use the spin coating technique for the thin film deposition. The spin coater, Spin 150 from SPS Europe is used for spin coating. The process can be schematically represented in Figure 1-6. The substrate is loaded on a vacuum chuck which holds it during the following high speed rotation. The polymer solution is then dispensed on this substrate and is rotated at a speed of 2000 rpm for 60S. The centripetal acceleration causes the solution to spread out leaving a thin layer of coating (polymer + solvent) on the substrate.

The final film thickness depends on the nature of the solution (for example: solution viscosity, solvent evaporation rate) and the parameters such as angular speed, spin time etc. chosen for the spin process. The dependence of the film thickness (h) to the solution viscosity (η) and the spin speed (ω) is as follows [9]:

$$h \propto \sqrt{\frac{\eta}{\omega}} \quad 1-8$$

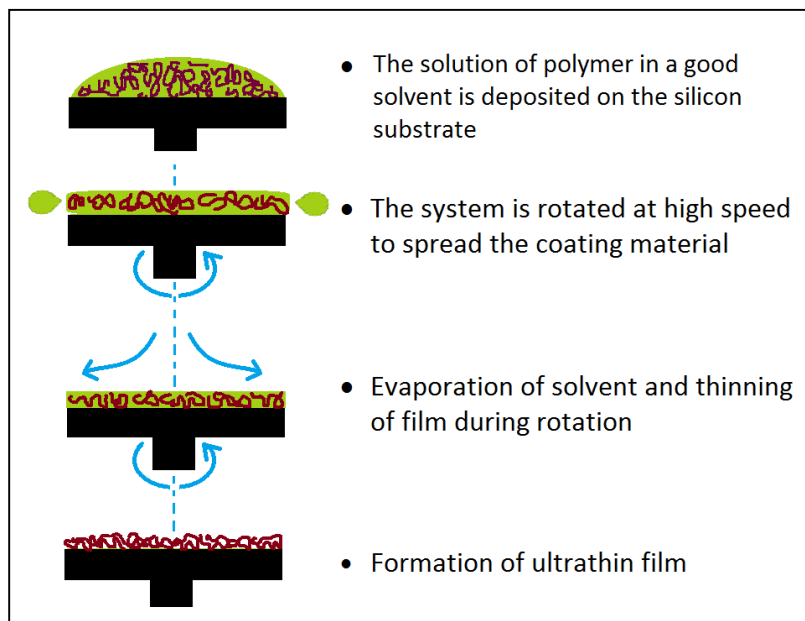


Figure 1-6: Schematic representation of the spin coating process. The substrate represented by black, solvent: green and the polymer: red respectively.

1.2.2.3 Annealing

The annealing refers to the process for keeping the samples at a temperature at 160°C (which is above the glass transition temperature of the polymers), for 24 hours in vacuum. The samples after the annealing are then allowed to reach the room temperature under the vacuum before usage. The annealing process helps the films to approach its thermodynamical equilibrium, which has been perturbed by the spin coating process due to the fast solvent evaporation [10]. The evidence that polymers in ultrathin films exist in an out of equilibrium structure has been used to account for the bizarre observation of negative thermal expansivity [11] and large residual stresses [12]. Annealing the films at temperatures above the glass transition temperature of the bulk polymer ($T_{g,bulk}$) for many hours reduces the residual stresses in spin coated thin polymer films but do not necessarily vanish even after long annealing. Annealing also helps to remove the residual solvent in the film. Since vitrification of spin-coated films generally occurs during solvent removal, it was pointed out that residual solvent could remain trapped inside the thin films. The work of Garcia-Turiel and Jérôme [13] using gas chromatography supports this idea which is not unanimously accepted.[14]

1.3 Characterization

1.3.1 Ellipsometry

The ellipsometry is an optical technique that measures the change of polarization upon reflection and compares it to a model. It can be used to characterize thickness, roughness, electrical conductivity etc. and various other material properties. We use this technique mainly to measure the thin film thickness, refractive index and to measure the glass transition temperature.

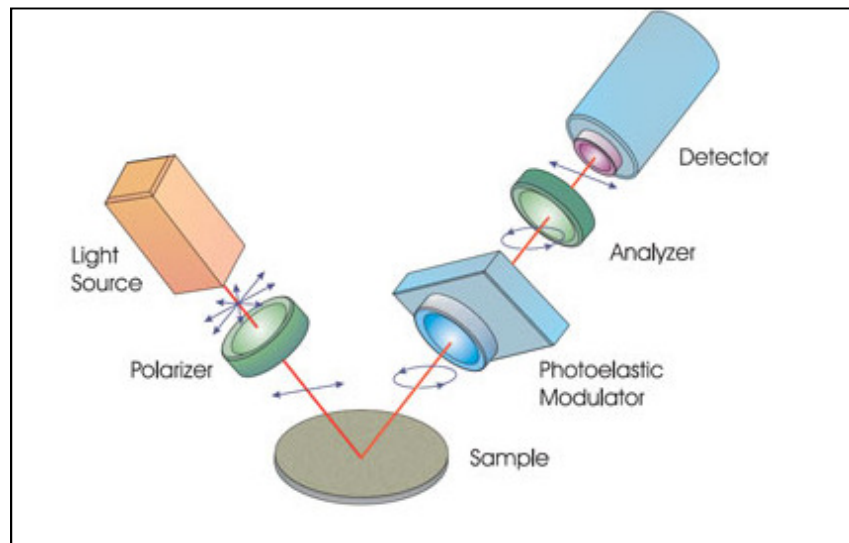


Figure 1-7: A schematic diagram showing the working principle of ellipsometry (Horiba scientific)

The system can be schematically represented as shown in Figure 1-7. It consists of a light source that emits the electromagnetic radiation which is linearly polarized by a polarizer. This linearly polarized light is allowed to fall on the sample and on reflection from the sample, the light becomes elliptically polarized. The output head comprises a photoelastic modulator and an analyzing polarizer that resolves the polarization state of the reflected beam. Both polarizers are held fixed during the measurement while the photoelastic modulator is used to induce a modulated phase shift of the reflected beam. The light is analyzed by a grating monochromator (analyzer) that directs sequentially the light for each individual wavelength onto the detector. The detector converts the light to electronic signal to determine the reflected polarization.

This information is compared to the known input polarization to determine the polarization change caused by the sample reflection. The exact nature of the polarization change is determined by the sample's properties such as thickness and refractive index.

The ellipsometer possess a well-established theory.[15], [16] The effect of the reflection of light from a film will depend on several variables such as the wavelength of light, the angle of incidence as well as the thickness and optical properties of all the films. The light beam can be described by defining an imaginary plane of incidence perpendicular to the film. On the other hand, the electric wave can be characterized by the orthogonal basis vectors, where E_p represents the amplitude of the wave in the plane of incidence (p -wave), E_s represents the amplitude of the wave perpendicular to the plane of incidence (s -wave).

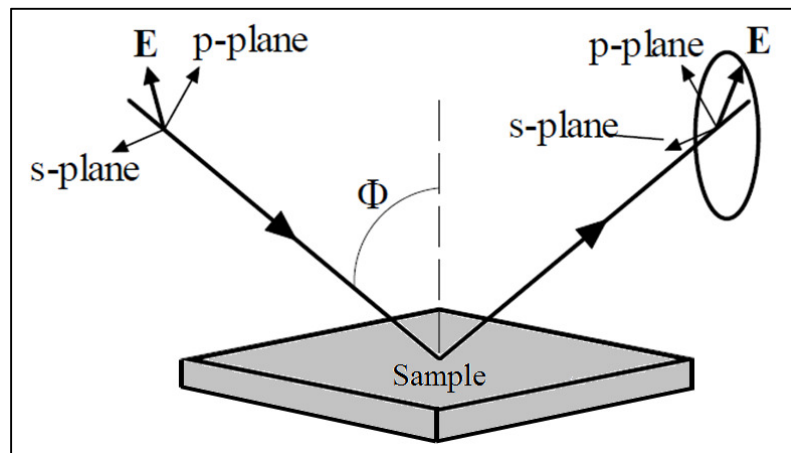


Figure 1-8: A typical geometry of an ellipsometric experiment showing the p - and s -directions. The light is linearly polarized initially and is elliptically polarized after being reflected from the sample.

Considering a single interference as shown in Figure 1-9, a), the ratio of the amplitude of the reflected beam to the incoming beam for the p - and s -waves can be given by the equations 1-9 and 1-10.

$$r_{1,2}^p = \frac{E_p^{out}}{E_p^{in}} = \frac{N_2 \cos\Phi_1 - N_1 \cos\Phi_2}{N_2 \cos\Phi_1 + N_1 \cos\Phi_2} \quad 1-9$$

$$r_{1,2}^s = \frac{E_p^{out}}{E_p^{in}} = \frac{N_2 \cos\phi_1 - N_1 \cos\phi_2}{N_2 \cos\phi_1 + N_1 \cos\phi_2} \quad 1-10$$

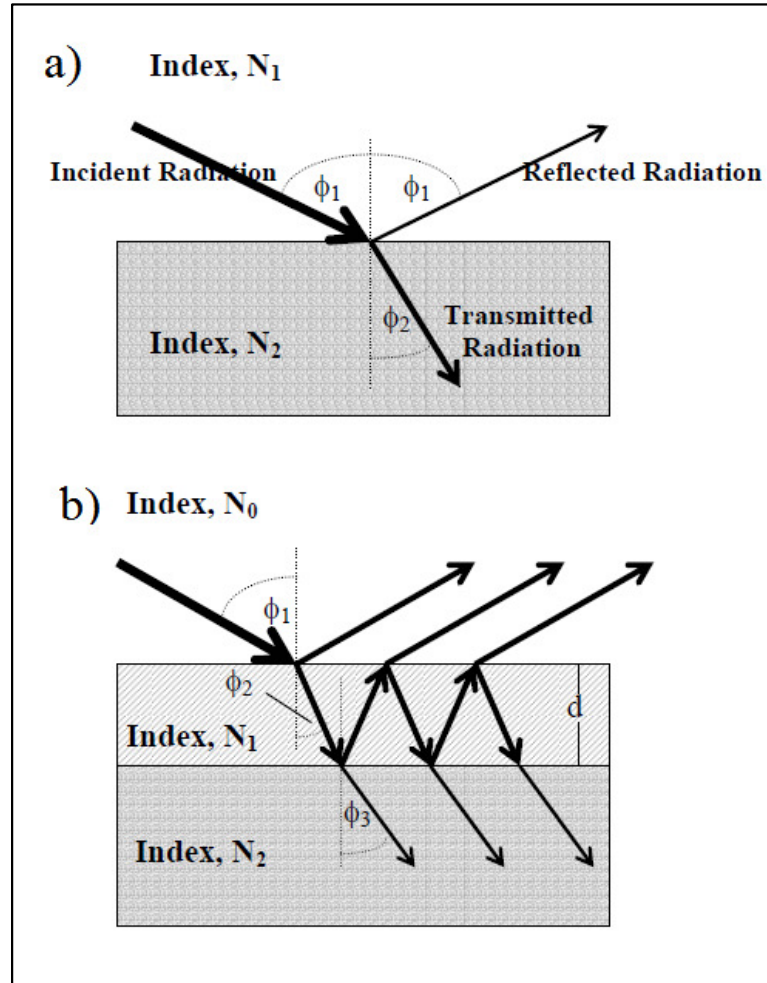


Figure 1-9: a.) Radiation interacting with a single plane parallel interface between Material 1, with refractive index N_1 , and Material 2, with refractive index N_2 . b.) Diagram of the beam path in a sample comprised of a film, with thickness d and refractive index N_1 , between Material 0, with refractive index N_0 , and Material 2, with refractive index N_2 . [17]

The complex refractive index of medium i , N_i is given by

$$N_i = n_i - jk \quad 1-11$$

where n_i is the real part of the refractive index, k is the extinction coefficient, and j is the imaginary number. In the special case of a single interface, r_p and r_s are more commonly referred to as the Fresnel reflection coefficients.

Considering the film on a substrate, that is considering the case where there are two interfaces, the equations describing the ratio of the amplitudes of the outgoing wave to the incoming wave are modified. This can be schematically represented as shown in Figure 1-9, b). Hence the resultant ratios of the p and s -waves can be written as given in equations 1-12 and 1-13.

$$R_p = \frac{E_p^{out}}{E_p^{in}} = \frac{r_{0,1}^p + r_{1,2}^p \exp(-j2\beta)}{1 + r_{0,1}^p r_{1,2}^p \exp(-j2\beta)} \quad 1-12$$

$$R_s = \frac{E_s^{out}}{E_s^{in}} = \frac{r_{0,1}^s + r_{1,2}^s \exp(-j2\beta)}{1 + r_{0,1}^s r_{1,2}^s \exp(-j2\beta)} \quad 1-13$$

where R_p and R_s are the total reflection coefficients, $r_{x,y}$ are the Fresnel reflection coefficients between interfaces x and y , and β is the optical thickness that describes the phase change of the wave as it moves from the top to the bottom of the film. [16], [17] The β can be given by the relation:

$$\beta = 2\pi \left(\frac{d}{\lambda} \right) N_2 \cos \phi_2 \quad 1-14$$

The fundamental equation of ellipsometry is [15]

$$\rho = \frac{R_p}{R_s} = \tan \Psi \exp(j\Delta) \quad 1-15$$

where Ψ and Δ are measured by the ellipsometer. Equations 1-12 and 1-13 provide the magnitude of the total reflection coefficients which is related to Ψ and the Δ term is related to the relative phase shift between the p and s -waves before and after reflection. Thus, by measuring Ψ and Δ with an ellipsometer, important information such as the thickness and refractive index of a film on a substrate can be extracted.

Typically this is done iteratively by assuming a model, such as that in Figure 1-9, b), and varying the thickness and optical constants in the model until the calculated values of Ψ and Δ match the experimentally measured values.[17]

We use the UVISEL spectroscopic ellipsometer for our studies which is purchased from Horiba Jobin Yvon. A photograph of the device is shown in Figure 1-10. It consists of a white light source, which is a 75W Xenon lamp that typically emits the light in a range of 190 to 2100 nm. The temperature controlled sample stage allows sample characterization at a range of temperatures for the investigation of material properties such as thermal transition analysis for polymers, band structure for compound alloys etc. The goniometer helps for automated variable angle measurements. Two types of detectors are employed: photomultipliers for UV-VIS applications, and InGaAs photodiodes for NIR applications.

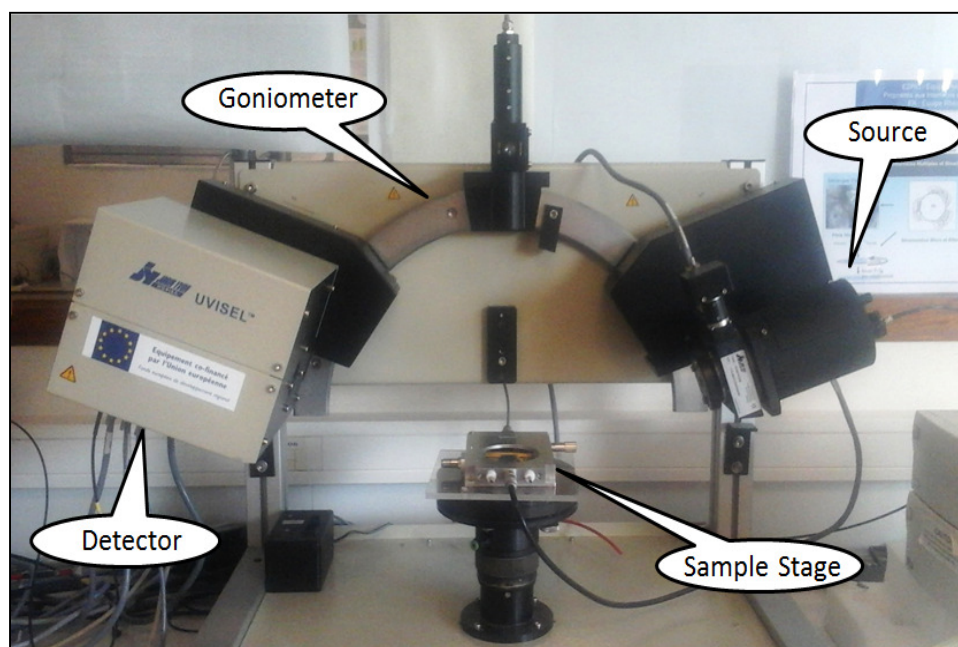


Figure 1-10: The photograph of Jobin-Yvon spectroscopic ellipsometer with labeled parts.

For the analysis, a multilayer model consisting of Si substrate, SiO₂ layer and the polymer was considered in case of polymer on SiO_x-Si. The refractive index spectrum was obtained by fixing the thickness value of SiO₂ at 17Å. Considering polymer on H-Si substrates, a single layer model is considered with polymer and Si substrate.

The incident angle is used as a fitting parameter. A transparent Sellmeier dispersion relation was used for modeling the refractive index of the polymer film as follows

$$n^2(\lambda) = 1 + B \frac{\lambda^2}{\lambda^2 - \lambda_0^2} \quad 1-16$$

Where λ is the wavelength of incident light, B is a dimensionless parameter that determines the shape of the refractive index in the visible range, and λ_0 is the resonance wavelength for which the refractive index diverges. The calculated optical constants were determined by simultaneously fitting the data obtained at three different incident angles (65° , 70° and 75°).

- **The Glass transition temperature (T_g) measurement**

When equipped with a hot stage (LinKAMTMS600), spectroscopic ellipsometer can be used to detect thermal variations and transitions in polymer samples. The sample is held in the temperature controlled stage. For each sample, the measurements were made at every 5°C interval from 25 to 160°C and before each measurement the sample was held at a fixed temperature for 5 min to equilibrate. During each of these temperature steps, the ellipsometric angles ψ and Δ are measured. The small changes in thickness and refractive index typical of most of the ellipsometry experiments can be shown to be linearly related to small changes in the ellipsometric measurable. Since both these quantities vary with the density of the sample, they necessarily exhibit a ‘kink’ at the glass transition temperature. [18] While the film is being heated, the ellipsometric angles linearly evolve as a function of the temperature, until the glass transition phase during which a change in slope takes place as can be seen from the figure 1-11. [19]

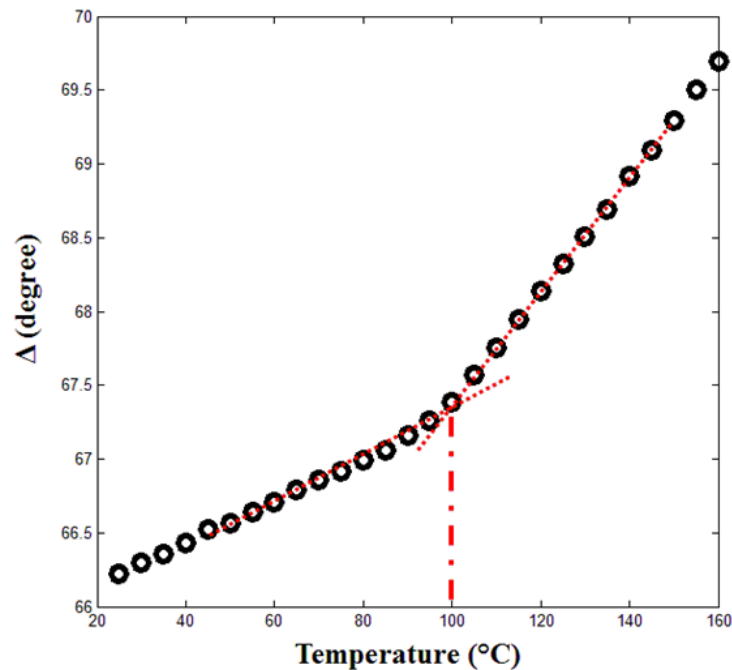


Figure 1-11: Raw ellipsometric curves showing Δ as function of temperature for 100 nm PS film on Si wafer with native oxide.

The T_g determination is done by selecting two linear regions of the data and finding the intersection point between the extrapolated lines. The data analysis with Matlab software, straight lines that best fit all of the points and their intersections was used for an accurate T_g determination.

1.3.2 Atomic force microscopy

The atomic force microscope (AFM) belongs to the broad family of scanning probe microscopes in which a proximal probe is exploited for investigating properties of surfaces with sub nanometer resolution [20]. Usually, the probe is a sharp tip, which is a 3-6 μm tall pyramid with 15-40 nm end radius.

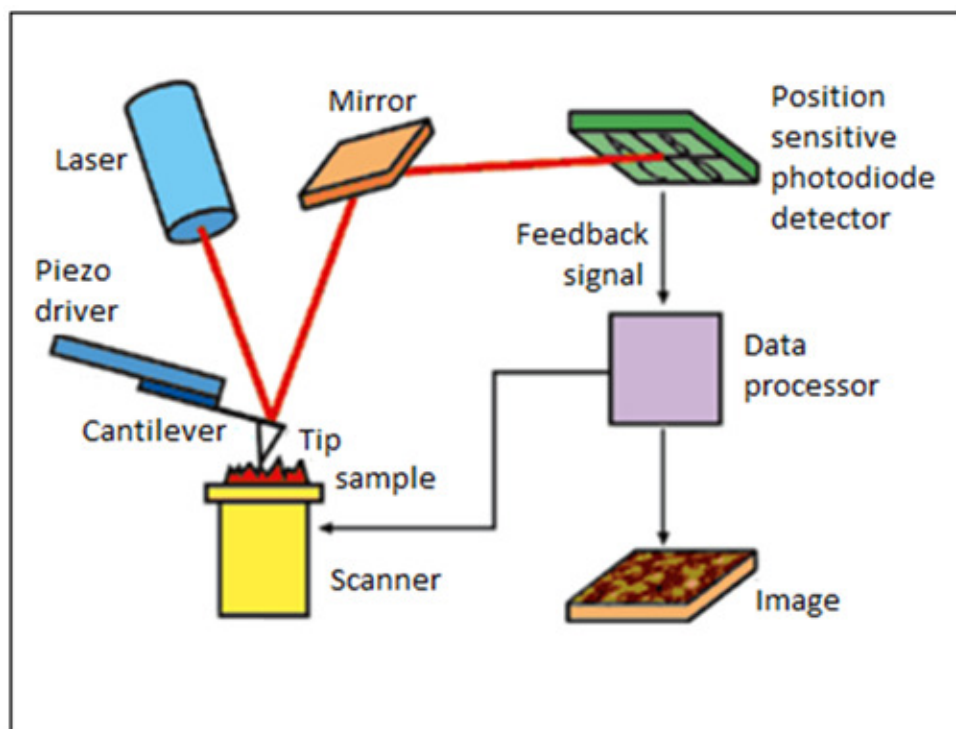


Figure 1-12: A schematic diagram showing the working principle of AFM.

Forces between the tip and the sample surface cause the cantilever to bend/ deflect. The amount of force between the probe and sample depends on the spring constant (stiffness) of the cantilever and the distance between the probe and sample surface.

This force, F can be described using Hooke's law [21]:

$$F = -k \cdot x \quad 1-17$$

Where, k , the spring constant and x is the cantilever deflection. The deflection of the cantilever is measured by detecting the deflection of a light beam reflected from the back of the cantilever onto a position sensitive detector (PSD) as shown in Figure 1-12.

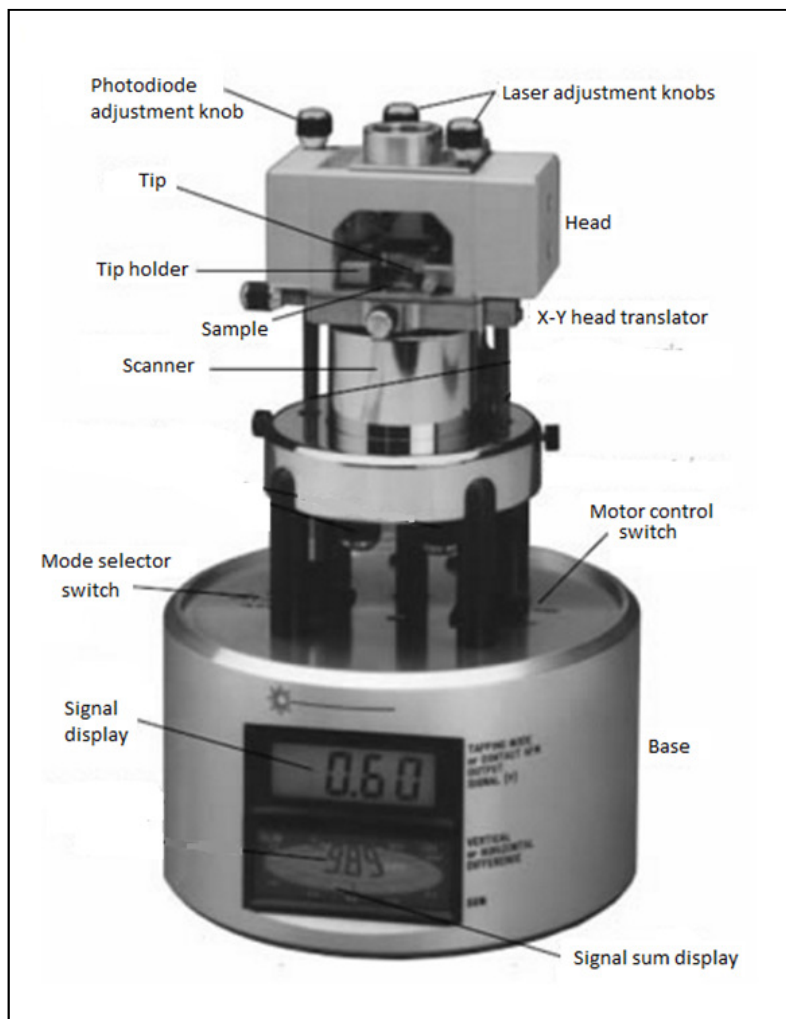


Figure 1-13: Photograph of Nanoscope IIIa with labeled parts.

The differences between the signals of photo-detector segments indicate the position of the laser spot on the detector and thus the angular deflections of the cantilever. The feedback loop consists of the tube scanner that controls the height of the tip; the cantilever and optical lever, which measures the local height of the sample; and a feedback circuit that attempts to keep the cantilever deflection constant by adjusting the voltage applied to the scanner. Hence as a function of the lateral sample position, the deflection measured from the cantilever allows the computer to generate the map of surface topography. The AFM not only measures the force on the sample but also regulates it, allowing acquisition of images at very low forces. We use Nanoscope IIIa Multimode8 AFM for our studies. The major components of this AFM/ its control units, as explained above are labeled in the photograph given in Figure 1-13.

- **Imaging modes**

There are three primary imaging modes in AFM: contact, non-contact and tapping mode. During contact mode, the probe is in contact with the sample and repulsive Van der Waals forces prevail, while the attractive Van der Waals forces are dominant when the tip moves further away from the sample surface.

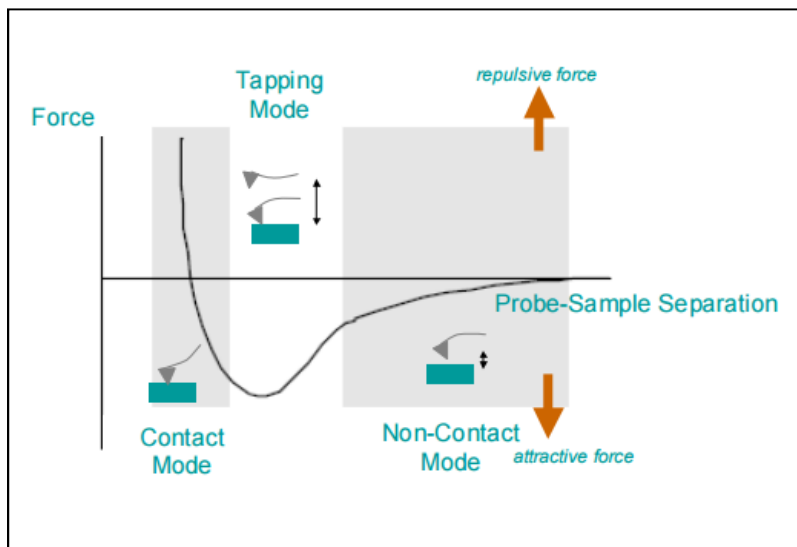


Figure 1-14: Inter atomic force vs. distance curve with different modes of operation.

i. Contact Mode

In contact mode, the tip is constantly in touch with the sample surface. The applied force is kept constant while the tip scans the surface, creating the surface image. This imaging mode is good for samples with rough and rigid surfaces as it provides fast scanning with high resolution. One disadvantage of this imaging mode is that soft samples like tissues can be deformed or damaged due to the applied force. This drawback can be solved by measuring the sample in aqueous environments to reduce the interaction force between the tip and the sample.

ii. Tapping Mode

In tapping mode, the tip is not in constant contact with the sample surface. Instead, the cantilever is oscillated at its resonant frequency, which makes the tip lightly tap on the surface during scanning. A piezo stack excites the cantilever's substrate vertically, causing the tip to bounce up and down. As the cantilever bounces vertically, the reflected laser beam is deflected in a regular pattern over a photodiode array, generating a sinusoidal electronic signal. The signal is converted to a root mean square (*rms*, R_q) amplitude value, which is displaced in AC volts. A constant tip-sample interaction is maintained by monitoring the oscillation amplitude and an image is obtained.

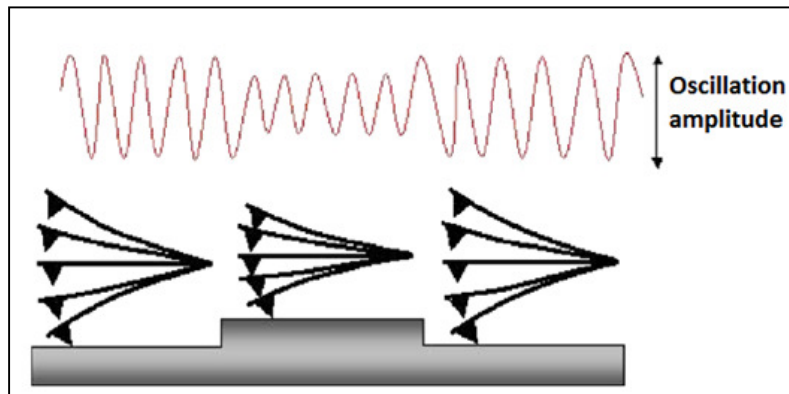


Figure 1-15: A schematic representation of AFM operating in tapping mode[20]

Several parameters that affect the image contrast are the height, phase signals and amplitude. As the dragging force during scanning is greatly reduced, this mode is useful where the samples are easily damageable or loosely bound to their surface [21]. The advantage of tapping the surface is an improved lateral resolution on soft samples. Resolution can reach atomic dimensions for flat surfaces.[22] However, this imaging mode requires a slower scanning speed. We use tapping mode for the imaging.

iii. **Non-contact mode**

There is no contact between the sample surface and the probe in non-contact mode. The probe oscillates above the sample surface, forming a weak attractive force between the tip apex atom and the sample surface atom.

Feedback signals are obtained by measuring a frequency shift in the mechanical oscillation of the cantilever. The force exerted on the surface sample is very low in this case. Moreover, as there is no contact between the probe and the surface, the probe lifetime can be extended. Another advantage of this operating mode is the possibility to observe an atomic defect if the very weak attractive force can be detected. The drawback of this mode is the reduction of resolution, and the oscillation of the cantilever is affected in case there are contaminants on the sample surface.

1.3.3 X-ray Reflectivity

XRR is a non-contact and non-destructive technique that can be used for thickness determination of thin films with a precision of about 1-3Å. In addition to thickness determination, this technique is also employed for measuring the density and roughness of films with a high precision. The basic idea behind the technique is to reflect a beam of x-rays from a flat surface and to measure the intensity of x-rays reflected in the specular direction, where the reflected angle is equal to the incident angle. In the absence of a perfectly sharp and smooth interface, the reflected intensity will deviate from that predicted by the law of Fresnel reflectivity. The deviations can then be analyzed to obtain the density profile of the interface normal to the surface.

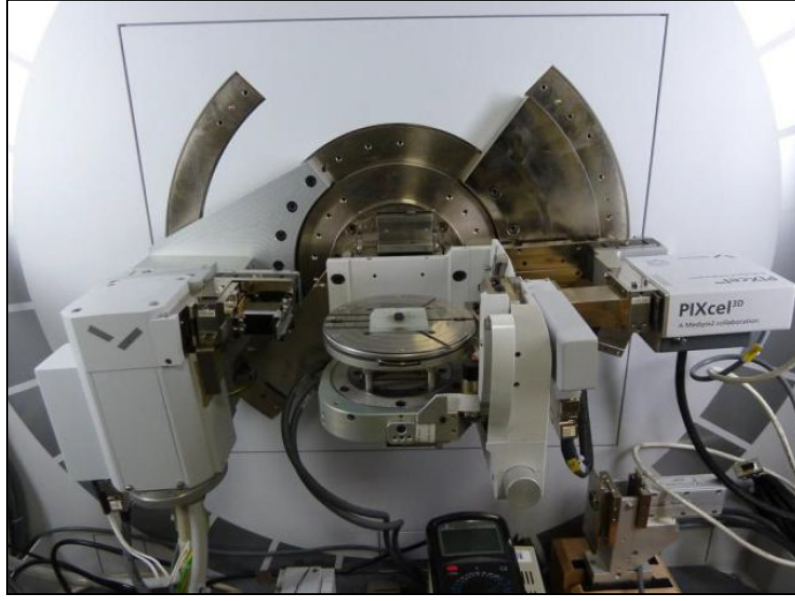


Figure 1-16: The photograph of Empyrean Panalytical reflectometer.

- **Refractive index and density determination**

Considering a plane wave travelling in medium 0 incident on the surface of medium 1, the refractive index n of a material for x-rays can be calculated using the following equations [23]:

$$n = 1 - \delta - i\beta \quad 1-18$$

$$\delta = \left(\frac{r_e \lambda^2}{2\pi} \right) N_0 \rho \sum_i x_i (Z_i + f_i') / \sum_i x_i M_i \quad 1-19$$

$$\beta = \left(\frac{r_e \lambda^2}{2\pi} \right) N_0 \rho \sum_i x_i (Z_i + f_i'') / \sum_i x_i M_i \quad 1-20$$

where r_e is the classical radius of electron (2.818×10^{-9} m), N_0 is the Avogadro number, λ , the x-ray wavelength, ρ is the density in (g/cm^3), z_i is the atomic number of i^{th} atom, M_i is the atomic weight of the i^{th} atom. x_i is the atomic/molar ratio of the i^{th} atom and f_i' , f_i'' are the atomic scattering factors of the i^{th} atom.

As from equation 1-18, the refractive index is expressed as a complex number. The value of the parameter δ varies from 10^{-5} to 10^{-6} for x-rays with wavelength approximately 1 Å. From equation 1-19, the value of δ depends on the x-ray wavelength, density and composition of the material. The parameter β is related to x-ray absorption, which is expressed by a linear absorption coefficient μ as shown below:

$$\beta = \lambda\mu/4\pi \quad 1-21$$

The critical angle θ_c for the total reflection is given by the following formula:

$$\theta_c = \sqrt{2\delta} \quad 1-22$$

Thus the density of the surface film can be obtained from the critical angle for total reflection θ_c . As by the equation 1-18, the refractive index of the material depends on the x-ray wavelength and the density of the material. When the x-ray wavelength is longer/ with lower material density, the θ_c is larger.

- **Thickness measurement**

The reflection of x-rays occurs at all the interfaces of a multilayer film. The x-ray reflectivity of a multilayer film as a function θ can be theoretically calculated using equation 1-23, where the vacuum or gas phase on the top of a film with n layers is regarded as the $j=1^{\text{st}}$ layer. Each layer in the multilayer film is numbered in sequence starting with $j=2$ and a substrate is considered as the $j= n+1$ layer. When the reflection coefficient at the interface between the j^{th} and $(j+1)^{\text{th}}$ layers is defined as $R_{j,j+1}$ where its value is calculated as follows:

$$R_{j,j+1} = \frac{R_{j+1,j+2} + F_{j,j+1}}{R_{j+1,j+2} \times F_{j,j+1} + 1} a_j^4 \quad 1-23$$

$$F_{j,j+1} = \frac{g_j - g_{j+1}}{g_j + g_{j+1}} \exp\left(\frac{-8\pi^2 g_j g_{j+1} \sigma_{j+1}^2}{\lambda^2}\right) \quad 1-24$$

$$a_j = \exp(-i\pi g_j d_j / \lambda) \quad 1-25$$

$$g_j = \sqrt{n_i^2 - \cos^2 \theta} \quad 1-26$$

The recurrence equation 1-23 together with equation 1-24, 1-25 and 1-26 can be used to calculate the values of $R_{j,j+1}$, starting at the interface on top of the substrate, and then the next upper interface in sequence up to the surface layer. The x-ray reflectivity $I/I_0 = R_{1,2}$ is finally calculated. Generally, an x-ray experimental reflectivity curve is compared to the theoretical curve calculated based on a layer structure model. The solution with optimal parameter values of thickness, density and roughness of the interface in the multilayer film is obtained when the residual between the measured and calculated reflectivity data reaches a minimum.

We used Empyrean Panalytical reflectometer, which has a Cu source (2kW) followed by a mirror to select and enhance Cu $K\alpha$ radiation with a wavelength of 1.543 Å. The measurements are carried out in symmetric θ - θ geometry, in which the sample was kept fixed during the measurements. The intensity was measured with a Pixel 3D detector using a fixed aperture of three channels (0.165°) in the 2θ direction. The photograph of Empyrean Panalytical reflectometer is given in Figure 1-16

1.3.4 Contact angle goniometry

Contact goniometry is a method to determine the wettability of a surface, to calculate the surface energy etc. The ‘contact angle’ is the angle at which a liquid/vapor interface meets the solid surface. It is specific for any given system and is determined by the interactions across the three interfaces –solid/ liquid, solid/gas and liquid/gas. The term ‘wetting’ describes the contact between a liquid and a solid surface and is a result of intermolecular interactions when the two are brought together. The amount of wetting depends on the energies (or surface tensions) of the interfaces involved such that the total energy is minimized. The degree of wetting is described by the contact angle. This is the angle at which the liquid/vapor interface meets the solid/liquid interface. [24]

The contact angle for a flat surface is measured from a drop of a suitable liquid resting on a surface (Figure 1-17)

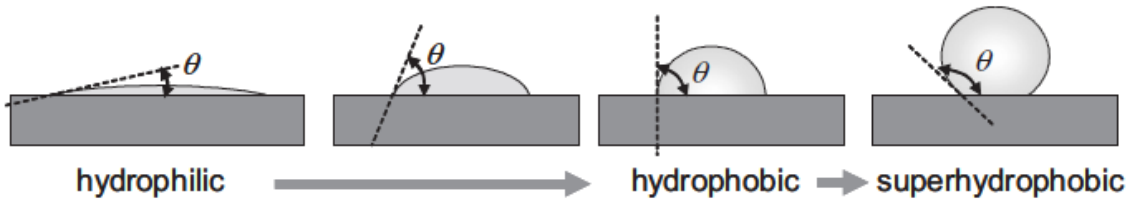


Figure 1-17: Schematic representation for the wettability of surface [24].

If the liquid is very strongly attracted to the solid surface, as for example, water on a hydrophilic solid, the droplet will completely spread out on the solid surface and the contact angle will be close to zero degrees. Less strongly hydrophilic solids will have a contact angle up to 90° . The contact angle will be larger than 90° for a hydrophobic solid surface. Surfaces are said to be super hydrophobic when the contact angle is greater than 150° . On these surfaces, water droplets simply rest on the surface, without actually wetting to any significant extent. The contact angle thus directly provides information on the interaction energy between the surface and the liquid.

The theoretical description of contact arises from the consideration of a thermodynamic equilibrium between the three phases: the liquid phase of the droplet (L), the solid phase of the substrate (S), and the gas/vapor phase of the ambient (V). The latter will be a mixture of ambient atmosphere and an equilibrium concentration of the liquid vapor or could alternatively be another immiscible liquid phase. At thermodynamic equilibrium, the chemical potential in the three phases should be equal. It is generally convenient to consider the interfacial energies involved.

Using the simplified planar geometry Young's equation [25] can be written as

$$0 = \gamma_{SG} - \gamma_{SL} - \gamma \cos \theta \quad 1-27$$

where γ_{SG} , γ_{sl} and γ are the interfacial energies at the solid/gas, solid/liquid and liquid/gas interface.

We use the Dig drop GBX contact angle goniometer in static sessile drop method where the angle formed between the liquid/solid interface and the liquid/vapor interface can be measured using a high-resolution camera. 1.5 μL of liquids are deposited on substrate at a speed of $3\mu\text{m/s}$ and the photos are captured at 20 ms after deposition. The Windrop software helps to capture and analyze the contact angle.

1.3.5 Solvent rinsing using dip coater

Dip coating refers to the immersing of a substrate into a tank containing coating material, removing the substrate from the tank, and allowing it to drain. It is a popular way of creating thin film coated materials along with the spin coating procedure.

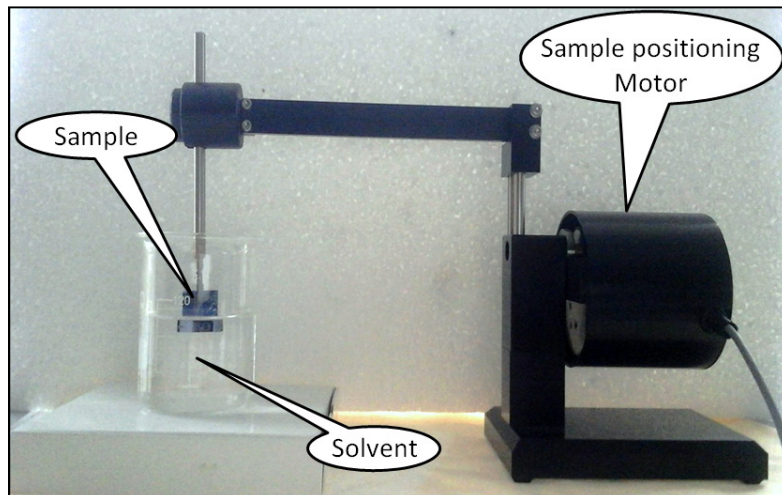


Figure 1-18: Photograph showing the solvent rinsing performed with dip coater.

Unlike its standard application, we used the dip coater for rinsing our supported thin films with various solvents. The advantage of using the dip coater for the solvent rinsing is that along with the software (Nima TR 8.1) provides control of the sample immersion and withdrawal speeds, rest positions, rest periods and number of cycles etc. The samples were dipped and withdrawn at a speed of 48.2 mm/min. The dip coater also helps to keep the samples steady at upright position for the desired amount of time.

REFERENCES

- [1] L. Qi, J. Fresnais, P. Muller, O. Theodoly, J.-F. Berret, and J.-P. Chapel, “Interfacial Activity of Phosphonated-Polyethylene Glycol Functionalized Cerium Oxide Nanoparticles.,” *Langmuir*, 2012.
- [2] L. Qi, A. Sehgal, J. C. Castaing, J. P. Chapel, J. Fresnais, J. F. Berret, and F. Cousin, “Redispersible hybrid nanopowders: Cerium oxide nanoparticle complexes with phosphonated-PEG oligomers,” *ACS Nano*, vol. 2, no. 5, pp. 879–888, 2008.
- [3] W. Kern, “The evolution of silicon wafer cleaning technology,” *J. Electrochem. Soc.*, vol. 137, no. 6, pp. 1887–1892, 1990.
- [4] H.-X. Wu, L. Tan, M.-Y. Yang, C.-J. Liu, and R.-X. Zhuo, “Protein-resistance performance of amphiphilic copolymer brushes consisting of fluorinated polymers and polyacrylamide grafted from silicon surfaces,” *RSC Adv.*, vol. 5, no. 16, pp. 12329–12337, 2015.
- [5] H. F. Okorn-Schmidt, “Characterization of silicon surface preparation processes for advanced gate dielectrics,” *IBM J. Res. Dev.*, vol. 43, no. 3, pp. 351–326, 1999.
- [6] H. F. Schmidt, I. Teerlinck, W. Storm, H. Bender, M. Meuris, P. W. Mertens, and M. M. Heyns, “Cleaning Technology in Semiconductor Device Manufacturing,” in *Proceedings of the 4th International Symposium on Cleaning Technology*, 1996, p. 480.
- [7] C. M. Hansen, *Hansen Solubility Parameters, A User’s Hand book*. Taylor & Francis, 2007.
- [8] T. Lindvig, M. L. Michelsen, and G. M. Kontogeorgis, “A Flory-Huggins model based on the Hansen solubility parameters,” *Fluid Phase Equilib.*, vol. 203, pp. 247–260, 2002.
- [9] S. Franssila, *Introduction to Microfabrication*, vol. 1. John Wiley & Sons, 2004.
- [10] G. Reiter and P. G. de Gennes, “Spin-cast, thin, glassy polymer films: Highly metastable forms of matter,” *Eur. Phys. J. E*, vol. 6, no. 1, pp. 25–28, 2001.

- [11] W. J. Orts, J. H. van Zanten, W. Wu, and S. K. Satija, "Observation of temperature dependent thicknesses in ultrathin polystyrene films on silicon," *Phys. Rev. Lett.*, vol. 71, no. 6, p. 867, 1993.
- [12] G. Reiter, M. Hamieh, P. Damman, S. Sclavons, S. Gabriele, T. Vilmin, and E. Raphael, "Residual stresses in thin polymer films cause rupture and dominate early stages of dewetting," *Nat. Mater.*, vol. 4, no. 10, pp. 754–758, Oct. 2005.
- [13] J. Garcia-Turiel and B. Jérôme, "Solvent retention in thin polymer films studied by gas chromatography," *Colloid Polym. Sci.*, vol. 285, no. 14, pp. 1617–1623, 2007.
- [14] X. Zhang, K. G. Yager, S. Kang, N. J. Fredin, B. Akgun, S. Satija, J. F. Douglas, A. Karim, and R. L. Jones, "Solvent retention in thin spin-coated polystyrene and poly (methyl methacrylate) homopolymer films studied by neutron reflectometry," *Macromolecules*, vol. 43, no. 2, pp. 1117–1123, 2009.
- [15] R. M. A. Azzam and N. M. Bashara, *Ellipsometry and Polarized Light* North-Holland Publ. 1977.
- [16] H. G. Tompkins and W. A. McGahan, *Spectroscopic ellipsometry and reflectometry: a user's guide*. Wiley New York, 1999.
- [17] Stephen Michael Sirard, "Structure and Interaction of Polymer Thin Films with Supercritical Carbon Dioxide," The University of Texas at Austin, 2003.
- [18] J. A. Forrest and K. Dalnoki-Veress, "The glass transition in thin polymer films," *Adv. Colloid Interface Sci.*, vol. 94, pp. 167–196, 2001.
- [19] A. El Ouakili, G. Vignaud, E. Balnois, J.-F. Bardeau, and Y. Grohens, "Multiple glass transition temperatures of polymer thin films as probed by multi-wavelength ellipsometry," *Thin Solid Films*, vol. 519, no. 6, pp. 2031–2036, Jan. 2011.
- [20] A. Alessandrini and P. Facci, "AFM: a versatile tool in biophysics," *Meas. Sci. Technol.*, vol. 16, no. 6, pp. R65–R92, 2005.

- [21] K. C. Khulbe, C. Y. Feng, and T. Matsuura, *Synthetic Polymeric Membranes Characterization by Atomic Force Microscopy*. Springer, 2008.
- [22] “NanoScope III Control System User’s Manual, ver 3.0.” Digital Instruments Inc., Santa Barbara, 1993.
- [23] M. Yasaka, “X-ray thin-film measurement techniques,” *Rigaku J.*, vol. 26, no. 2, pp. 1–9, 2010.
- [24] R. Förch, H. Schönherr, and A. T. A. Jenkins, “Appendix C: Contact Angle Goniometry,” in *Surface Design: Applications in Bioscience and Nanotechnology*, Wiley-VCH Verlag GmbH & Co. KGaA, 2009, pp. 471–473.
- [25] J. N. Israelachvili, *Intermolecular and surface forces*. Academic Press London, 1991.

Chapter 2. Density variations of polymer thin films under confinement; a study based on Ceria nanoparticle adsorption

Summary

The density variation in confined polymer films still remains a puzzling problem subject to controversy as the methods utilized to determine the density are often model dependent. In this chapter, we propose a direct and model independent method to detect the density/refractive index variations in polymer thin films through adsorption of ceria nanoparticles (NPs) onto their surface. The amount of adsorbed NP scales with the polymer film refractive index, hence any increase/decrease in the NP surface coverage directly indicates an increase/decrease in the film refractive index and density. The nanoparticle adsorption experiments conducted on two well studied polymers, Polystyrene and Poly (methyl methacrylate) is discussed.

2.1 Introduction

The polymer thin films in a confined state show-up many anomalous behavior in their viscosity, [1], [2] physical aging, [3], [4] stability, [5], [6] density [7] etc. The mass density is an important fundamental property of polymer thin films, on which many of the other properties like free volume, glass transition temperature (T_g), stability, coefficient of thermal expansion (CTE) etc. are related. Considering the relation of density to other thin film properties, molecular dynamics simulation showed that the enhancement of the mobility of the polymer chains due to the lowering of density of the polymer films at polymer vacuum interface results in the reduction of the glass transition temperature. [8] Later in an experimental study on the effect interfacial interactions on the glass transition properties of supported thin films, Tsui *et. al.* showed that a decrease in mass density of a mobile layer could interpret the depression of T_g . [9] Considering the relation of density to the stability of polymer thin films, Sharma *et. al.* found that the increase in the density with the increasing film thickness can actually stabilize a thermodynamically unstable film, whereas due to decrease in the density with increasing film thickness, a thermodynamically stable thin film can be destabilized. [10] Yet another main approach to interpret the anomalous behavior of films under confinement is by the free volume theory, [11]–[13] where the density scales with free volume. [14] Considering the traditional concepts of free volume, the motion of individual particles in a glass forming material requires sufficient free volume into which the particles can move. [15] The molecular motion in a fluid of hard spheres is conditioned by the presence of located interstitial holes where there are vacancies of atoms. [16] The specific free volume is given as $V_f = V - V_{occ}$, where V is the total specific volume and V_{occ} is the occupied volume including the interstitial free volume and the van der Waals volume of molecules. The movement of a molecule into a hole within a cage by the immediate neighbors of the moving particle becomes only possible when the hole has a greater size than some critical value v^* . In such a case, the temperature dependent redistribution of free volume is assumed to be the reason for the formation of critical void. As the temperature is decreased, the density increases and it becomes increasingly difficult for a particle to find sufficient free volume for motion to occur on a reasonable time scale.

Recently, Napolitano *et al.* [17] put forward the concept of *interfacial free volume* (the space available for molecular relaxations at the polymer/substrate interface) which can differ from the bulk free volume due to the packing frustration of the adsorbed layer. They have evidenced that the knowledge of the film thickness together with interfacial interactions are not sufficient to fully describe the properties of macromolecules under confinement. [17]–[20] Indeed, this local free volume can alter the long-range structural dynamics from the substrate and consequently the T_g . [18], [20] Thus the information about the density of polymer thin films can lead us to understand many other properties which are linked to it. Hence a natural question is how we can probe the density of polymer films that are confined by their thickness?

Even after more than 2 decades of intense research, the density variation in confined polymer films still remains a puzzling problem subject to controversy, as the methods utilized to determine the density are model dependent. Vignaud *et al.* [14] showed by combining Spectroscopic Ellipsometry (SE) and X-ray reflectivity (XRR) that the average density of polystyrene (PS) thin films on oxide-free H-terminated silicon wafer (H-Si) increases when reducing the film thickness. This result is in line with the recent results of Gin *et. al* [21] revealing by X-ray and neutron reflectivity experiments that the PS chains at the polymer/substrate interface exhibit a more flattened conformation and thus possesses a higher density than in the bulk. At odds with these results, XRR measurements reported either no systematic change in density with the film thickness [22] or even a decreased electron density near the PS substrate interface. [23] Some of these discrepancies can possibly arise from the sample preparation conditions like the quality and evaporation rate of the spin-coating solvent [24] (acting on the entanglement density), the nature of the substrate [25] (acting on interfacial interactions), the annealing time [26] (acting on the monomer density at the polymer/substrate interface). Another possible source of controversy is related to the way experimental results coming from ellipsometry and XRR are analyzed. For XRR, the density profile is determined according to a guessed model that is refined by fitting the model dependent calculated data to the measured ones. [27] This approach has however a serious limitation as the phase of the reflected radiation is lost. This prevents the uniqueness of the density profile determination from the data. [28] For ellipsometric measurements, the thickness and refractive index values are strongly correlated in particular for thinner films ($h < 10$ nm).[29]

Because ellipsometry is sensitive to the product of the refractive index and the film thickness (i.e., the optical path length) the absolute value of the index of refraction may be dubious for an unknown thickness. Hence, probing small changes in the density of ultrathin films remains a very challenging issue till date.

In this chapter, we propose a novel method based on the adsorption of ceria (CeO_2) nanoparticles at the surface of polymer thin films to get this most demanding information. The study is carried out on two well studied polymers, namely polystyrene (PS) and poly methyl methacrylate (PMMA). The proposed method allows a direct assessment of the film density without relying on any model. The amount of adsorbed nanoparticles scales with the polymer film refractive index, hence any increase/decrease in the nanoparticle surface coverage directly indicates an increase/decrease in the film refractive index. The refractive index, n is linked to the density, ρ by the Clausius and Mossotti equation as follows:

$$\frac{(n^2 - 1)}{(n^2 + 2)} = \frac{\alpha N_a}{3M\epsilon_0} \rho \quad 2-1$$

where N_a is Avogadro number, M is the molecular weight of the polymer repeating unit, ϵ_0 is the vacuum permittivity and α being the average polarizability of polymer repeat unit whose unit is (Cm^2/V). Hence a variation in the refractive index is directly indicating the density variations.

2.2 Ceria NP adsorption for sensing the density variations

The principle for using is Ceria NPS for sensing the variations of polymer thin film density is straightforward. High dielectric constant Ceria NPs [30] adsorb strongly onto any hydrophobic polymer surface mainly through dispersive van der Waals (LW) interactions. The total Hamaker constant A_{Total} of a particle interacting with a surface in a solution is the sum of a zero-frequency, $A_{\nu=0}$ and a dispersive $A_{\nu \neq 0}$ Hamaker constants. [31]

$$A_{Total} = A_{\nu=0} + A_{\nu \neq 0} \quad 2-2$$

where

$$A_{v=0} \approx \frac{3}{4} kT \left(\frac{\epsilon_P - \epsilon_{sol}}{\epsilon_P + \epsilon_{sol}} \right) \left(\frac{\epsilon_{NP} - \epsilon_{sol}}{\epsilon_{NP} + \epsilon_{sol}} \right) \quad 2-3$$

$$A_{v \neq 0} = \frac{3h\nu_e}{8\sqrt{2}} (n_p^2 - n_{sol}^2)(n_{NP}^2 - n_{sol}^2) / \left\{ (n_{NP}^2 + n_{sol}^2)^{1/2} (n_p^2 + n_{sol}^2)^{1/2} \left[(n_p^2 + n_{sol}^2)^{1/2} + (n_{NP}^2 + n_{sol}^2)^{1/2} \right] \right\} \quad 2-4$$

where h and k are the Planck and Boltzmann constants respectively, ν_e is the main electronic absorption frequency in the UV typically around $3 \times 10^{15} s^{-1}$, T is the temperature, n_p , n_{sol} , n_{NP} and ϵ_P , ϵ_{sol} , ϵ_{NP} are the refractive index and the relative permittivity of the polymer, the solution, and the nanoparticles respectively. A simulation of $A_{v=0}$ and $A_{v \neq 0}$ for Ceria NPs interacting with polymers, Figure 2-1 clearly shows that the contribution of $A_{v \neq 0}$ is much higher than $A_{v=0}$ and dominates the behavior of A_{Total} . It clearly shows that the dispersive contribution is much higher than the zero-frequency term and dominates then the total Hamaker constant. It is also to be noted that the Hamaker constant is a monotonous growing function of the polymer film refractive index n_p .

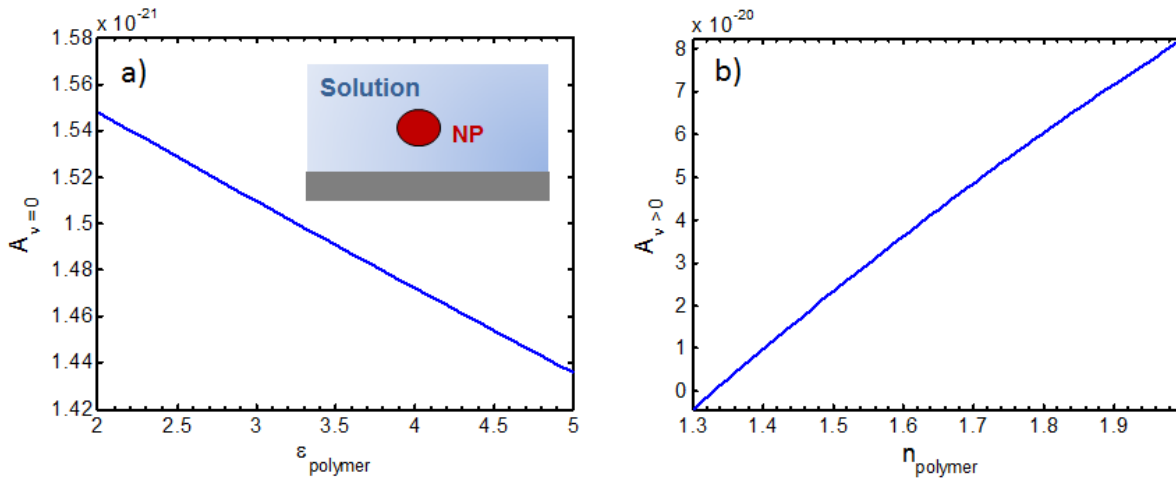


Figure 2-1. a) Zero-frequency (eq. 2-3) and b) dispersive (eq. 2-4) contributions of the Hamaker constant as a function of the dielectric and the refractive index of the polymer surface for a given CeO_2 NP dispersion (with $n_{NP}=1.9$, $\epsilon_{NP}=25$, $n_{sol}=1.33$ and $\epsilon_{sol}=80$).

Thus the bigger n_p , the stronger the van der Waals interactions. Assuming that the interaction between NPs and a polymer is mainly governed by A_{Total} , evidence for a change in the refractive index of the polymer can be monitored by measuring the adsorption of ceria NPs at the surface of the polymer. In the framework of this model, one can indeed expect that Ceria NPs will adsorb more strongly on polymer films having a bigger index of refraction. Conversely the higher the adsorption of NPs, the bigger the index of refraction of the polymer film. This model can thus be validated if one can observe large variation in the amount of adsorbed NPs on polymer films having different index of refraction.

2.3 NP deposition on polymer thin films and data acquisition

Thin films of PS ($M_w = 136$ Kg/mol and polydispersity index (PDI), $M_w/M_n=1.05$) and PMMA ($M_w = 152.8$ Kg/mol and PDI, $M_w/M_n=1.08$) were spin-coated on Si (100) wafers. Their thickness was varied by tuning the concentration of polymer/toluene solutions at a speed of 2000 rpm for 1 min. The silicon wafers were diced into pieces of dimension 1×1 cm² and were immersed in a piranha solution to remove the organic contamination. All the substrates were then rinsed thoroughly by Milli-Q water (resistivity ≈ 18.2 M Ω -cm) and dried with N₂. The native oxide thickness was measured to be around 1.7 nm by ellipsometry. Prior to spin-coating of the PS films, the oxide layer is removed through HF treatment (wafers immersed in 5% HF for 5 mins). After spin-coating, the films are annealed at 160°C during 24h under vacuum. AFM images also revealed that the films were homogeneous and extremely flat with typical roughness (root mean square) of the order of 4Å on a large area (100 μm^2).

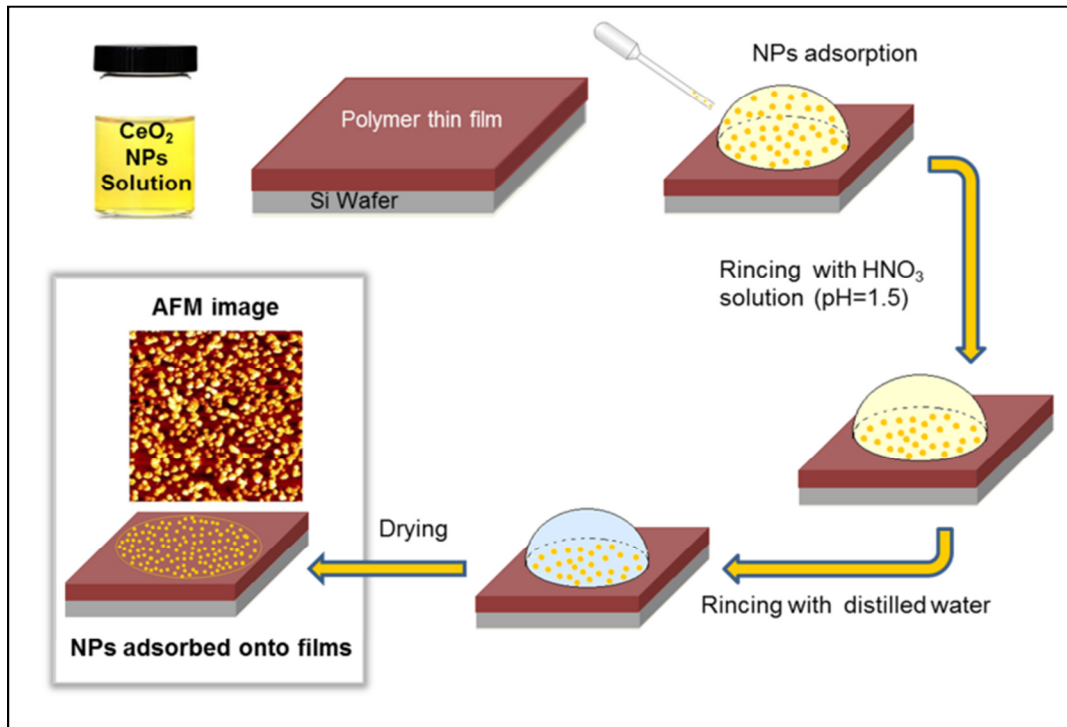


Figure 2-2. Schematic illustration of the ceria NPs adsorption process. The key parameters are the adsorption time, the refractive index of the polymer thin film and the NP dispersion, which allows tuning the surface coverage on samples of any shape and size.

Cerium oxide / ceria NP [32], [33] dispersions (10%/w, pH 1.5) were kindly supplied by the Rhodia-Solvay chemical company (Belgium). The size distribution of the NPs was found to be log-normal with median diameter 8.3 nm and a polydispersity 0.26 as measured from dynamic light scattering. The CeO₂ NPs were stabilized at low pH by a combination of long range electrostatic forces and short range hydration interactions. The NPs were then adsorbed from solution onto both types of polymer thin films as shown in Figure 2-2. For PS, a 0.03% /w NP dispersion was dropped over each sample and allowed to adsorb for 30s (a 100 μ L droplet was used for a 1x1 cm² Si wafer). The solution was then removed and the surface was rinsed with pure nitric acid solution at pH~1.5. Finally, the surface was cleaned with distilled water (pH~5.6). The intermediate cleaning step with nitric acid was performed to avoid the precipitation of the NPs that occurs when one directly cleans with water (due do an increase of the pH). For PMMA we used instead a 0.1% /w dispersion and an adsorption time of 20 min (due to a much lower adsorption resulting from a lower PMMA refractive index).

AFM measurements were performed in tapping mode using a Silicon cantilever. Two different samples were measured for each thickness and polymer. At least 3 AFM images were acquired on different zone of the sample (i.e. 2x3 AFM images for one film thickness) in order to have good reproducibility and statistics avoiding image artifacts, which provides the error value. The NP surface coverage was computed from AFM images using Image J software.

2.4 Nanoparticle adsorption as a function of refractive index value of polymers

One of the best ways to validate our model is check the amount of absorbed NPs on polymer films having different index of refraction. Hence experiments were conducted on PMMA, polypropylene (PP) and PS films having a similar thickness of about 200 nm for which the index of refraction n_p was increasing. [34], [35] (Figure 2-3)

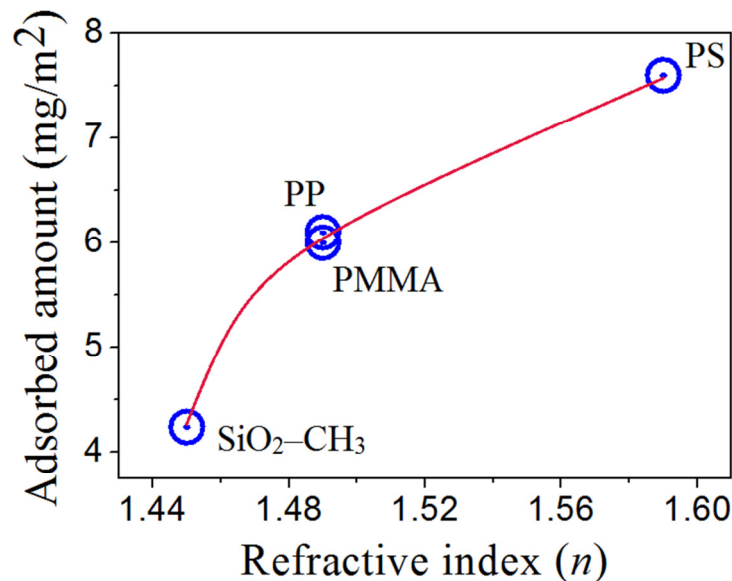


Figure 2-3. Amount of ceria NPs adsorbed onto various hydrophobic (polymer) thin films as a function of the film refractive index.

In addition, a silane hydrophobic silica layer $\text{SiO}_2\text{-CH}_3$ (water contact angle of 115°) made by silanization of the $\text{SiO}_2\text{-Si}$ wafer with the help of ODTs molecules (octadecyltriethoxysilane) was also used.

In this case, (i. e. for thick films of PMMA, PP, PS and SiO₂-CH₃ layer) an adsorption time of 2h with the same concentration was used. As shown in Figure 2-3, the adsorbed amount of NPs was found to change by almost a factor of two for films having an index of refraction, n_p going from 1.45 to 1.59 clearly illustrating the sensitivity of this novel approach. The fact that PP and PMMA films roughly show the same adsorbed amount clearly signs that the van der Waals interaction rather than the surface energy dictates the process since PP and PMMA have different contact angles (102° and 71° respectively). As the refractive index of ceria nanoparticles is large (~1.8-2.0), their adsorption onto a PS surface for example is strong and follows a high affinity adsorption isotherm as shown in Figure 2-4.

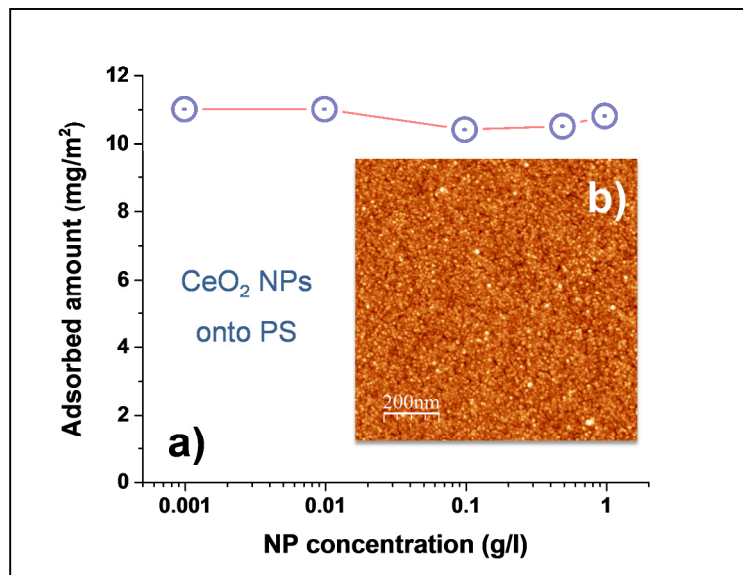


Figure 2-4. a) Adsorption of CeO₂ NP onto polystyrene surface as a function of the NP solution concentration monitored by optical reflectometry during 2 hours. b) AFM topographic image (1x1 μm²) showing the surface of the PS film densely covered with CeO₂ NP.

In Figure 2-4, the irreversible strong adsorption of the NPs onto the PS surface give rise to a high affinity isotherm as anticipated from the high refractive indexes of both the PS film and the CeO₂ NP. Here the pH of the dispersion is 1.5 with 0.1M of NaNO₃ (κ^{-1} ~1 nm) to minimize the mutual NP repulsion and to increase the surface coverage

2.5 Density and NP adsorption of PS thin films

Figure 2-5 shows the evolution of refractive index (n) with respect to the film thickness of PS coated on HF treated Si wafer (PS/H-Si) obtained from spectroscopic ellipsometry measurements at a wavelength of 605 nm.

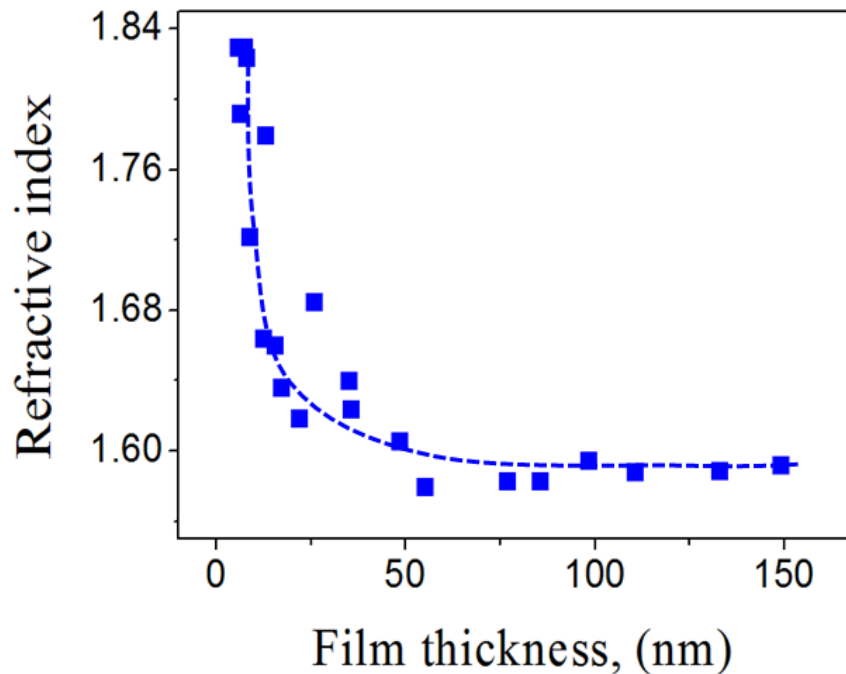


Figure 2-5: Refractive index of PS/H-Si as a function of the film thickness calculated at 605 nm by ellipsometry. [14](dotted line is the guide for eyes)

The Sellmeier model is used to find out the wavelength and thickness dependency of n . It can be observed that the refractive index decrease with the increasing thickness of PS thin films. For the thicker films, the n converge towards the value of 1.589 and is accordance with the previously reported value of bulk polystyrene at the same wavelength. [36] The refractive index of PS films obtained from the effective Hamaker of the system [37] and the one obtained with multiple angle spectroscopic ellipsometry [7] also reported such a trend of increasing refractive index with the decreasing film thickness. An estimation of the amount of ceria NPs adsorbed onto PS/H-Si films at different film thickness (h) was obtained from AFM topographic images as shown in Figure 2-6.

Considering three images for instance for easiness (a, c and f), One can clearly observe that the 6.7 nm thick film (a) is densely covered by the ceria NPs whereas the coverage on the 143.6 nm thick PS film (f) is comparatively very low; the 18.8 nm film falling in between (c). These AFM images, along with the evolution of percentage area of adsorbed NPs with respect to the PS film thickness (Figure 2-7) clearly shows that the percentage area of adsorbed nanoparticles decreases with increasing PS film thickness.

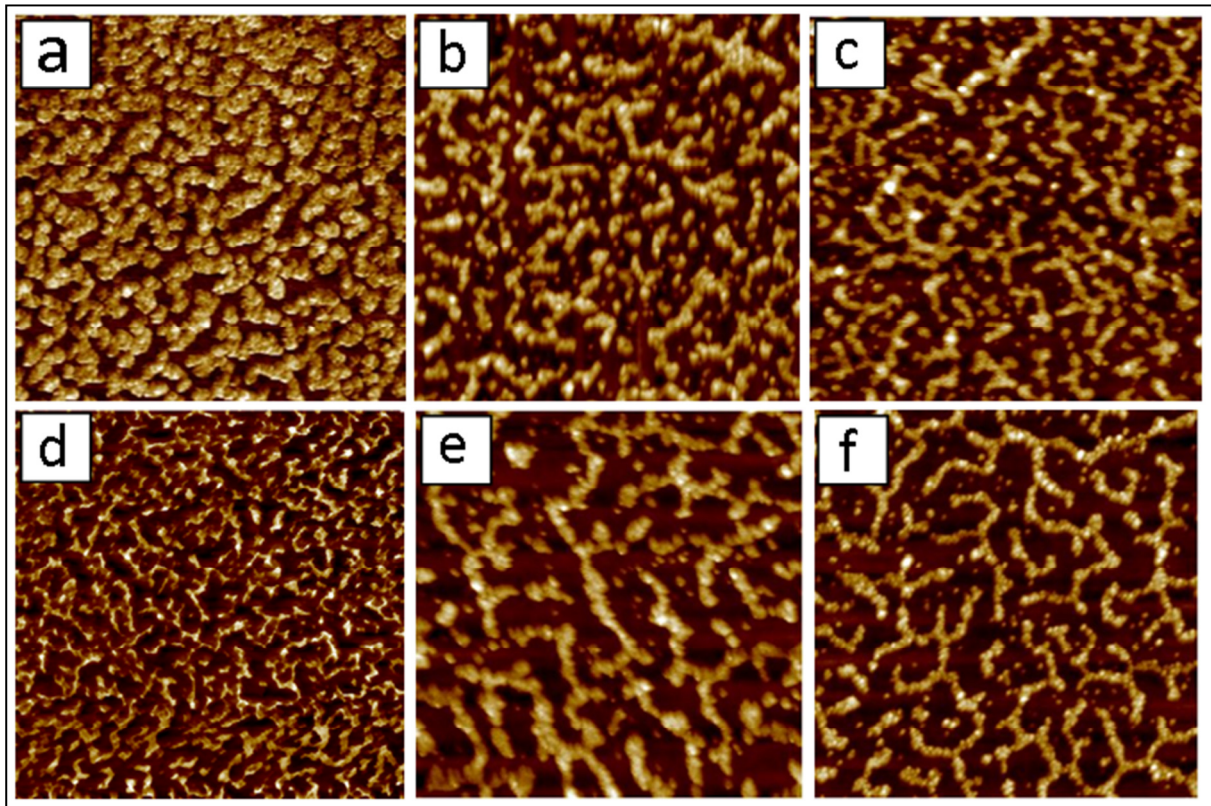


Figure 2-6: AFM topographic images showing the adsorbed ceria nanoparticles to the PS/H- Si surface of PS film thickness, h : (a) 6.7 nm, (b) 13.99 nm, (c) 18.84 nm, (d) 36 nm, (e) 75.26 nm, (f) 143.55 nm. (Scan size $1 \times 1 \mu\text{m}^2$)

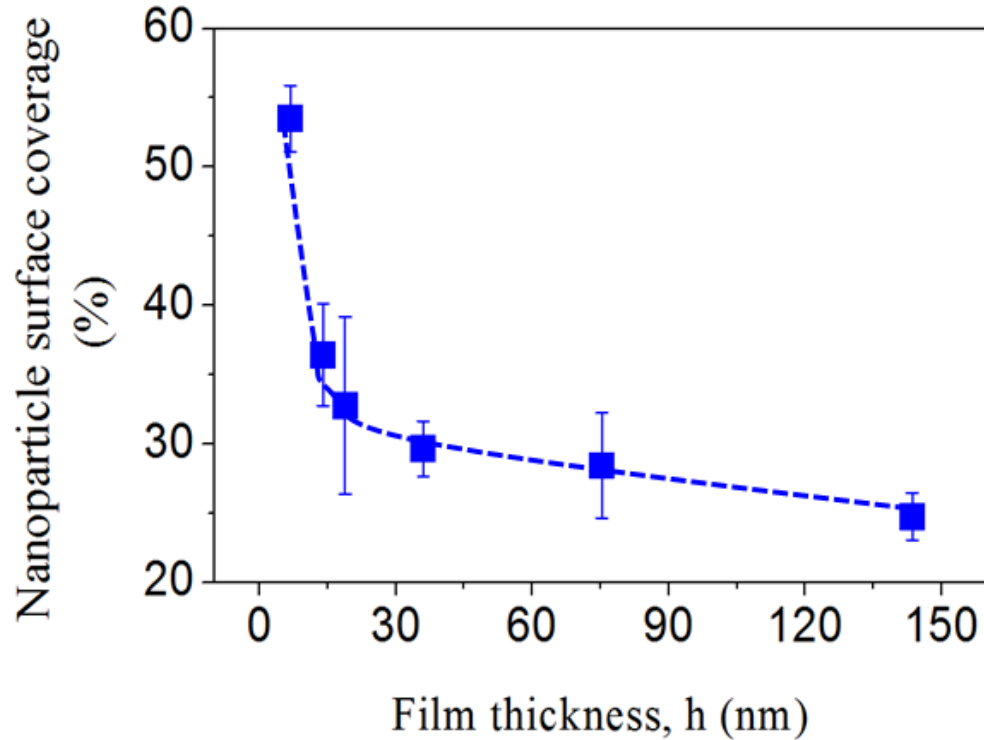


Figure 2-7: NP coverage (in percentage %) as a function of PS film thickness h computed from AFM images

Comparing this evolution of percentage area of adsorbed nanoparticles to the evolution of refractive index with thickness (Figure 2-5) one can observe that both follow the same trend. In other words, the increase percentage area of adsorbed nanoparticles directly indicates an increase in the refractive index (thus in density) of the film. Among the various factors which influence the density, the chain conformations of polymer molecules parallel to the solid surface accommodated at the solid-polymer interfaces, supports the densification of PS films with decreasing film thickness. [38], [39] In addition, the nature of the interactions between PS film and the hydrophobic Si-H terminated surface [40], [41], the time of annealing of the samples above its T_g [26] etc. can also generate a densification.

2.6 Density and NP adsorption of PMMA thin films

Following the observations of PS thin films, it is interesting to check how the percentage adsorption of the nanoparticle can sense the refractive index for PMMA on silicon wafer (SiO_x-Si) with an oxide layer of 1.7 nm. Figure 2-8 shows the adsorption percentage of ceria nanoparticles on PMMA/SiO_x-Si at various thicknesses. Contrary to what observed with the PS/H-Si, an increased adsorption of nanoparticle with increasing film thickness can be observed through the AFM images.

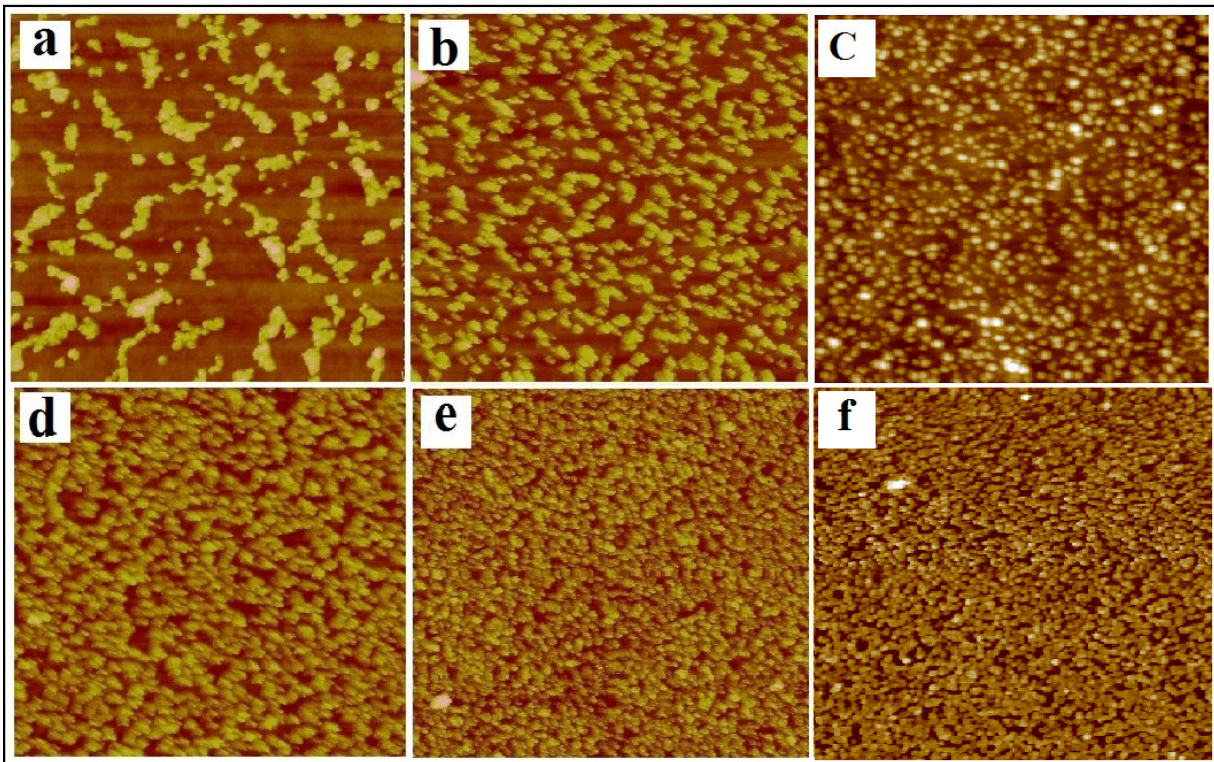


Figure 2-8: AFM topographic images showing the adsorbed ceria nanoparticles to the PMMA/SiO_x-Si surface of PMMA film thickness, h : (a) 6.66 nm, (b) 12.43 nm, (c) 32.1 nm, (d) 41.1 nm, (e) 66.74 nm, (f) 95.11 nm. (Scan size 1*1 μm^2)

The trend can be clearly observed with the percentage area of adsorbed nanoparticles as a function of PMMA film thickness as given in the Figure 2-9. Hence from Figure 2-9, one should expect a decrease in the refractive index of the PMMA films with decreasing film thickness. This is exactly the case, as observed by the ellipsometric measurements as shown in Figure 2-10.

Refractive index is measured to be 1.5 at a thickness of 95.1 nm which comparable to the bulk value 1.49 of the PMMA. [36] So from Figure 2-8 and Figure 2-9, the decrease in the refractive index of PMMA/ SiO_x-Si is detected by the decreased NP adsorption corresponding to the decreasing film thickness.

A study of PMMA thin films by neutron reflectivity also reported similar decreased density when the films become thinner. [42] To explain the difference in density between PS and PMMA, a key parameter could be the nature of the interactions between the polymer and SiO_x layer. Unlike PS chains that do not form hydrogen bond with the hydrophobic H-Si substrate, PMMA chains are bonded to the substrate by acid-base interactions involving the carbonyl and the hydroxyl -OH. For a given chain of atactic PMMA, the number of carbonyl in capacity to form hydrogen bonds is limited [43] and reduces the number of conformations that a chain can have. These conformational restrictions may lead to situations where larger segments of the chains can no longer arrange themselves in the same dense way as in the bulk.

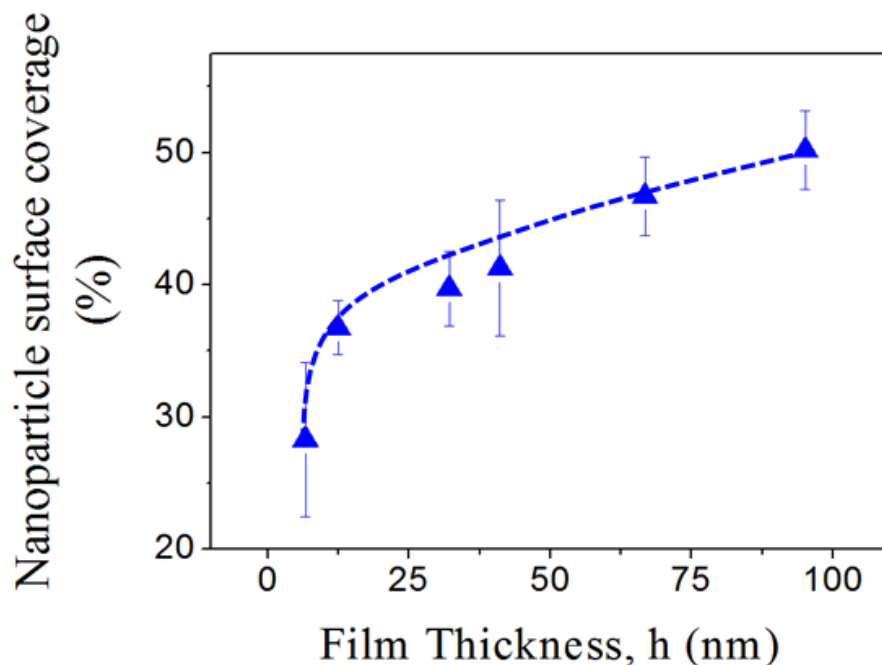


Figure 2-9: NP surface coverage (in percentage %) as a function of PMMA film thickness

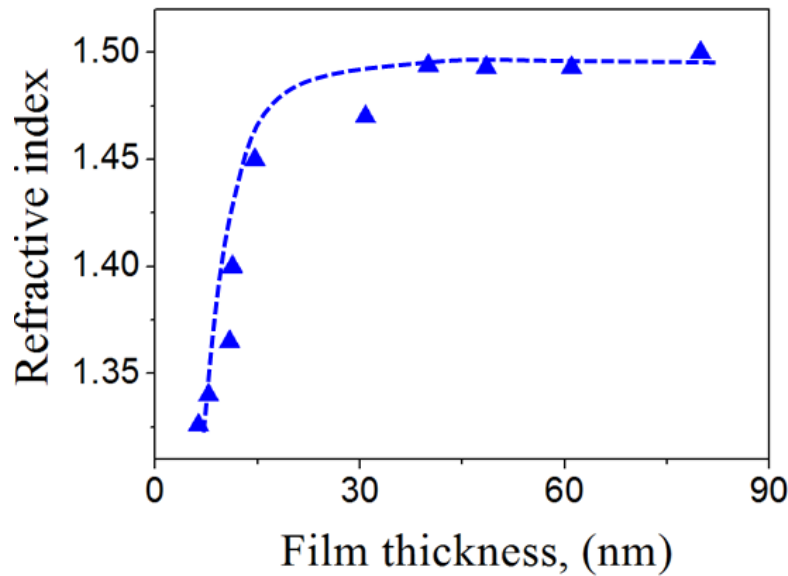


Figure 2-10: Refractive index of PMMA-SiO_x-Si as a function of the PMMA film thickness.

2.7 Influence of substrate on NP adsorption

All our studies are employed with films of thickness ranging few nanometers (4-100 nm). A lot of studies have reported that there is a significance influence of the substrate on various properties of thin films. [44]–[47] Hence a natural question that can arise is whether there is any influence of the substrate on the percentage adsorption of nanoparticles. In a study on the effect of long range interactions on glass transition temperature of thin polystyrene films, Zhang *et. al.* [48] portrays the influence of oxide layer thickness on the long range effective interfacial potential, $\phi(d)_{vdW}$ as shown in Figure 2-11. This study shows that the relationship between the PS thickness and the long-range interactions is strongly dependent on the thickness of the oxide layer. The substrate effects are clearly observed when the thickness of the film falls below 10 nm. In order to check the same, experiments were done on 30 nm films with various silicon oxide thicknesses. For the films around 30 nm, there was no observable variation the percentage of the adsorbed NPs as given in the Table 2-1. It was not possible to carry out the experiments with low thickness PS samples, as the films are found to be dewetted on substrate with oxide layer.

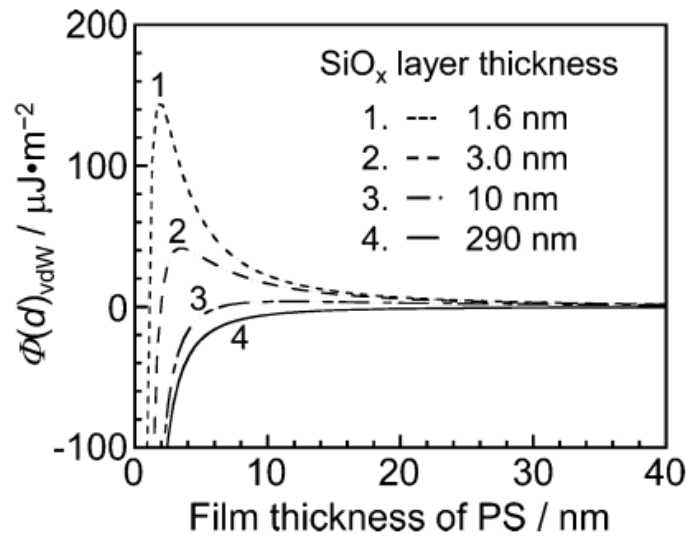


Figure 2-11. PS film thickness vs. long-range effective interfacial potential as a function of the SiO_x layer thickness[48]

Table 2-1. Nanoparticle coverage obtained on ~30 nm PS films with various oxide thicknesses.

| | NP surface Coverage (%) | Error (%) | Refractive index at 610 nm |
|---------------------------------------|----------------------------|-----------|-------------------------------|
| (a) Substrate without oxide | 29.64 | 2.6 | 1.59 |
| (b) Substrate with 1.7 nm oxide layer | 29.24 | 1.59 | 1.58 |
| (c) Substrate with 424 nm oxide layer | 30.41 | 1.6 | 1.57 |

As it is not possible to obtain the details on the influence of substrate nature with very thin films of PS, we tried the substrate influence test on PMMA samples. The experiments are done on PMMA films at two thickness regions, (1) around 30 nm and case (2) around 4nm. Figure 2-12 shows the ceria nanoparticles adsorbed on films of PMMA film ~30 nm on Si wafer a) without oxide layer on the substrate b) Oxide thickness of 1.7 nm on the substrate c) oxide thickness of 424 nm on the substrate. The measured amount of NPs adsorbed onto the film is given in the Table 2-2.

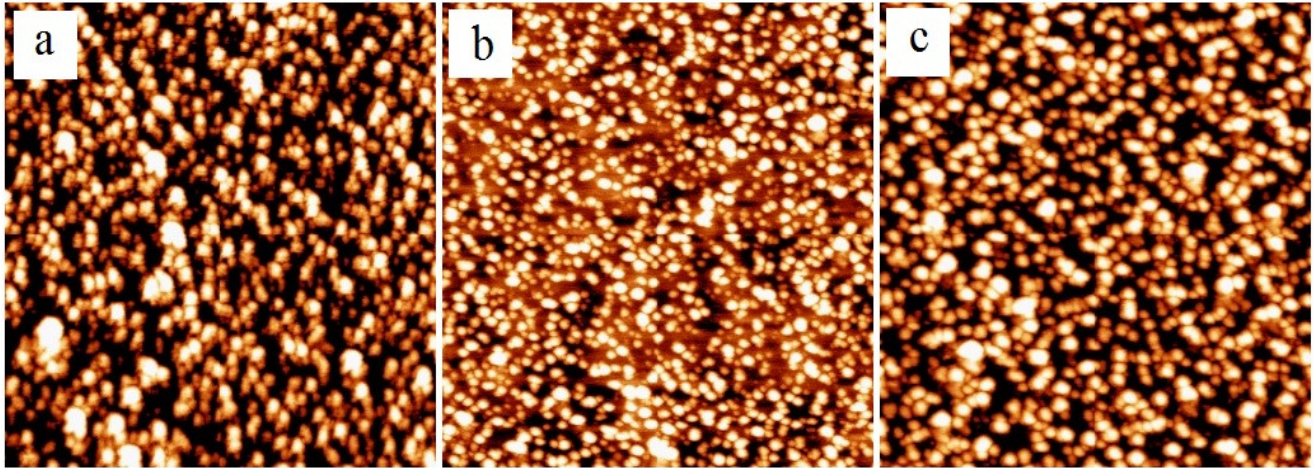


Figure 2-12: AFM topographic images showing the adsorbed ceria nanoparticles on films of PMMA film ~ 30 nm on Si wafer a) without oxide layer on the substrate b) Oxide thickness of 1.7 nm on the substrate c) oxide thickness of 424 nm on the substrate. Scan area of $1 \times 1 \mu\text{m}$.

| | NP surface Coverage (%) | Error (%) | Refractive index at 610 nm |
|---------------------------------------|-------------------------|-----------|----------------------------|
| (a) Substrate without oxide | 40.885 | 1.185 | 1.481 |
| (b) Substrate with 1.7 nm oxide layer | 39.73 | 2.83 | 1.480 |
| (c) Substrate with 424 nm oxide layer | 43.56 | 3.92 | 1.493 |

Table 2-2. Nanoparticle coverage obtained on ~ 30 nm PMMA films with various oxide thicknesses.

It can be observed that the NP surface coverage possess a close value for all the films of thickness ~ 30 nm, irrespective of their oxide thickness. Considering the NP surface coverage of PMMA films with thickness of around 4 nm, it was tested on the H terminated Si wafer and Si with a 424 nm oxide layer. Figure 2-13 shows the ceria nanoparticles adsorbed on films of PMMA film whose values are tabulated in Table 2-3.

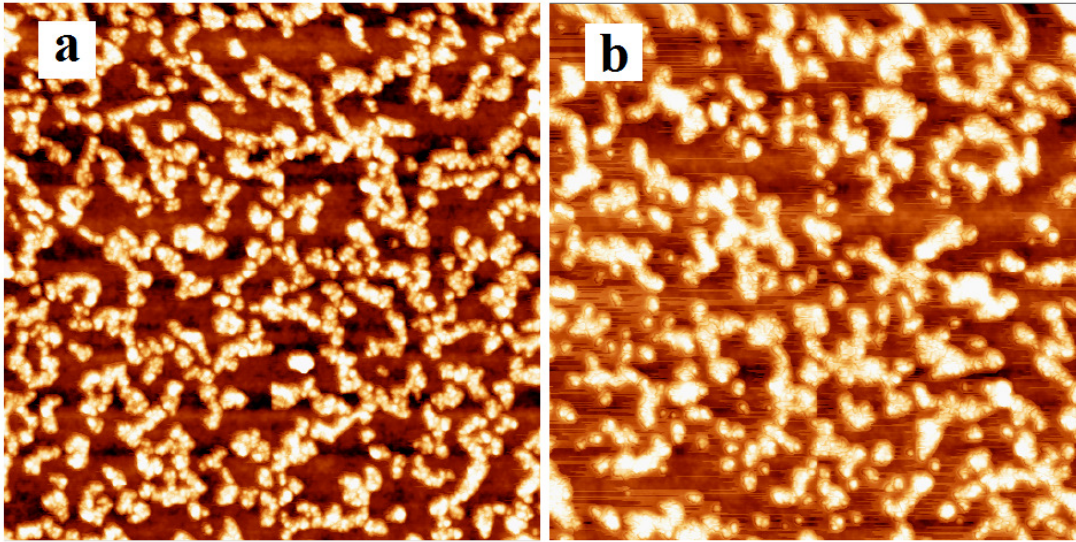


Figure 2-13: AFM topographic images showing the adsorbed ceria nanoparticles on films of PMMA film ~4 nm on Si wafer a) without oxide layer on the substrate b) oxide thickness of 424 nm on the substrate. Scan area of 1*1 μm .

Table 2-3. Nanoparticle coverage obtained on ~4 nm PMMA films with various oxide thicknesses.

| | NP surface Coverage (%) | Error (%) |
|---------------------------------------|----------------------------|-----------|
| (a) Substrate without oxide | 35.16 | 1.56 |
| (c) Substrate with 424 nm oxide layer | 35.97 | 1.44 |

Unlike expected, it was not possible to observe a significant variation in the surface coverage of NPs at lower thickness on different substrates. Hence following the approach of Zhang et al. we simulated the of interfacial potential vs. film thickness of PMMA films as a function of the SiO_x layer thickness as shown in Figure 2-14. Which is drawn from the Lifshitz-van der Waals theory. The effective interfacial potential, $\Delta F_{LW}(h)$ of a 3-layered system like Si/SiO_x/PMMA can be written as,

$$\Delta F_{LW}(h) = \left(\frac{-A_{Si/Polymer/Air}}{12\pi(h+d_{SiO_x})^2} \right) + \left(\frac{-A_{SiO_x/Polymer/Air}}{12\pi h^2} \right) - \left(\frac{-A_{SiO_x/Polymer/Air}}{12\pi(h+d_{SiO_x})^2} \right) \quad 2-5$$

where $A_{Si/Polymer/Air}$ and $A_{SiO_x/Polymer/Air}$ are the effective Hamaker constants of the Si/Polymer/Air and SiOx/Polymer/Air 3 layer systems, respectively. This is calculated using the relation;

$$A_{Substrate/Polymer/Air} = A_{Polymer/Polymer} - \sqrt{A_{Polymer/Polymer} \times A_{Substrate/Substrate}} \quad 2-6$$

The average values of Hamaker constant obtained from the literature are used for the calculations, where $A_{Si/Si} = 22.3 \times 10^{-20} \text{ J}$, $A_{SiO_2/SiO_2} = 5.8 \times 10^{-20} \text{ J}$, $A_{PMMA/PMMA} = 7.11 \times 10^{-20} \text{ J}$ respectively. [6], [31], [49]–[52] From the evolution of interfacial potential with respect to the oxide layer thickness, we can expect a difference in the percentage adsorption of the nanoparticles only when the film thickness is less than 1 nm. Hence the similar NP adsorption percentage observed on PMMA films (even around 4nm) with substrates of varying oxide thickness can be justified.

Thus considering the influence of substrate on the NP adsorption, for PS, no significant influence was observed for the film thickness around 30 nm whereas we were unable to probe the effect below 10 nm due to film dewetting. In case of PMMA, the nanoparticle adsorption is found to be independent of the substrate nature even for films of thickness around 4 nm.

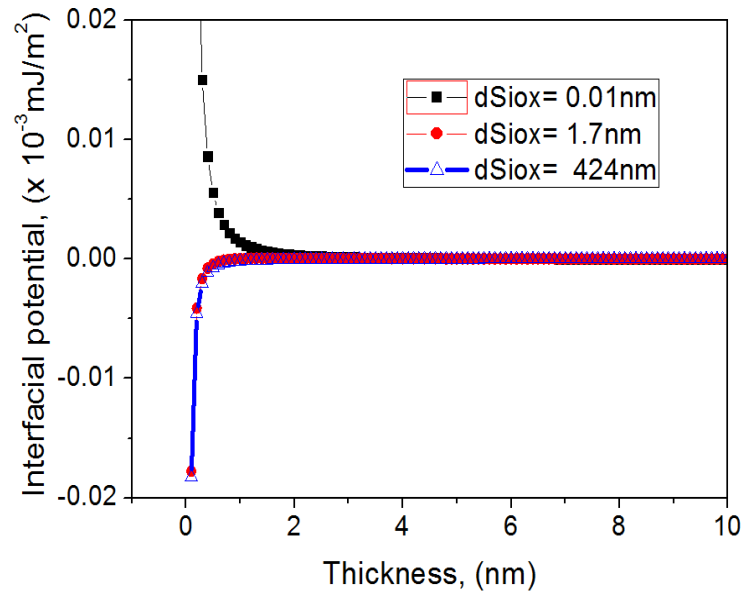


Figure 2-14: Interfacial potential vs. film thickness of PMMA films as function of SiOx layer thickness.

2.8 Correlation of density with thin film thermal behavior

Even if the thermal behavior of the system is not within the scope of this chapter, as we observed the opposing trends for the density evolution of PS and PMMA with film thickness, it is interesting to have a short mention to the related thermal behavior which can lead to future investigations. Considering PS, the ellipsometric studies together with X ray reflectivity showed that the free volume of a thin film is smaller than the one of a thick film below the glass transition temperature; it reaches a characteristic value v^* at a lower temperature which is near the glass transition temperature as schematically shown in Figure 2-15. As the density of the films scales as the free volume, thinner films are found to be denser than thicker ones. Thus for PS, when film thickness is reduced, T_g decreases, [53] coefficient of thermal expansion (CTE) [53]–[56] and density increase [7], [14].

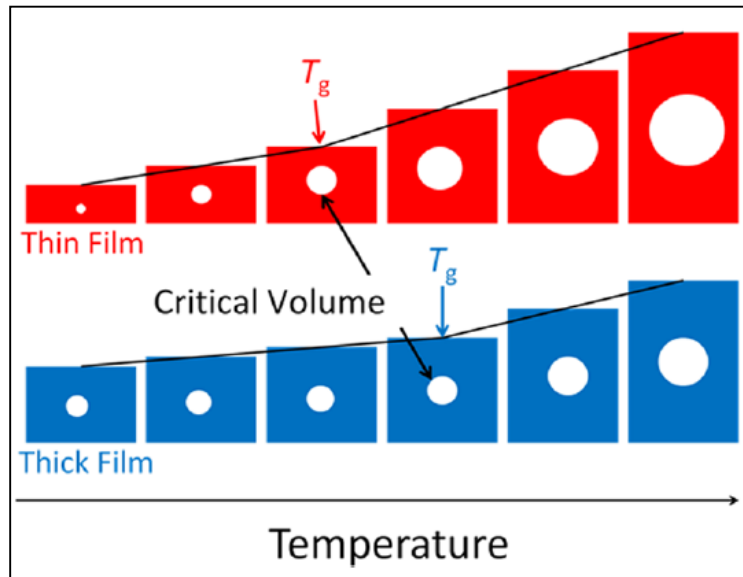


Figure 2-15: Schematic representation showing that the critical volume is reached at a lower temperature for the thinner film.[14]

This is just the opposite for PMMA thin films whose glass transition temperature increase [45], [57], [58] along with the coefficient of thermal expansion [59] and film density [42]. Although counterintuitive, a reduction of T_g for PS (increase for PMMA) when density is higher than the bulk (lower for PMMA) can be justified by an increase in CTE (decrease for PMMA) with decreasing film thickness. Based on our previous work, [14] a reduction in thermal expansion with decreasing film thickness indicates that the increase in free volume with temperature is less rapid in the thinner films of PMMA. The thermal behavior of the two studied polymers extracted from the literature and compiled in Table 2-4.

Thus the thinner films reaches its critical volume v^* (which is the minimum space needed to allow molecules rearrangement) later compared to the thick films, which is exactly the contrary for the PS films. This behavior can be illustrated as shown in Figure 2-16.

Table 2-4. Shows the increase (\uparrow) or decrease (\downarrow) of Glass transition temperature (T_g), Coefficient of thermal expansion (CTE) and the density (ρ) with decrease in film thickness of PS and PMMA.

| $h \downarrow$ | T_g | CTE | ρ |
|----------------|--------------|--------------|--------------|
| PS | \downarrow | \uparrow | \uparrow |
| PMMA | \uparrow | \downarrow | \downarrow |

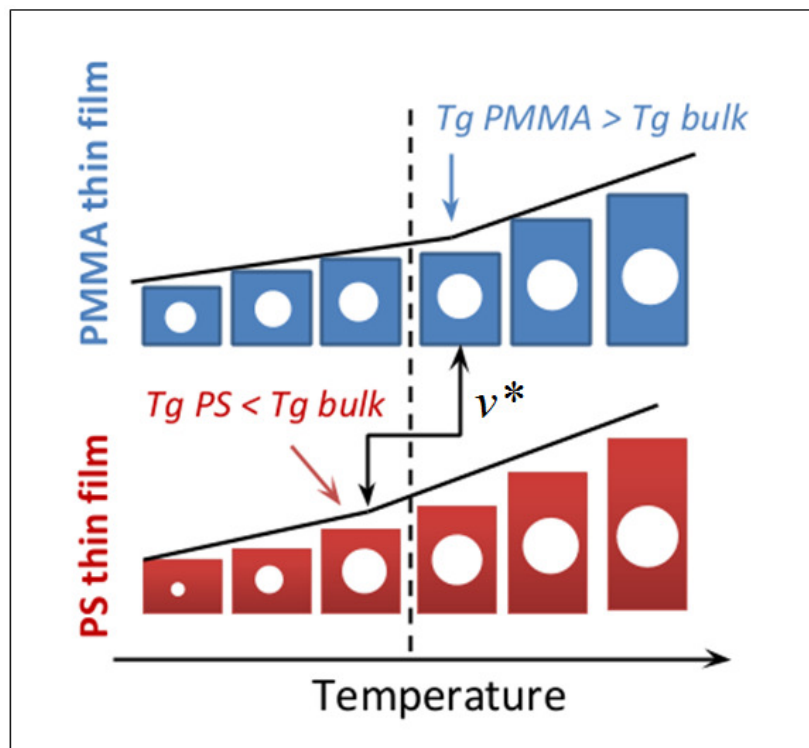


Figure 2-16: The schematic representation of the free volume that evolves with temperature, for PMMA and PS films. v^* stands for the critical volume.

2.9 Conclusion

A novel and simple approach is put forward to assess/detect the refractive index/density variations in polymer thin films through the adsorption of ceria NPs onto the polymer film surface. The NP adsorbed amount being a monotonic function of the polymer surface refractive index, any increase/decrease in the NP surface coverage can be directly ascribed to an increase/decrease in the thin film refractive index and density. Furthermore, using this approach we found that the density of PS thin films on high energy oxide-free Si wafer increases with a reduction of the film thickness whereas the investigation performed on PMMA films spin-casted on low energy SiO_x-Si wafers shows a reverse trend: a decrease of the density with the film thickness. A better understanding on how confinement and interfaces perturb T_g in polymer thin films clearly substantiate any further works on the coefficient of thermal expansion (*CTE*) - dependent density in particular because *CTE* provides the evolution of the free volume/density as a function of the temperature. [14]

REFERENCES

- [1] H. Bodiguel and C. Fretigny, “Reduced viscosity in thin polymer films,” *Phys. Rev. Lett.*, vol. 97, no. 26, pp. 266105, 1–4, 2006.
- [2] F. Chen, D. Peng, C.-H. Lam, and O. K. C. Tsui, “Viscosity and Surface-Promoted Slippage of Thin Polymer Films Supported by a Solid Substrate,” *Macromolecules*, vol. 48, no. 14, pp. 5034–5039, Jul. 2015.
- [3] D. Cangialosi, V. M. Boucher, A. Alegria, and J. Colmenero, “Direct Evidence of Two Equilibration Mechanisms in Glassy Polymers,” *Phys. Rev. Lett.*, vol. 111, no. 9, p. 95701, 2013.
- [4] D. Cangialosi, V. M. Boucher, A. Alegria, and J. Colmenero, “Physical aging in polymers and polymer nanocomposites: recent results and open questions,” *Soft Matter*, vol. 9, no. 36, pp. 8619–8630, 2013.
- [5] R. Xie, A. Karim, J. Douglas, C. Han, and R. Weiss, “Spinodal Dewetting of Thin Polymer Films,” *Phys. Rev. Lett.*, vol. 81, no. 6, pp. 1251–1254, 1998.
- [6] A. Sharma and G. Reiter, “Instability of Thin Polymer Films on Coated Substrates: Rupture, Dewetting, and Drop Formation,” *J. Colloid Interface Sci.*, vol. 178, no. 2, pp. 383–399, 1996.
- [7] S. Ata, K. Kuboyama, K. Ito, Y. Kobayashi, and T. Ougizawa, “Anisotropy and densification of polymer ultrathin films as seen by multi-angle ellipsometry and X-ray reflectometry,” *Polymer.*, vol. 53, no. 4, pp. 1028–1033, 2012.
- [8] K. F. Mansfield and D. N. Theodorou, “Molecular dynamics simulation of a glassy polymer surface,” *Macromolecules*, vol. 24, no. 23, pp. 6283–6294, Nov. 1991.

- [9] O. K. C. Tsui, T. P. Russell, and C. J. Hawker, “Effect of Interfacial Interactions on the Glass Transition of Polymer Thin Films,” *Macromolecules*, vol. 34, no. 16, pp. 5535–5539, Jul. 2001.
- [10] A. Sharma, J. Mittal, and R. Verma, “Instability and Dewetting of Thin Films Induced by Density Variations,” *Langmuir*, vol. 18, no. 26, pp. 10213–10220, Dec. 2002.
- [11] V. M. Boucher, D. Cangialosi, A. Alegría, and J. Colmenero, “Accounting for the thickness dependence of the T_g in supported PS films via the volume holes diffusion model,” *Thermochim. Acta*, vol. 575, pp. 233–237, Jan. 2014.
- [12] S. Herminghaus, K. Jacobs, and R. Seemann, “The glass transition of thin polymer films: some questions, and a possible answer,” *Eur. Phys. J. E*, vol. 5, pp. 531–538, Aug. 2001.
- [13] D. Long and F. Lequeux, “Heterogeneous dynamics at the glass transition in van der Waals liquids, in the bulk and in thin films,” *Eur. Phys. J. E*, vol. 4, no. 3, pp. 371–387, 2001.
- [14] G. Vignaud, M. S. Chebil, J. K. Bal, N. Delorme, T. Beuvier, Y. Grohens, and A. Gibaud, “Densification and Depression in Glass Transition Temperature in Polystyrene Thin Films,” *Langmuir*, vol. 30, no. 39, pp. 11599–11608, 2014.
- [15] M. H. Cohen and D. Turnbull, “Molecular Transport in Liquids and Glasses,” *J. Chem. Phys.*, vol. 31, no. 5, pp. 1164–1169, 1959.
- [16] D. Turnbull and M. H. Cohen, “Free-Volume Model of the Amorphous Phase: Glass Transition,” *J. Chem. Phys.*, vol. 34, no. 1, pp. 120–125, 1961.
- [17] S. Napolitano, C. Rotella, and M. Wübbenhorst, “Can Thickness and Interfacial Interactions Univocally Determine the Behavior of Polymers Confined at the Nanoscale?,” *ACS Macro Lett.*, vol. 1, no. 10, pp. 1189–1193, Oct. 2012.

- [18] S. Napolitano, A. Pilleri, P. Rolla, and M. Wübbenhorst, “Unusual Deviations from Bulk Behavior in Ultrathin Films of Poly(tert-butylstyrene): Can Dead Layers Induce a Reduction of Tg?,” *ACS Nano*, vol. 4, no. 2, pp. 841–848, Feb. 2010.
- [19] S. Napolitano and D. Cangialosi, “Interfacial Free Volume and Vitrification: Reduction in Tg,” *Macromolecules*, vol. 46, pp. 8051–8053, 2013.
- [20] S. Napolitano, S. Capponi, and B. Vanroy, “Glassy dynamics of soft matter under 1D confinement: How irreversible adsorption affects molecular packing, mobility gradients and orientational polarization in thin films,” *Eur. Phys. J. E*, vol. 36, no. 6, p. 61, 2013.
- [21] P. Gin, N. Jiang, C. Liang, T. Taniguchi, B. Akgun, S. K. Satija, M. K. Endoh, and T. Koga, “Revealed Architectures of Adsorbed Polymer Chains at Solid-Polymer Melt Interfaces,” *Phys. Rev. Lett.*, vol. 109, no. 26, p. 265501, Dec. 2012.
- [22] W. E. Wallace, N. C. B. Tan, W. L. Wu, and S. Satija, “Mass density of polystyrene thin films measured by twin neutron reflectivity,” *J. Chem. Phys.*, vol. 108, no. 9, pp. 3798–3804, 1998.
- [23] G. Reiter, “Mobility of polymers in films thinner than their unperturbed size,” *Europhys. Lett.*, vol. 23, no. 8, p. 579, 1993.
- [24] R. N. Li, A. Clough, Z. Yang, and O. K. C. Tsui, “Equilibration of Polymer Films Cast from Solutions with Different Solvent Qualities,” *Macromolecules*, vol. 45, no. 2, pp. 1085–1089, Jan. 2012.
- [25] D. S. Fryer, R. D. Peters, E. J. Kim, J. E. Tomaszewski, J. J. de Pablo, P. F. Nealey, C. C. White, and W. Wu, “Dependence of the Glass Transition Temperature of Polymer Films on Interfacial Energy and Thickness,” *Macromolecules*, vol. 34, no. 16, pp. 5627–5634, Jul. 2001.
- [26] S. Napolitano and M. Wübbenhorst, “The lifetime of the deviations from bulk behaviour in polymers confined at the nanoscale,” *Nat. Commun.*, vol. 2, p. 260, Mar. 2011.

- [27] A. Gibaud and G. Vignaud, “Specular Reflectivity from Smooth and Rough Surfaces,” in *X-ray and Neutron Reflectivity: Principles and Applications*, Springer, 2009, pp. 85–131.
- [28] B. Bataillou, H. Moriceau, and F. Rieutord, “Direct inversion of interfacial reflectivity data using the Patterson function,” *J. Appl. Crystallogr.*, vol. 36, no. 6, pp. 1352–1355, 2003.
- [29] H. G. Tompkins and E. A. Irene, *Handbook of Ellipsometry*, vol. 30, no. 7. William Andrew, 2005.
- [30] T. Yamamoto, H. Momida, T. Hamada, T. Uda, and T. Ohno, “First-principles study of dielectric properties of cerium oxide,” *Thin Solid Films*, vol. 486, no. 1–2, pp. 136–140, Aug. 2005.
- [31] J. N. Israelachvili, *Intermolecular and surface forces*. Academic Press London, 1991.
- [32] L. Qi, A. Sehgal, J. C. Castaing, J. P. Chapel, J. Fresnais, J. F. Berret, and F. Cousin, “Redispersible hybrid nanopowders: Cerium oxide nanoparticle complexes with phosphonated-PEG oligomers,” *ACS Nano*, vol. 2, no. 5, pp. 879–888, 2008.
- [33] L. Qi, J. Fresnais, P. Muller, O. Theodoly, J.-F. Berret, and J.-P. Chapel, “Interfacial Activity of Phosphonated-Polyethylene Glycol Functionalized Cerium Oxide Nanoparticles.,” *Langmuir*, 2012.
- [34] J. P. Chapel and M. Morvan, “Modified surfaces and method for modifying a surface,” WO2007126925 A2, 2007.
- [35] S. Sekar, J. Giermanska, and J.-P. Chapel, “Reusable and recyclable quartz crystal microbalance sensors,” *Sensors Actuators B Chem.*, vol. 212, pp. 196–199, Jun. 2015.
- [36] S. N. Kasarova, N. G. Sultanova, C. D. Ivanov, and I. D. Nikolov, “Analysis of the dispersion of optical plastic materials,” *Opt. Mater. (Amst.)*, vol. 11, no. 29, pp. 1481–1490, 2007.

- [37] Y. Li, J. Q. Pham, K. P. Johnston, and P. F. Green, “Contact Angle of Water on Polystyrene Thin Films : Effects of CO₂ Environment and Film Thickness,” *Langmuir*, vol. 23, pp. 9785–9793, 2007.
- [38] D. Hudzinsky, A. V. Lyulin, A. R. C. Baljon, N. K. Balabaev, and M. A. J. Michels, “Effects of strong confinement on the glass-transition temperature in simulated atactic polystyrene films,” *Macromolecules*, vol. 44, no. 7, pp. 2299–2310, Apr. 2011.
- [39] R. L. Jones, S. K. Kumar, D. L. Ho, R. M. Briber, and T. P. Russell, “Chain conformation in ultrathin polymer films,” *Nature*, vol. 400, pp. 146–149, 1999.
- [40] Y. Fujii, Z. Yang, J. Leach, H. Atarashi, K. Tanaka, and O. K. C. Tsui, “Affinity of Polystyrene Films to Hydrogen-Passivated Silicon and Its Relevance to the T_g of the Films,” *Macromolecules*, vol. 42, no. 19, pp. 7418–7422, Oct. 2009.
- [41] P. T. Wilson, L. J. Richter, W. E. Wallace, K. A. Briggman, and J. C. Stephenson, “Correlation of molecular orientation with adhesion at polystyrene/solid interfaces,” *Chem. Phys. Lett.*, vol. 363, no. 1–2, pp. 161–168, 2002.
- [42] W. Wu, W. J. Orts, J. H. Van Zanten, and B. M. Fanconi, “Density profile of spin cast polymethylmethacrylate thin films,” *J. Polym. Sci. Part B Polym. Phys.*, vol. 32, no. 15, pp. 2475–2480, 1994.
- [43] Y. Grohens, M. Brogly, C. Labbe, M.-O. David, and J. Schultz, “Glass Transition of Stereoregular Poly(methyl methacrylate) at Interfaces,” *Langmuir*, vol. 14, no. 11, pp. 2929–2932, May 1998.
- [44] D. Qi, Z. Fakhraai, and J. A. Forrest, “Substrate and chain size dependence of near surface dynamics of glassy polymers,” *Phys. Rev. Lett.*, vol. 101, no. 9, pp. 1–4, 2008.
- [45] R. P. White, C. C. Price, and J. E. G. Lipson, “Effect of Interfaces on the Glass Transition of Supported and Freestanding Polymer Thin Films,” *Macromolecules*, vol. 48, no. 12, pp. 4132–4141, Jun. 2015.

- [46] X. Zheng, M. H. Rafailovich, J. Sokolov, Y. Strzhemechny, S. A. Schwarz, B. B. Sauer, and M. Rubinstein, “Long-Range Effects on Polymer Diffusion Induced by a Bounding Interface,” *Phys. Rev. Lett.*, vol. 79, no. 2, pp. 241–244, 1997.
- [47] R. D. Priestley, C. J. Ellison, L. J. Broadbelt, and J. M. Torkelson, “Structural relaxation of polymer glasses at surfaces, interfaces, and in between.,” *Science*, vol. 309, no. 5733, pp. 456–9, Jul. 2005.
- [48] C. Zhang, Y. Fujii, and K. Tanaka, “Effect of Long Range Interactions on the Glass Transition Temperature of Thin Polystyrene Films,” *ACS Macro Lett.*, vol. 1, pp. 1317–1320, 2012.
- [49] T. Kerle, R. Yerushalmi-Rozen, J. Klein, and L. J. Fetters, “van der Waals stable thin liquid films : Correlated undulations and ultimate dewetting,” *Eur. Lett.*, vol. 44, no. 4, pp. 484–490, 1998.
- [50] L. Bergström, “Hamaker constants of inorganic materials,” *Adv. Colloid Interface Sci.*, vol. 70, pp. 125–169, 1997.
- [51] H. D. Ackler, R. H. French, and Y.-M. Chiang, “Comparisons of Hamaker constants for ceramic systems with intervening vacuum or water: From force laws and physical properties,” *J. Colloid Interface Sci.*, vol. 179, pp. 460–469, 1996.
- [52] H. Zhao, Y. J. Wang, and O. K. C. Tsui, “Dewetting induced by complete versus nonretarded van der Waals forces.,” *Langmuir*, vol. 21, no. 13, pp. 5817–24, Jun. 2005.
- [53] J. L. I. Keddie, R. A. L. Jones, and R. A. Cory, “Size-Dependent Depression of the Glass Transition Temperature in Polymer Films .,” *Europhys. Lett.*, vol. 27, no. July, pp. 59–64, 1994.
- [54] J. E. Pye and C. B. Roth, “Above, below, and in-between the two glass transitions of ultrathin free-standing polystyrene films: Thermal expansion coefficient and physical aging,” *J. Polym. Sci. Part B Polym. Phys.*, vol. 53, no. 1, pp. 64–75, Jan. 2015.

- [55] S. Kawana and R. A. L. Jones, “Character of the glass transition in thin supported polymer films,” *Phys. Rev. E*, vol. 63, no. 2, p. 21501, 2001.
- [56] L. Singh, P. J. Ludovice, and C. L. Henderson, “Influence of molecular weight and film thickness on the glass transition temperature and coefficient of thermal expansion of supported ultrathin polymer films,” *Thin Solid Films*, vol. 449, no. 1–2, pp. 231–241, Feb. 2004.
- [57] J. L. Keddie, R. A. L. Jones, and R. A. Cory, “Interface and surface effects on the glass-transition temperature in thin polymer films,” *Faraday Discuss.*, vol. 98, pp. 219–230, 1994.
- [58] T. Lan and J. M. Torkelson, “Methacrylate-based polymer films useful in lithographic applications exhibit different glass transition temperature-confinement effects at high and low molecular weight,” *Polymer.*, vol. 55, no. 5, pp. 1249–1258, Mar. 2014.
- [59] W. Wu, J. H. van Zanten, and W. J. Orts, “Film Thickness Dependent Thermal Expansion in Ultrathin Poly(methyl methacrylate) Films on Silicon,” *Macromolecules*, vol. 28, no. 3, pp. 771–774, Jan. 1995.

Chapter 3. Stable ultrathin polymer films (<7nm) made by solvent rinsing

Parts of this chapter are extracted from:

“Stability of Polymer Ultrathin Films (<7 nm) Made by a Top-Down Approach”

Adapted with permission from,

Bal, J. K.; Beuvier, T.; Unni, A. B.; Chavez Panduro, E. A.; Vignaud, G.; Delorme, N.; Chebil, M. S.; Grohens, Y.; Gibaud, A. *ACS Nano* **2015**, *9*, 8184–8193

Copyright © (2015) American Chemical Society

Summary

Succeeding the discussion about density variations observed when polymer thin films are confined by their thickness in chapter1, this chapter deals with stability issues observed when the thickness of polymer films are reduced. Polystyrene films on Si wafer with different surface treatment are employed for the study, with an aim to investigate the causes of instability in polymer thin films and to find a route to obtain ultrathin stable polymer films. The bulk PS films are rinsed with a good solvent toluene to obtain the polymer residual layer, whose thickness is in the order of few nanometers. Its stability is experimentally analyzed and further understanding of the results is achieved with the help of Lifshitz van der Waals intermolecular theory.

3.1 Introduction

The stability of thin polymer films is of paramount importance for a variety of applications such as sensors, [1] coating, [2] adhesives, [3] biomedical devices, [4] organic solar cells, [5], [6] thin-film transistors (OTFTs) [7] etc. Despite a notably growing literature, it is not yet clear why polymer thin films often exhibit strong deviations from bulk behavior. For example, under certain conditions thin films show undesirable rupture although they are expected to be energetically stable. [8] Key issues in interpreting these results are originating from sample preparation. The induction of residual stress during spin-coating due to out of equilibrium chain conformations that arise from rapid solvent loss has been frequently considered as the main source of instabilities. [9] It has been shown recently that the reduction of mechanical stresses can be achieved by severe thermal annealing for durations exceeding by far the reptation time. [10] However when the film thickness becomes very small (typically of the order of a few R_g), numerous experiments show that annealing above the glass transition temperature (T_g) reveals their instability through the formation of holes. It is therefore of fundamental interest to address how one can predict the stability of a thin film and more importantly to propose a strategy for the stabilization of ultrathin films.

Considering the concept of stability, when there is fluid on a substrate, the fluid will not form a stable film on the substrate if the substrate has a lower surface tension than a fluid. Consequently such an unstable fluid film will retract from this substrate by a dewetting process, [11]–[14] which is characterized by the formation of holes, their growth, and coalescence, finally leading to a set of droplets on the substrate. [15] The distinction among the stable, metastable and the unstable states can be understood with the help of the effective interfacial potential, $\Delta F(h)$ and its second derivative, $\Delta F''(h_0)$. $\Delta F(h)$ is defined as the excess free energy per unit area necessary to bring two interfaces (the substrate-polymer and the polymer-solvent interfaces) from infinity to a certain distance h . The distance h defines the thickness of the polymer layer separating the two interfaces. From its definition and as shown in Figure 3-1, it is clear that as $\Delta F(h) \rightarrow 0$ as h tends to infinity. [16]

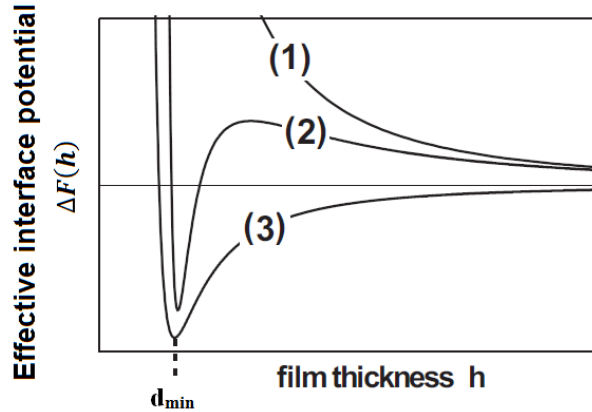


Figure 3-1: Sketch of the effective interface potential as a function of film thickness for stable (1), unstable (2), and metastable (3) films.

The film is said to be stable when $\Delta F(h) > 0$ and the global minimum lies at infinite thickness (curve 1). Considering the curve 2, the film is unstable for small film thickness $\Delta F''(h_0) < 0$, (h_0 is the initial film thickness) whereas the film is metastable for larger film thicknesses $\Delta F''(h_0) > 0$. In the metastable case, the system has to overcome a potential barrier in order to reach its state of lowest energy at $h = d_{\min}$. Some kind of nuclei, e.g. dust particles or defects, are required to lower $\Delta F(h)$ and can therefore induce rupture of the film by a mechanism called “heterogeneous nucleation”. [17] The system is unstable when the second derivative of ΔF w.r.t. the film thickness is negative (curve 3). In this case, the capillary waves on the film surface are spontaneously amplified under thermal annealing and the rupture mechanism is termed “spinodal dewetting”. [18], [19] The spinodal wavelength λ is the key to clearly identify a spinodal dewetting process in experimental systems which is related to the second derivative of interfacial potential as follows: [12], [16]

$$\lambda(h) = \sqrt{\frac{-8\pi^2 \sigma_{lv}}{F''(h)}} \quad 3-1$$

Where σ_{lv} is the surface tension between the film and surrounding media. Considering the interfacial potential, Lifshitz van der Waals intermolecular potential provides a convincing starting point to calculate free energy per unit area of a film $\Delta F(h)$ of thickness h on a flat surface as follows: [11], [20]

$$\Delta F^{VDW}(h) = \frac{-A_{Substrate / Film / Air}}{12\pi h^2} \quad 3-2$$

Here, $A_{Substrate/Film/Air}$ is the effective Hamaker constant of the three-layered component system (Substrate/Film/Air) which takes into account the substrate/film and the film/air interfaces. This expression doesn't consider the residual stress and the density variations inside the films. The effective Hamaker constant can be expressed by the following mixing rule: [11], [20]–[22]

$$A_{Substrate / Film / Air} = A_{Film / Film} - \sqrt{A_{Film / Film} \times A_{Substrate / Substrate}} \quad 3-3$$

with A_{ij} the Hamaker constants of materials i and j interacting across a vacuum. In the case of polystyrene (PS) film deposited on silicon (Si) wafer, it is found from the literature that the Hamaker constant of PS, $A_{PS/PS}$, is varying between 6.1 and 7.9×10^{-20} J [20], [23], [24] while the one of Si, $A_{Si/Si}$, is much higher (between 19 and 25.6×10^{-20} J [20]–[22], [25] compared to the one of silica $A_{SiO_2/SiO_2} = 5.0$ to -6.6×10^{-20} J [20], [26]–[28]). Considering these values it turns out that the Hamaker constant for flat interfaces of the system Si/PS/Air is negative *i.e.* $A_{Si/PS/Air} = -4.4$ to -6.0×10^{-20} J (using equation 3-3). The sign of Hamaker constant can also play a crucial for determining the stability of a thin film. [29] When $A_{Sub/PS/Air} < 0$, the film is stable while if $A_{Sub/PS/Air} > 0$, the film is unstable. Thus if a PS film is attempted to be deposited on oxide-free Si then the negative value of A should impose a stable film. Yet this is not the case and films usually dewet through hole nucleation. Apart from heterogeneous nucleation process has been already discussed, The films are found to be unstable (1) by the possible presence of a silica layer ($A_{SiO_2/SiO_2} = 5.0$ to -6.6×10^{-20} J [2], [8], [10]) at the substrate-polymer interface inducing a rupture called thermal nucleation or homogeneous nucleation, or (2) by the spatial density variations due to film confinement leading to variations in the Hamaker constants, [30] or (3) by the release of stress coming from the spin-coating preparation. Among these various causes of film instability, it is really difficult to choose the correct one because most of the times films encounter instability or metastability as soon as they are spin-coated.

The underlying question that still remains open is the following: Is it necessary to revise the theoretical approach or is it possible to preclude any of the responsible causes for the dewetting? Recently, Xue and Han [31] discussed various methods for inhibiting or slowing down the

dewetting of polymer films. However, these approaches involve a change in the composition of the film (new end-groups, cross-linking agents or additives) and are more over difficult to set up for ultrathin films. In this context, we have explored a new strategy to inhibit the dewetting of ultrathin films without modifying the composition of the films. Inspired by the works of Koga, [32], [33] Fujii [34] and Napolitano [10] who reported that thick polymer films can be thinned down after a good solvent rinsing, in this chapter we are investigating the stability/instability behavior of PS films with thicknesses ranging from ≈ 1.3 nm to 7.0 nm made on Si substrates with and without a native oxide layer following the top-down approach (i.e. construction of a bulk film proceeded by good solvent rinsing). The experimentally obtained results which are then compared with the Lifshitz van der Waals intermolecular theory could provide better understanding of the results.

3.2 Ultrathin polymer films

3.2.1 Formation of ultrathin film (< 7 nm) by direct spin-coating

The general trends observed when a thin film of PS is deposited by spin-coating a diluted solution ($c < 1$ g/L, where c stands for the concentration of PS in the toluene solution) on Si surfaces are briefly reported in this section. Figure 3-2 shows AFM topographies immediately after depositing PS films by spin-coating dilute solutions at 2000 rpm.

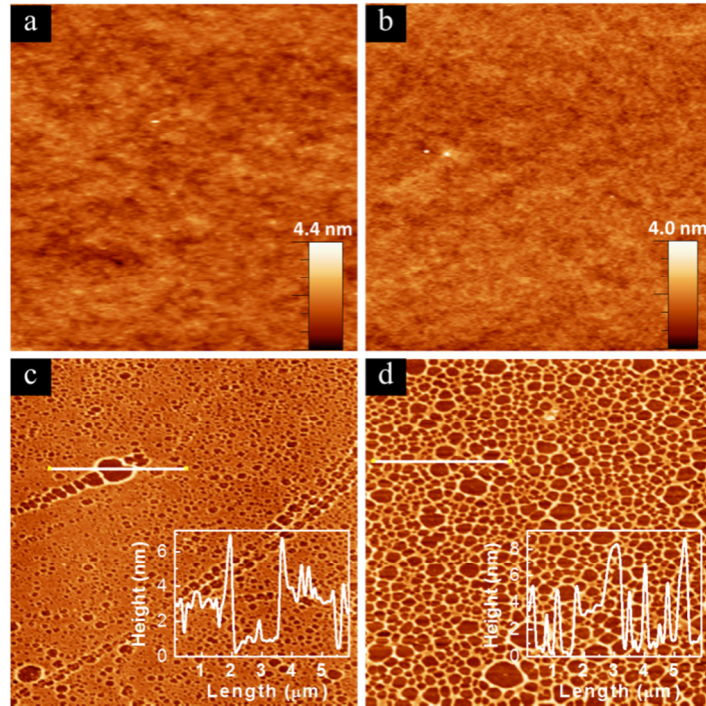


Figure 3-2: AFM images of PS films spin-coated at 2000 rpm on (a) SiO_x-Si and (b) H-Si surfaces from a 1.5 g/L solution (scan size = 5×5 μm²) and on (c) SiO_x-Si and (d) H-Si surfaces from a 0.75 g/L solution (scan size = 15×15 μm²). The thicknesses of the films determined by XRR are ≈ 6.8 nm, 7.1 nm, 3.2 nm and 4.3 nm for the images (a), (b), (c) and (d), respectively. The insets of figures (c) and (d) correspond to the evolution of the height along the drawn line.

At $c = 1.5$ g/L and for higher concentration films are perfectly smooth on both native oxide Si (labeled as SiO_x-Si) and oxide-free Si (labeled as H-Si) substrates (shown in Figure 3-2, a and b respectively). However, at $c = 0.75$ g/L (*i.e.* 30 times less than the overlap concentration $c^* \sim 21$ g/L), films exhibit dewetting with a large number of randomly distributed holes as shown in Figure 3-2, c and d. The average thickness obtained from AFM (inset of Figure, c and d) and also from XRR is ≈ 3-4 nm (shown in Figure 3-3).

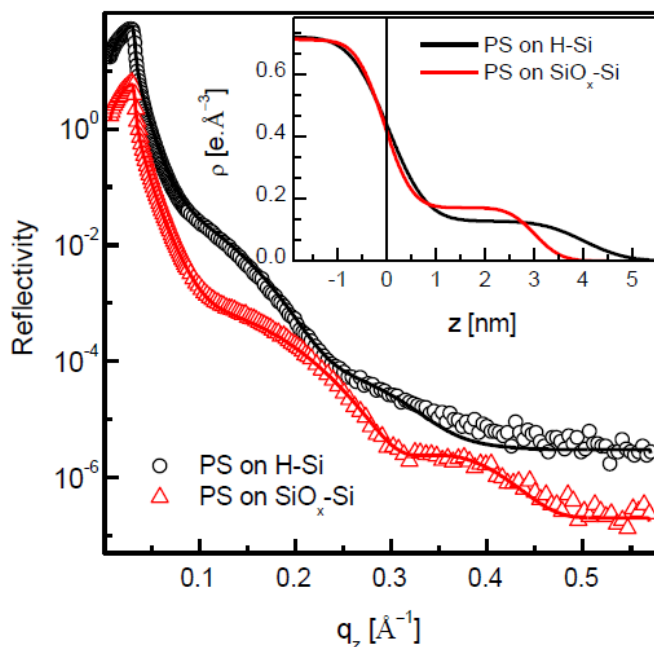


Figure 3-3: XRR and EDP profiles showing dewetting of directly spin-coated ultrathin films. XRR data (different symbols) and analyzed curves (solid line) of as-prepared PS films on H-Si and SiO_x-Si substrates by direct spin-coating of 0.75 g/L solution (curves are shifted vertically for clarity). Insets: corresponding EDPs showing very low coverage of the PS films with respect to the bulk electron density $\approx 0.344 e \cdot \text{\AA}^{-3}$.

The ruptures observed on the films made from diluted solution can not be explained by the van der Waals interaction according to the formalism mentioned in the introduction. It may probably come from residual stress during the fast evaporation of the solvent followed by a relaxation during the early stages of the film or from density heterogeneities. As a consequence, uniform ultrathin films of PS ($M_w = 1.36 \times 10^5$ g/mol) with a thickness less than 7 nm are very difficult to obtain directly by spin-coating. The unexplained dewetting of thinner films on both Si surfaces together with the quest to produce uniform ultrathin films motivated us to adopt a new strategy.

3.2.2 Formation of ultrathin films (≤ 7 nm) by solvent rinsing treatment

Following the same leaching route as the one proposed by Guiselin *et al.* [35] and used by the research groups of Koga, [32], [33] Tsui, [34] and Napolitano, [10] flat films of initial thickness equal or greater than 7 nm were prepared by spin coating both on oxide Si (SiO_x-Si) and oxide-

free Si (H-Si) substrates (shown in Figure 3-2, a and b). They were then sequentially immersed in toluene for 10 min and dried by mild flow of N₂ at ambient temperature and pressure. XRR data and the corresponding analyzed curves of pre- and post-rinsing (up to 70 min of rinsing) for a PS film on SiO_x-Si are shown in Figure 3-4, a. The Kiessig fringes for the 10 min rinsed film (blue curve) are well visible up to $q_z = 0.45 \text{ \AA}^{-1}$ highlighting a smooth surface (presumably no dewetting) and a film thickness close to 2.9 nm.

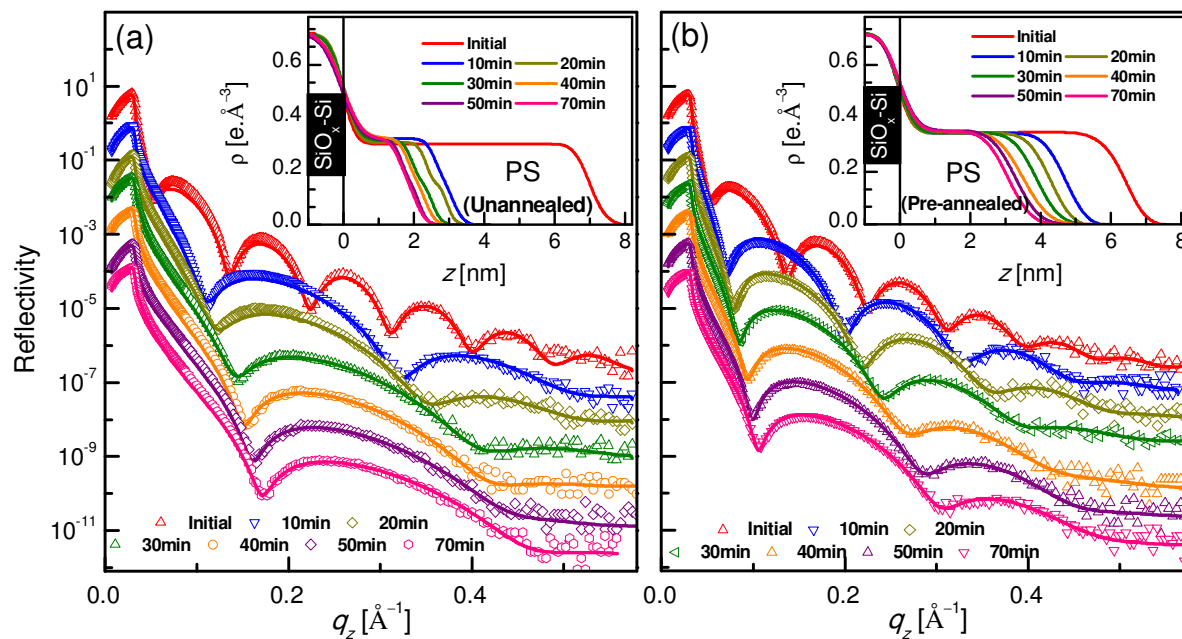


Figure 3-4: Structural evolution as a result of solvent rinsing. XRR data (different symbols) and analyzed curves (solid line) of unannealed (a) and pre-annealed (b) 7 nm PS films on SiO_x-Si substrates before and after toluene rinsing during different durations (curves are shifted vertically for clarity). Insets: corresponding EDPs showing different thicknesses of the PS films with different toluene rinsing time.

According to the study of Koga's group, [32], [33] we can assume that during this first rinsing, the loosely attached layer was partly removed. This rinsing process was repeated several times on the same sample as shown in Figure 3-4, (a) As expected from work of Gin *et al.*, [32] we observed that after the second rinsing the thickness decreased slowly. This decrement progressively increased upon further rinsing and the film thickness reached about 1.7 nm after 70 min (*i.e.* after 7 rinsings). We attribute this progressive decay of the film thickness to the desorption of the residual loosely attached layer.

In contradiction with the work of Fujii *et al.* [34] in which no residual film was found after just 30 min of toluene rinsing, the existence of a non-zero residual film even after “prolonged” toluene rinsing can be observed in Figure 3-5 or when starting with a higher initial thickness $h_0 \approx 130$ nm, Figure 3-6 is a clear signature that an adsorbed layer near the substrate/PS interface already forms in the early times of spin-coating even though no annealing treatment has been performed.

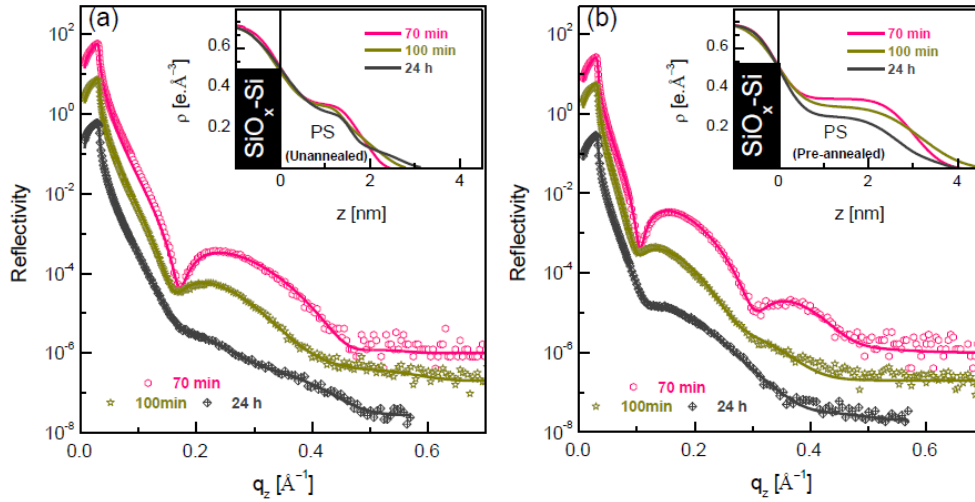


Figure 3-5: Solvent rinsing of a thick ($h_0 \approx 130$ nm) PS film. XRR data (different symbols) and analyzed curves (solid line) of a thick PS film on a $\text{SiO}_x\text{-Si}$ substrates before and after toluene rinsing during different durations as mentioned in the legend. Insets: corresponding EDPs showing different thicknesses of the PS films with different toluene rinsing times.

These observations match well with the observation of Napolitano *et al.* [10] who have shown a non-zero adsorbed layer ($h_{ads}(t_{an} = 0) \neq 0$) (where t_{an} is the annealing time) without annealing. Johnson and Granick [36] estimated that the net segment-surface interaction energy between PS dissolved in carbon tetrachloride and an oxidized Si substrate is quite weak ($\sim 1.3 kT$ at 25°C , k is the Boltzmann constant and T is the absolute temperature) compare to the one for PMMA ($\sim 4 kT$). This weak interaction combined with the low segment-surface interaction number may explain why PS chains adsorbed at ambient temperature can desorb progressively in toluene with time. When films are annealed at 160°C during 24 h before rinsing, ascribed as pre-annealed films, the decrement of thickness after the first rinsing is smaller as shown in Figure 3-4,(b) The adsorption of PS segments initiated during the spin-coating is thus favored by annealing the samples above T_g .

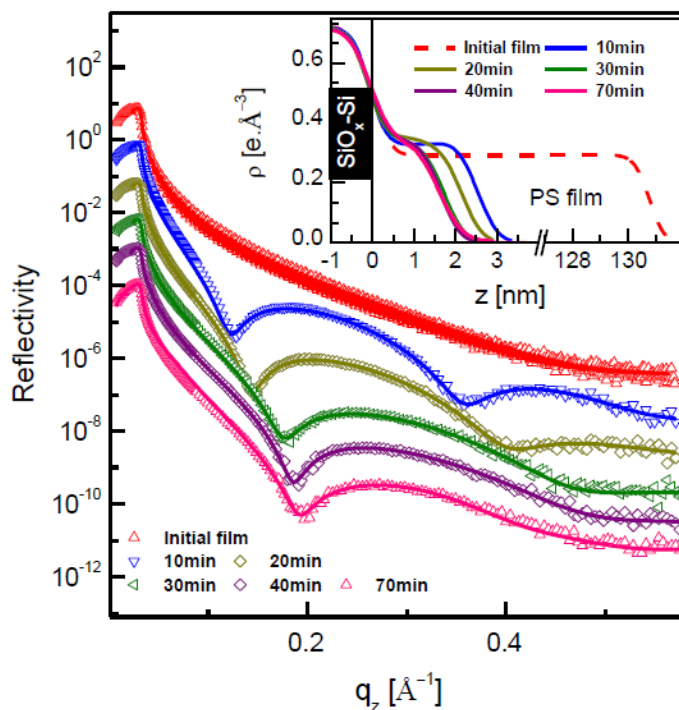


Figure 3-6: Solvent rinsing of a 7 nm preannealed PS film grown on H-Si substrate. XRR data (different symbols) and analyzed curves (solid line) of a preannealed 7 nm PS film on H-Si substrates before and after toluene rinsing during different durations as mentioned in the legend (curves are shifted vertically for clarity). Insets: corresponding EDPs showing different thicknesses of the PS films with different toluene rinsing times.

A similar kind of behavior was also encountered in films grown on H-Si as shown in Figure 3-7. This confirms that annealing increases the thickness of the adsorbed layer probably by enhancing the entanglement between the polymer chains and by increasing the number of segment-surface contacts with the substrate. Corresponding EDPs (shown in the inset of Figure 3-4, a and b) show that the electron density of the film remains nearly constant to about $0.33 \text{ e}/\text{\AA}^3$ (corresponding to a mass density of $1.02 \text{ g}/\text{cm}^3$ close to the one of the bulk $1.06 \text{ g}/\text{cm}^3$ [37], [38]) for the unannealed samples and slightly higher for the pre-annealed films. The higher density for thin and annealed PS films was already reported. [39], [40] On the contrary to the work of Jiang *et al.* [33] and despite trying other density models we were not able to prove that the adsorbed layer was composed of 2 layers with different densities coming from the loosely attached layer and a denser flattened layer. The best fits were obtained by putting a single layer of PS with a constant density.

The rinsing procedure may remove the density variation inside the film or probing the existence of such a layer would need measurements at higher q wave vector transfers with a high statistics. The thinnest good quality residual films were found to be ≈ 1.7 nm thick for unannealed films and ≈ 2.9 nm thick for pre-annealed films after 100 min of toluene rinsing. Yet after 100 min of rinsing, the quality of the film declines with a boost up of the top surface roughness while the film thickness does not change appreciably as can be observed from Figure 3-5. One can thus infer that after 100 min of rinsing, the loosely attached residual layer constituting the adsorbed layer is completely removed after 24 h of immersion. This observation is in agreement with Jiang *et al.*'s report. [33] Hence a rinsing time (t_{rins}) below 100 min was chosen for exploring the stability of such smooth ultrathin residual films presented in the following section of this chapter.

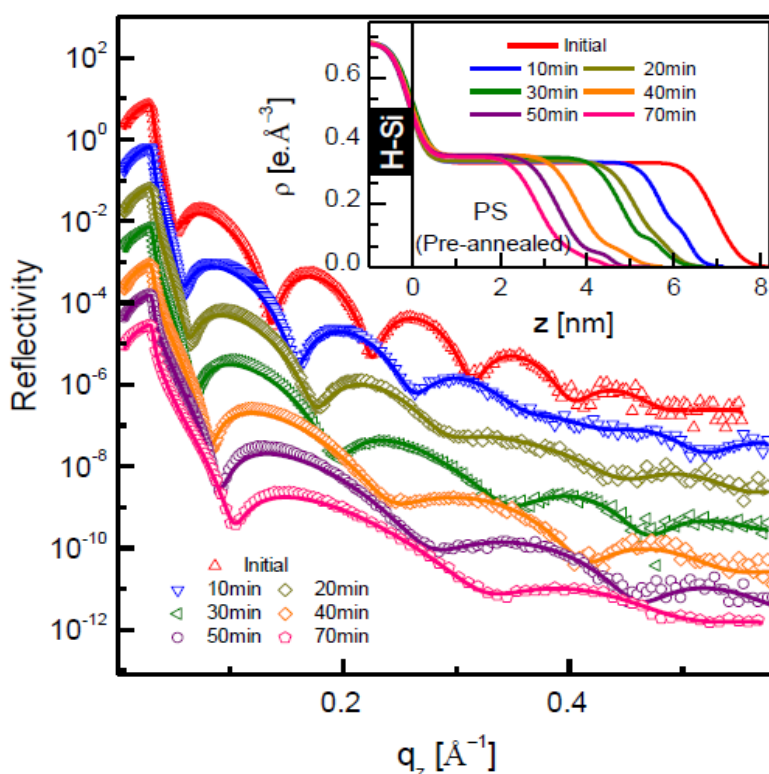


Figure 3-7: Solvent rinsing of a 7 nm preannealed PS film grown on a H-Si substrate. XRR data (different symbols) and analyzed curves (solid line) of a preannealed 7 nm PS film on a H-Si substrates before and after toluene rinsing during different durations as mentioned in the legend (curves are shifted vertically for clarity). Insets: corresponding EDPs showing different thicknesses of the PS films with different toluene rinsing times.

Additionally, we observed that in pre-annealed samples the adsorbed layer thickness obtained after 10 min of toluene rinsing was found to increase almost linearly with the radius of gyration (*e.g.* R_g) of PS as shown in the Figure 3-8. The films deposited on SiOx-Si are pre-annealed at 160 °C during 24 h and have thicknesses of 7 nm (± 0.5 nm). h_{res} is the value obtained after 10 min of toluene rinsing. This time of rinsing is expected to remove the unbound layer and probably only a small part of the adsorbed layer. The dotted line represents the relation published by Fujii *et al.* [34] $h_{res} = 0.47 R_g$ (h_{res} and R_g in nm). Results are quite similar to those of Fujii for native oxide covered Si ($h_{ads} \approx 0.47 \times R_g$) and confirm that the longer the PS chains, the thicker the adsorbed layer as reported also by Housmans *et al.* [41] The radius of gyration is deduced from the relation $R_g = 1.20 \times 10^{-2} M_w^{0.595}$ [42].

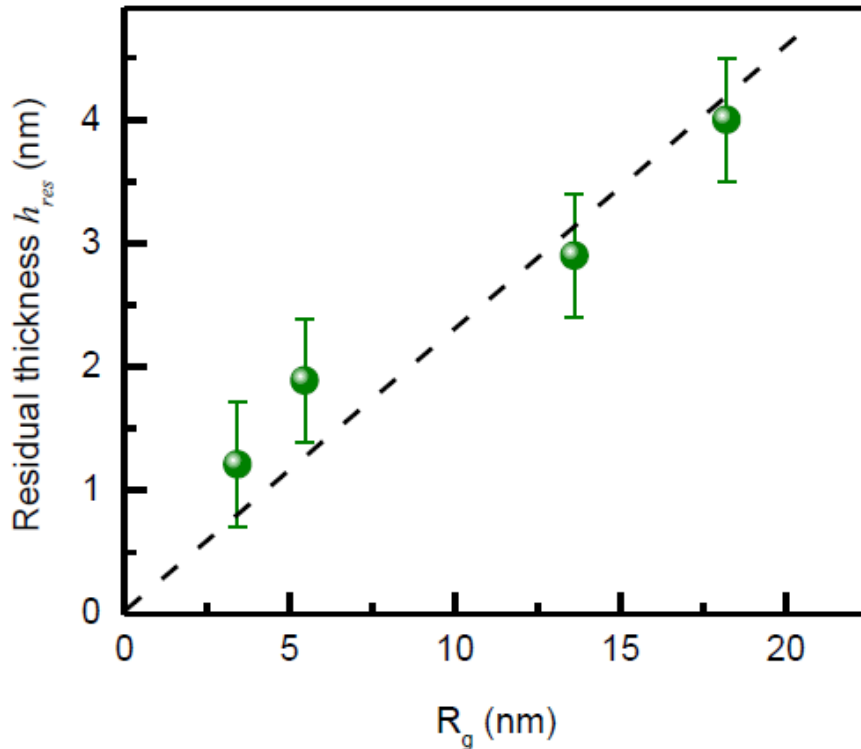


Figure 3-8: Residual layer thickness h_{res} as a function of R_g .

3.3 Correlation between the kinetics of dissolution and annealing

The residual thickness (h_{res}) deduced from the fit to the data and from the EDPs is plotted in Figure 3-9 (a), as a function of the rinsing time t_{rins} .

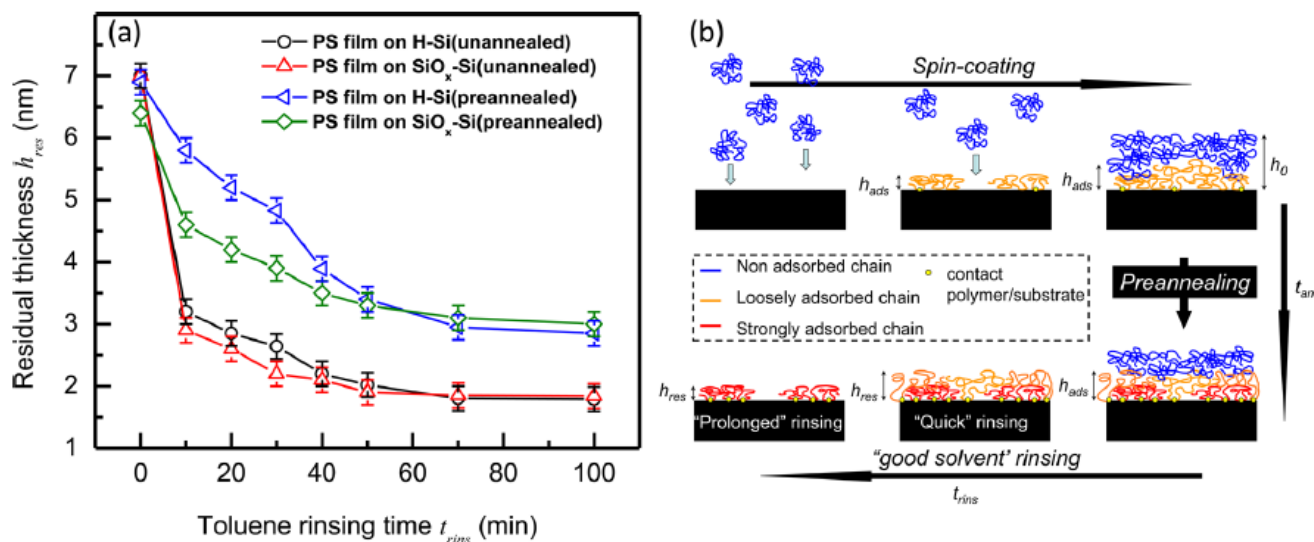


Figure 3-9: Correlation between the kinetics of dissolution and annealing. (a) Residual thickness (h_{res}) of pre-annealed and unannealed PS film of $h_0 \approx 7$ nm grown on SiO_x-Si and H-Si substrates as a function of rinsing time (t_{rins}). (b) Schematic illustration of the formation of an adsorbed layer h_{ads}

From figure 3-9, it is evident that the film thickness can be controlled by tuning the rinsing time t_{rins} . A similar trend was witnessed by Gin *et al.* [32] A careful observation of Figure 3-9,(a) reveals that h_{res} is higher for the H-Si supported pre-annealed PS film than for the SiO_x-Si supported one but only up to 40 min of rinsing. The difference for "quick" rinsed samples is in agreement with the work of Fujii [34]. For longer times, differences only arise when films are pre-annealed or not. The value of h_{res} for pre-annealed films is always greater than for unannealed films. For $h_0 \approx 7$ nm, after 70 min of toluene rinsing h_{res} is found to be ≈ 2.9 nm and ≈ 1.7 nm for pre-annealed and unannealed films, respectively. The formation of an adsorbed layer h_{ads} is illustrated in Figure 3-9, (b) the schematic during the spin-coating (prior to preparing a film of thickness h_0 , shown in top panel) and pre-annealing (right panel) processes of PS film followed by toluene rinsing (bottom panel) that gives rise to a residual layer of thickness h_{res} . Pre-annealing incites the thickening of adsorbed layer h_{ads} and increases the number of polymer-surface interac-

tions or contacts (labeled by small circle at the interface). Hence pre-annealed films exhibit greater residual thickness h_{res} after toluene rinsing. Note that h_{ads} is equivalent to h_{res} . The two quantities only differ in the sense that h_{ads} corresponds to the thickness of the adsorbed layer before rinsing whereas h_{res} corresponds to the one of the adsorbed layer after rinsing known as residual layer. During spin-coating, the adsorption process favors a transition from a chain's random-coil conformation in the solvent to a flat conformation on the substrate surface. It is accomplished by the diffusion of chains towards the interface. Hence empty spaces should be there for incoming chains to attach with the substrate.

For 7 nm thick films prepared from a solution of concentration $c \approx 1.5$ g/L, one can expect flat conformations (as shown in the top panel of Figure 3-9, (b) of adsorbed segments leading to a thin adsorbed layer (h_{ads}) as proposed by Napolitano *et al.* [10] The thickness of this layer is limited by the number of chains that are initially adsorbed at the interface. This layer is linked to the substrate (contact point is labeled by a small circle) and is very difficult to remove by toluene rinsing. It probably determines the residual thickness (h_{res}) of the toluene-rinsed films. Annealing promotes the thickening of this adsorbed layer (shown in the right panel of Figure 3-9, (b) by providing more activation energy to fill more empty spaces at the polymer/Si interface. As a result, the chains reaching the surface in the later stages encounter a more crowded surface and can only attach by a reduced number of segments. Thus a transition from a flat to a more vertical configuration takes place which probably leads to a thicker residual layer (given by h_{res} in Figure 3-9, (a) in pre-annealed films). Surprisingly the electron density of the films remains nearly constant though the thickness is strongly reduced during the rinsing. This implies that the dissolution of polymeric chains is most likely occurring from the top surface leaving the lower part unaffected.

3.4 Morphology and verification of residual layer on substrates surface

AFM images depicting the surface morphology of these residual films after 70 min of toluene are shown in Figure 3-10, a and b. Images show a smooth (RMS roughness < 5 Å) and uniform residual PS film on both type of surfaces, such as on SiO_x-Si (Figure 3-10, a) and H-Si (Figure 3-10, b).

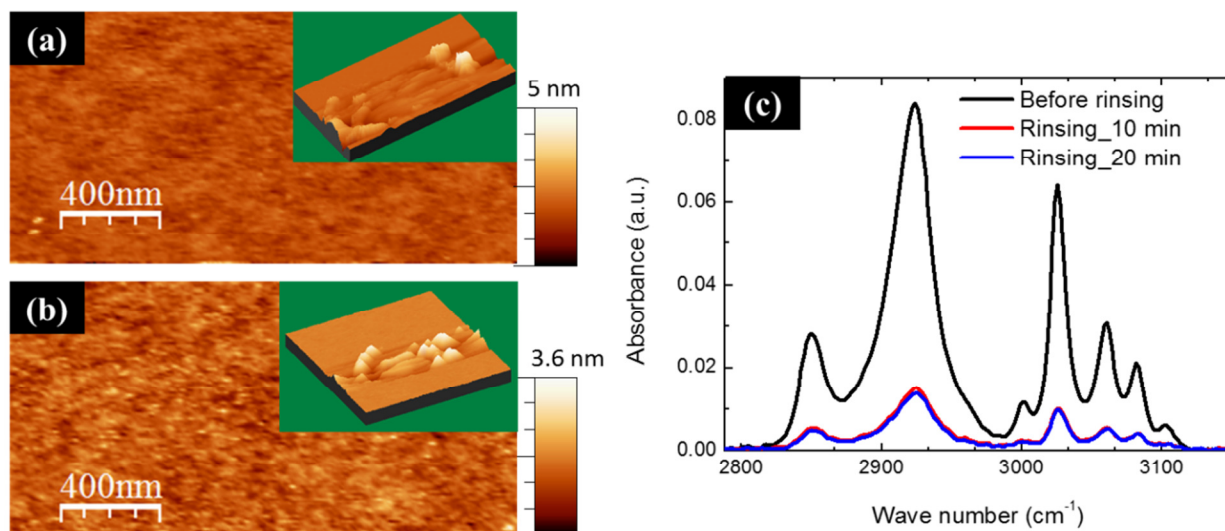


Figure 3-10: AFM topography image of pre-annealed residual films on (a) SiO_x-Si and (b) H-Si substrates obtained after 70 min of toluene rinsing. Inset of (a) and (b) show the 3D AFM images after scratching some regions of residual film by AFM tip in order to confirm that this is polymer rather than Si substrate. (c) Attenuated total reflectance absorbance spectra of a PS ultrathin film before ($h_0 \approx 18.0$ nm) and after ($h_{ads} \approx 5.2$ nm) a "quick" toluene rinsing (up to 20 min) confirming the existence of PS residual layer on Si substrate.

In order to confirm that the observed topography comes from the soft polymer film and not from the Si surface, we scratched the surface of the film on both substrates by the AFM tip (shown in the inset of Figure 3-10, a and b). We thus observed some patches of soft material confirming the existence of a residual film residing on the Si surface. It should be mentioned here that despite the application of high force (~ 2 nN) in AFM scan prior to testing the existence of the residual film, we observe some patches instead of complete empty spaces through the scan area. It can be an indication that PS chains are strongly adsorbed to the substrate since when such a force is applied during scanning of soft materials the bare substrate is generally observed after removing the soft film as previously reported in the case of amphiphilic molecules grown on Si. [43] In addition, ATR spectroscopy was performed before and after toluene rinsing of an 18 nm (h_0) PS film grown on H-Si (shown in Figure 3-10, c) to ascertain the presence of this residual film. Peaks located at 3000, 3030, 3060, 3085 and 3105 cm⁻¹ are due to the C-H stretching modes of the C-H groups located in the benzene ring on the PS side chain. The bands with peak positions of 2930 and 2850 cm⁻¹ are due to the C-H stretching vibration of the CH₂ and CH groups on the main PS chain, respectively. [44] The intensity of all the peaks decreases by about a factor of 4 after 10

min of toluene rinsing. This decrease is due to the removal of loosely attached PS chains during the rinsing. The thickness of the residual film obtained after 10 min of toluene rinsing (≈ 5.5 nm) is also in agreement with the ATR results. Furthermore, beyond the first 10 min of toluene rinsing, the kinetics of dissolution drastically slows down (blue curve in Figure 3-10, c) supporting the kinetics illustrated in Figure 3-9, a. Hence this series of experimental results consistently confirms the existence of a residual PS layer and their kinetics on the substrate upon toluene rinsing.

Having proved that it is possible to produce uniform films of controlled thickness using this simple top-down approach by playing (1) on the nature of the substrate, (2) on the gyration radius of the polymer (R_g), (3) on the pre-annealing time (t_{an}) and (4) on the rinsing time (t_{rins}), we want to address now the stability of the rinsed PS films when they are post-annealed above T_g depending on the type of treatment the Si substrate.

3.5 Stability or instability of residual films of tunable thickness

The stability of thin films strongly depends on their thickness and on the chemical treatment of the Si substrate. [29] Therefore 12 films were initially spin-coated on both SiO_x -Si (6 films) and H-Si (6 films) surfaces with thicknesses mostly of 7 nm and few of 16 nm prior to carrying out the rinsing. Films having different h_{res} values were thus obtained by playing either on the rinsing time or on the pre-annealing treatment as tabulated in Table 3-1. Their stability was then scrutinized after they were annealed (at 120 °C) above the T_g of bulk polystyrene. For the sake of clarity, this annealing treatment performed after rinsing is labeled as “post-annealing”. We first report the results obtained on H-Si before commenting the ones on SiO_x -Si.

3.5.1 The stability of residual films on H-Si wafers

Let us recall that PS ultrathin films on H-Si wafers usually dewet the surface of the substrate thus violating the prediction given by the Lifshitz-van der Waals theory. Our aim here was to test again if this violation was pertained for a series of uniform films of different thickness having undergone a leaching treatment. Residual uniform films with thickness ranging from 1.5 nm to 6.0 nm were thus obtained on H-Si wafers (see Table 3-1) by tuning both the annealing time of the films before rinsing and the duration of toluene rinsing.

The procurement of such uniform films is a “*sine qua non*” condition to apprehend their stability upon annealing. Indeed to apply physical models such as the one based on Lifshitz van der Waals interaction, it is compulsory to start with uniform films of known thickness (as shown by equation 3-2).

Table 3-1: Preparation of the PS rinsed films on Si substrates (6 samples on H-Si and 6 samples on SiO_x-Si). Pre-annealing time t_{an} of the film (before the rinsing procedure) and the duration of toluene rinsing t_{rins} determine the thicknesses of residual layer (h_{res}).

| Sample name | Silicon treatment | Initial PS thickness h_0 (nm) | Pre-annealing time t_{an} at 160 °C | Rinsing time t_{rins} (min) | Residual PS film thickness h_{res} (nm) | Stability after post-annealing at 120°C for 24h |
|------------------------|-------------------|---------------------------------|---------------------------------------|-------------------------------|---|---|
| H-Si-a | HF | 7 | 0h | 100 | 1.5 | no dewetting |
| H-Si-b | HF | 7 | 0h | 50 | 2.5 | no dewetting |
| H-Si-c | HF | 7 | 24h | 40 | 4.0 | no dewetting |
| H-Si-d | HF | 7 | 24h | 20 | 4.6 | no dewetting |
| H-Si-e | HF | 7 | 24h | 10 | 5.0 | no dewetting |
| H-Si-f | HF | 16 | 24h | 2 | 6.0 | no dewetting |
| SiO _x -Si-a | RCA | 7 | 0h | 100 | 1.3 | dewetting |
| SiO _x -Si-b | RCA | 7 | 0h | 50 | 1.7 | dewetting |
| SiO _x -Si-c | RCA | 7 | 0h | 30 | 2.2 | dewetting |
| SiO _x -Si-d | RCA | 7 | 0h | 10 | 3.5 | no dewetting |
| SiO _x -Si-e | RCA | 7 | 24h | 10 | 4.9 | no dewetting |
| SiO _x -Si-f | RCA | 16 | 24h | 1 | 6.8 | no dewetting |

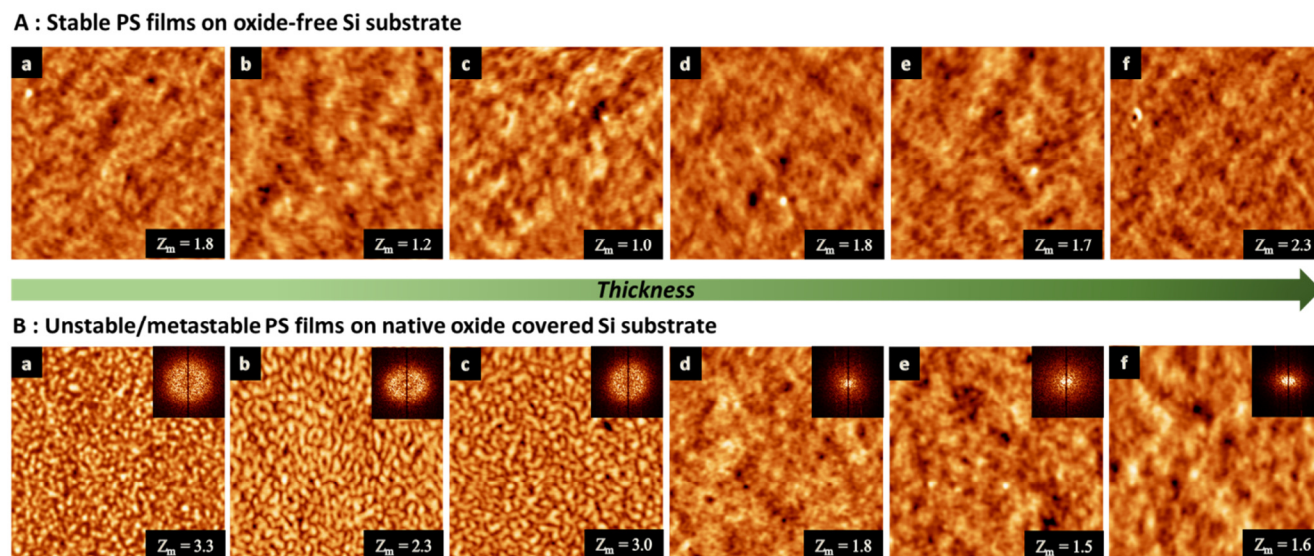


Figure 3-11: AFM topographic images (scan size = $1 \times 1 \mu\text{m}^2$) presented in the top panel (A) show the morphologies of residual films of thickness h_{res} (a) ≈ 1.5 nm, (b) ≈ 2.5 nm, (c) ≈ 4.0 nm, (d) ≈ 4.6 nm, (e) ≈ 5.0 nm and (f) ≈ 6.0 nm on H-Si after post-annealing. In the bottom panel (B) are shown similar results for h_{res} (a) ≈ 1.3 nm, (b) ≈ 1.7 nm, (c) ≈ 2.2 nm, (d) ≈ 3.5 nm, (e) ≈ 4.9 nm and (f) ≈ 6.8 nm thick films on SiO_x -Si. Inset shows their corresponding 2D FFT image. Morphologies were obtained after post-annealing at 120°C during 24 h. Note that the thicknesses that are mentioned here are the thicknesses of the residual films just before the post-annealing. Z_m represents the maximum height in nm.

The best way to probe the stability of such films is to perform AFM imaging of the surface of the residual PS films after post-annealing above the T_g of bulk PS. Figure 3-11. A. shows such images for residual PS films of thickness ranging from ≈ 1.5 nm to ≈ 6.0 nm on H-Si after post-annealing at 120°C for 24h. Further rise in annealing temperature to 170°C does not show any kind of dewetting as can be observed from Figure 3-12. On the contrary to what was obtained for films of similar thickness which were directly spin-coated on the same type of surface, we found that continuous and flat films were always obtained. No dewetting occurred in this case thus reconciling our experimental observations with the prediction of the Lifshitz-van der Waals theory. With this in mind, it was natural to consider the behavior of films prepared in the same way but deposited on SiO_x -Si substrates.

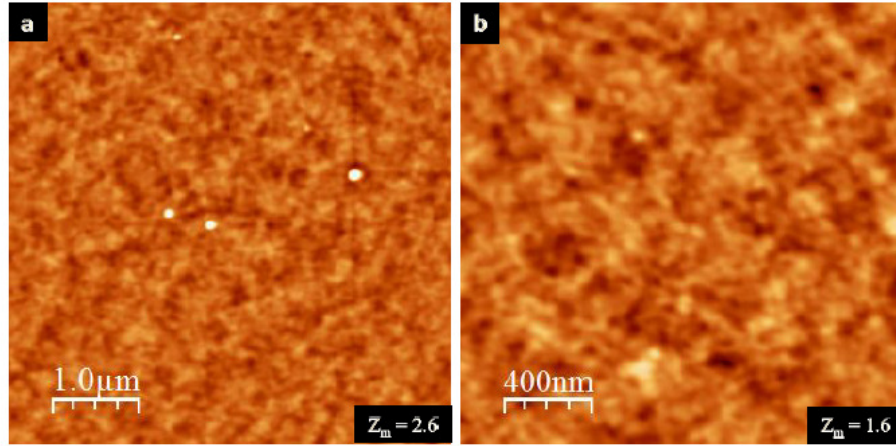


Figure 3-12: AFM topography images illustrate a 2.3 nm thick PS film (residual) on an oxide-free Si substrate. (a) Scan size = $5 \times 5 \mu\text{m}^2$ (RMS roughness $\approx 0.16 \text{ nm}$) and (b) Scan size = $2 \times 2 \mu\text{m}^2$ (RMS roughness $\approx 0.16 \text{ nm}$). The images were taken after post annealing at 170°C during 24 h.

3.5.2 The instability/metastability of residual films on SiO_x-Si wafers

AFM images of residual films with h_{res} in the range 1.3 nm to 6.8 nm on SiO_x-Si followed by post-annealing at 120°C during 24 h under vacuum are shown in Figure 3-11 (B). The results observed in this AFM study are in marked contrast with the ones obtained on H-Si substrates. AFM images of thinner films ($h_{res} < 2.9 \text{ nm}$) shown in Figure 3-11 (B). a, b, and c reveal a bicontinuous surface pattern. [18], [19], [45] For thicker films ($h_{res} > 2.9 \text{ nm}$) shown in Figure 3-11 (B). d, e, and f, we clearly observed a smooth, flat and continuous morphology. Therefore there is a threshold in thickness of about 2.9 nm above which residual films (or adsorbed layer) remain stable. Below this threshold, the formation of bicontinuous structures can be understood in terms of spinodal dewetting. [18], [19], [45] In order to extract the characteristic features of these dewetted patterns, Fast Fourier Transform (FFT) of topographic images were conducted with results shown in the corresponding insets of each figure. In the case of spinodal dewetting, the FFT yielded ring patterns indicating the existence of a correlation peak consistent with a definite correlation length λ . A radial averaging of the FFT images or power spectral density (PSD) calculation of topographic images was then achieved to extract the value of $\lambda \approx 53 - 63 \text{ nm}$ from Figure 3-13. This value is comparable to the value reported by Seeman *et al.* [29] with low PS

molar mass ($M_w = 2 \times 10^3$ g/mol). No need to say that flat featureless films studied by the same procedure did not show any correlation peak.

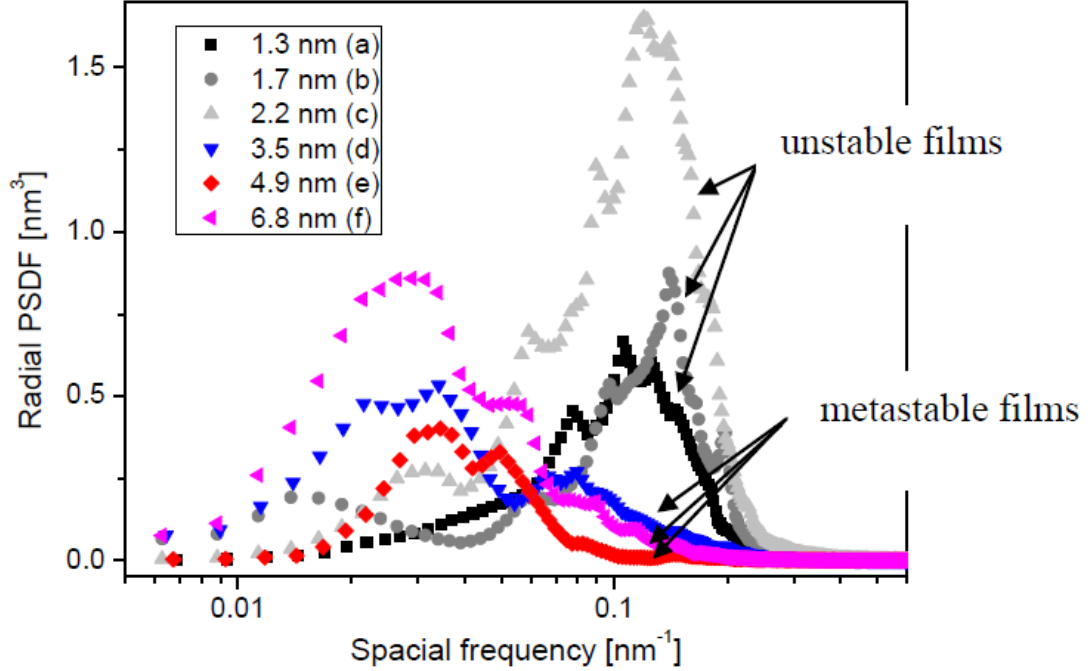


Figure 3-13: Power spectral density (PSD) curves of residual PS films grown on SiO_x -Si substrates having different thicknesses calculated from AFM images presented in Figure 3-11. B.

The full interpretation of these results can be once again apprehended *via* the Lifshitz –van der Waals interaction potential. Yet, it is necessary to now consider the presence of the silicon oxide layer to explain our results. The system that needs to be considered is thus made of 4 media Si/ SiO_x /PS/Air in which the thickness of the oxide layer is denoted d_{SiO_x} . Application of equation 3-2 assuming pair wise addition leads to the following expression for the free energy. [46], [47]

$$\Delta F_{LW}(h) = \left(\frac{-A_{\text{Si/PS/Air}}}{12\pi(h + d_{\text{SiO}_x})^2} \right) + \left(\frac{-A_{\text{SiO}_x/\text{PS/Air}}}{12\pi h^2} \right) - \left(\frac{-A_{\text{SiO}_x/\text{PS/Air}}}{12\pi(h + d_{\text{SiO}_x})^2} \right) \quad 3-4$$

where $A_{\text{Si/PS/Air}}$ and $A_{\text{SiO}_x/\text{PS/Air}}$ are the effective Hamaker constants of the Si/PS/Air and the SiO_x /PS/Air systems, respectively. We assume that $d_{\text{SiO}_x} = 2$ nm, from Figure 3-14 in the case of the SiO_x -Si substrate.

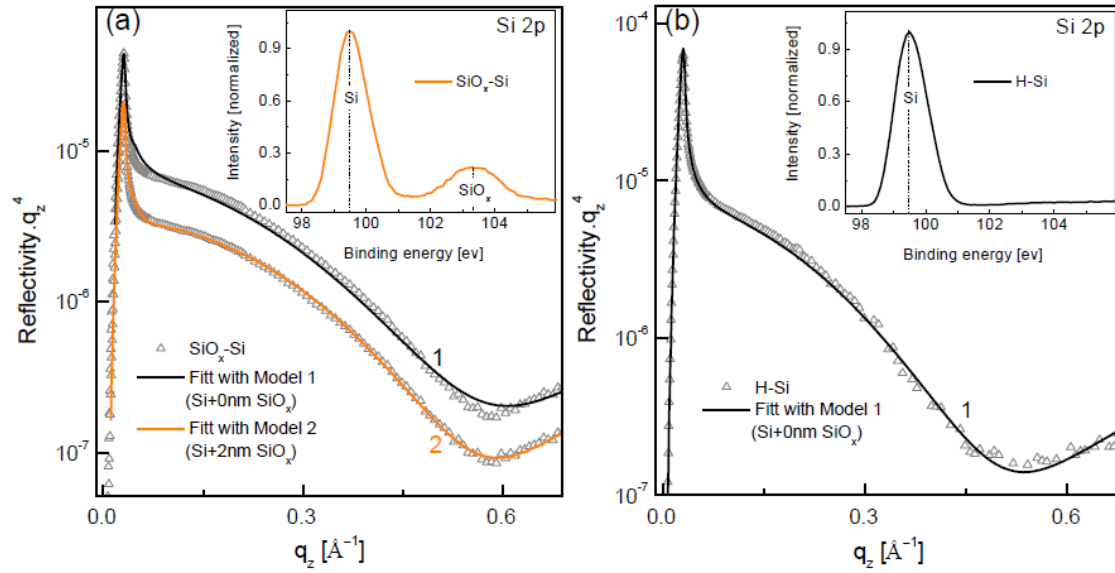


Figure 3-14: (a) Normalized XRR data (symbol) of RCA-cleaned Si and analyzed curves (solid lines. Inset: XPS spectrum of RCA-cleaned Si substrate demonstrating the existence of SiO_x layer on top of Si. (b) Normalized XRR data (symbol) of HF-cleaned Si substrate and fitted curve (solid line) using model 1 without oxide layer. Inset: XPS spectrum confirming the absence of an oxide layer on H-Si substrate after HF-treatment.

The normalized XRR data (symbol) of RCA-cleaned Si and analysed curves (solid lines) using model 1 and model 2. In model 1, a SiO_x layer was not included whereas in model 2, the introduction of a 2 nm thick layer of SiO_x yielded a much better fit. The fitting reliability was also appreciated from the χ^2 value: in case of model 1, $\chi^2 = 0.020122$ whereas for model 2, $\chi^2 = 0.002106$. Hence the fit confirms the existence of a 2 nm SiO_x layer on the Si substrate. Note that it is very difficult to evidence the presence of this layer because (i) it is very thin and (ii) its electron density is very close to the one of silicon. The XPS spectrum of RCA-cleaned Si substrate demonstrating the existence of SiO_x layer on top of Si is given in the inset. Figure 3-14, b shows the normalized XRR data (symbol) of HF-cleaned Si substrate and fitted curve (solid line) using model 1 without oxide layer. The fitting reliability $\chi^2 (= 0.007472)$ is quite good. The XPS spectrum confirming the absence of an oxide layer on H-Si substrate after HF-treatment is given in the inset. Note that the insets were taken from a previous work reported. [48] The values of the Hamaker constants are not very well defined in the literature and are ranging from $A_{\text{Si/PS/Air}} = -4.4$ to -6.0×10^{-20} J and $A_{\text{SiO}_x/\text{PS/Air}} = -0.22$ to 1.6×10^{-20} J, hence $\Delta F_{LW}(h)$ can vary considerably depending on the values of $A_{\text{Si/PS/Air}}$ and $A_{\text{SiO}_x/\text{PS/Air}}$ (as given in Table 3-2).

| | $A_{Si/Si}$ $\times 10^{-20} J$ | $A_{PS/PS}$ $\times 10^{-20} J$ | $A_{SiOx/SiOx}$ $\times 10^{-20} J$ | $A_{Si/PS/Air}$ $\times 10^{-20} J$ | $A_{SiOx/PS/Air}$ $\times 10^{-20} J$ | State of PS for $d_{SiOx} = 2$ nm |
|----------------|------------------------------------|------------------------------------|--|--|--|--------------------------------------|
| Curve A | 24.0 | 6.15 | 6.6 | -6.0 | -0.2 | Stable |
| Curve B | 19.0 | 7.9 | 5.0 | -4.4 | 1.6 | Unstable |
| Curve C | 20.3 | 6.5 | 5.2 | -5.0 | 0.7 | Unstable/Metastable |

Table 3-2: Correlation between the Hamaker constant values of $A_{Si/Si}$, $A_{PS/PS}$ and $A_{SiOx/SiOx}$ and the resulting effective Hamaker constants $A_{Si/PS/Air}$ and $A_{SiOx/PS/Air}$ from the "mixing rule" of equation 3-3. Curves A, B and C refer to the three different states as shown in Figure 3-15.

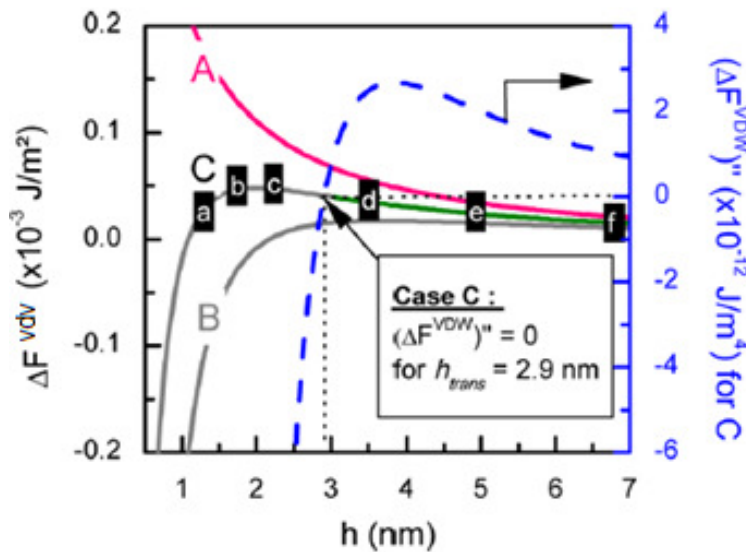


Figure 3-15: Simulated $\Delta F^{VDW}(h)$ (solid lines) and $[\Delta F^{VDW}(h)]''$ (dashed line) curves using Eq.3-4 assuming 2 nm native oxides present on SiO_x -Si substrate. Curve 'A', drawn by choosing $A_{Si/PS/Air} = -6.0 \times 10^{-20} J$ and $A_{SiOx/PS/Air} = -0.2 \times 10^{-20} J$, corresponds to a stable state. Curve 'B', deduced with $A_{Si/PS/Air} = -4.4 \times 10^{-20} J$ and $A_{SiOx/PS/Air} = 1.6 \times 10^{-20} J$, depicts an unstable state. Curve 'C', plotted assuming $A_{Si/PS/Air} = -5 \times 10^{-20} J$ and $A_{SiOx/PS/Air} = 0.7 \times 10^{-20} J$, corresponds to either a metastable state above $h_{trans} \approx 2.9$ nm and unstable films below h_{trans} . The letters a,b,c,d,e and f are corresponding to the AFM images presented in Figure 3-11. Color of state : stable in pink, unstable in grey, metastable in green.

For instance in Figure 3-15, we have plotted $\Delta F_{LW}(h)$ or $(\Delta F^{VDW}(h))$ with the values of the effective Hamaker constants given in Table 3-2. Curve A that was calculated with $A_{Si/PS/Air} = -6.0 \times 10^{-20} J$ and $A_{SiOx/PS/Air} = -0.22 \times 10^{-20} J$ corresponds to a stable state since the second derivate

of the free energy is always positive. On the contrary, curve B calculated with $A_{\text{Si/PS/Air}} = -4.4 \times 10^{-20}$ J and $A_{\text{SiOx/PS/Air}} = 1.6 \times 10^{-20}$ J depicts an unstable state since the second derivative is always negative. The interpretation of a spinodal decomposition for $h < 2.9$ nm can only be explained if the variation of $\Delta F^{\text{VDW}}(h)$ would be similar to the one plotted in curve C. Curve C was obtained by adjusting the Hamaker constant to $A_{\text{Si/PS/Air}} = -5 \times 10^{-20}$ J and to $A_{\text{SiOx/PS/Air}} = 0.7 \times 10^{-20}$ J. Note that these values are almost in the middle range of the ones found in the literature. Additionally they dictate the value of the threshold thickness h_{trans} delimiting the unstable from the metastable zones. In dash line shown in Figure 3-15 (right y-axis) is the plot of second derivative of the free energy *i.e.* $[\Delta F^{\text{VDW}}(h)]''$ corresponding to the C curve. For $h < 2.9$ nm, $[\Delta F^{\text{VDW}}(h)]'' < 0$, films are unstable and dewet as it is observed in the AFM images *a*, *b* and *c* of Figure 3-11, B. For $h > 2.9$ nm, $[\Delta F^{\text{VDW}}(h)]'' > 0$, films are metastable and do not dewet as it is observed in the AFM images *d*, *e* and *f* of Figure 3-11, B. The threshold thickness $h_{\text{trans}} = 2.9$ nm corresponds to the zero value of the second derivative. Notably the thickness of native oxide layer is found to be crucial for determining h_{trans} value as shown in Figure 3-16. It has a linear dependency with the oxide thickness ($h_{\text{trans}} \sim d_{\text{SiOx}}$).

In the introduction of this chapter, we mentioned that the behaviour of polymer ultrathin films confined at the surface of chemically etched silicon was still a mystery. The underlying reason was that the most recognized theory utilized for predicting the stability of such films was failing when films were deposited on oxide-free silicon surfaces. Solving this issue never succeeded and it was natural to either question the validity of the theory or to consider that one of the four stated hypotheses in the introduction section would be at the origin of observed phenomena. So far none of these possibilities could be ruled out. However the validity of the Lifshitz- van der Waals interaction potential was difficult to distrust and for this reason it was clear to us that the reconciliation between the theory and the experimental observation could come from a modification of the sample preparation.

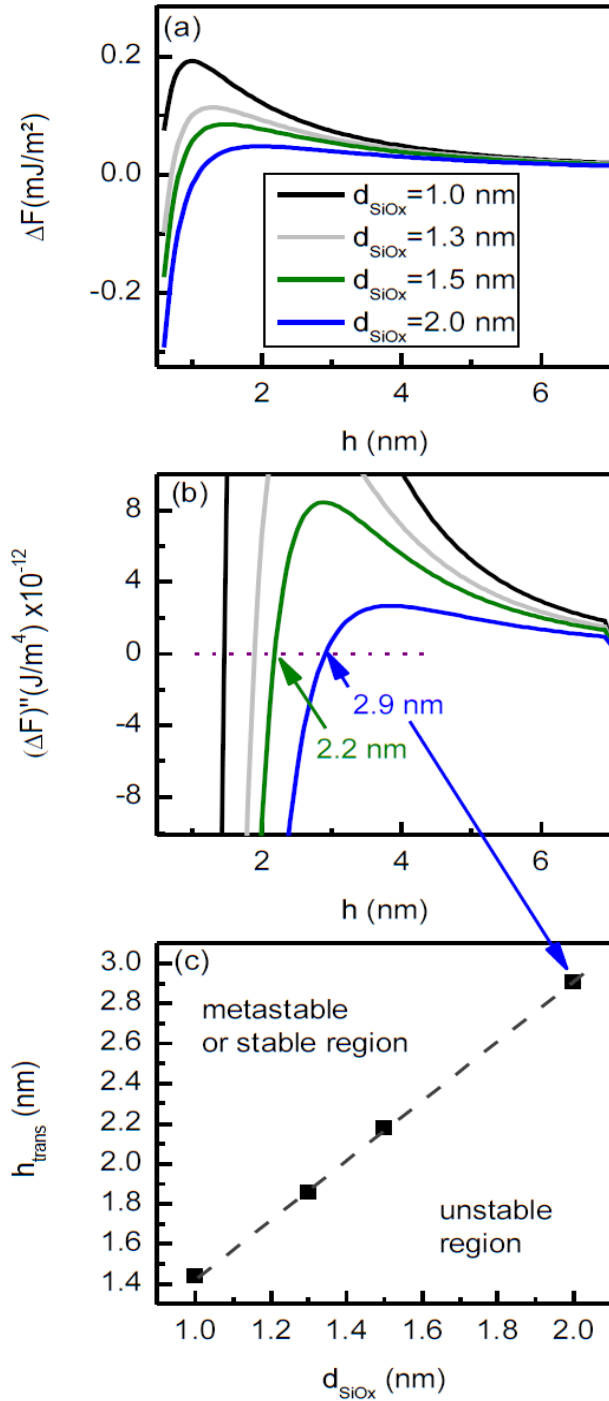


Figure 3-16: Evolution of the free energy as a function of SiO_x thickness. Simulated (a) (b) curves using equation 3-4 considering 4 different thicknesses (d_{SiO_x}) of native oxides in SiO_x-Si substrate. All the curves are plotted with $A_{\text{Si/PS/Air}} = -5.0 \times 10^{-20}$ J and $A_{\text{SiO}_x/\text{PS/Air}} = 0.7 \times 10^{-20}$ J. The intercept point of curves to the x-axis indicates the value of h_{trans} . (c) Plot of h_{trans} as a function of d_{SiO_x} . Fitted linear curve (dashed line) draws a border line between stable or metastable and unstable regimes.

Following the solvent rinsing route, we are now confident that the first two hypotheses *i.e.* the dewetting due to heterogeneities or the presence of silica can be excluded. Indeed, if there were any heterogeneities and/or an oxide layer on the Si surface causing the dewetting of directly spin-coated films, there should be no reason to get a stable residual film on H-Si after the leaching procedure. Also it is not feasible to assume that the oxide layer and the heterogeneities present at the dewetted PS film-Si interface would be removed by rinsing treatment. Thus the application of this novel technique narrowed the possible reasons for the common discrepancy between experimental results (Figure 3-2, c and d) and theoretical expectations (equation 3-2). The two other hypotheses for the dewetting *i.e.* the negative stresses induced by the spin-coating procedure and/or density variation could not yet be excluded. The leached films were then post-annealed at 120 °C and their stability was revisited. The observed results were then confronted to the theory in a very successful way since the behaviour of PS films both on oxide-free and on SiO_x silicon surfaces was fully explained. The good agreement between the observed domains of stability of the residual films and the underlying theory promotes the idea that the leaching route has removed residual stresses and/or local density variations originating from the spin-coating and from the fast evaporation of the solvent. Such stresses are usually considered to be at the origin of the dewetting of directly spin-coated PS films both on oxide-free (H-Si) and native oxide covered (SiO_x-Si) Si surfaces (as shown in Figure 3-2, a and b). In contrast, the leached films of identical thicknesses are amazingly stable on H-Si surfaces. One can thus conclude that the leaching procedure combined to a post-annealing leads to stable films on H-Si substrates. In addition all residual films on H-Si were found to be stable at ambient conditions up to ~ 2 months without post-annealing as can be seen from Figure 3-17.

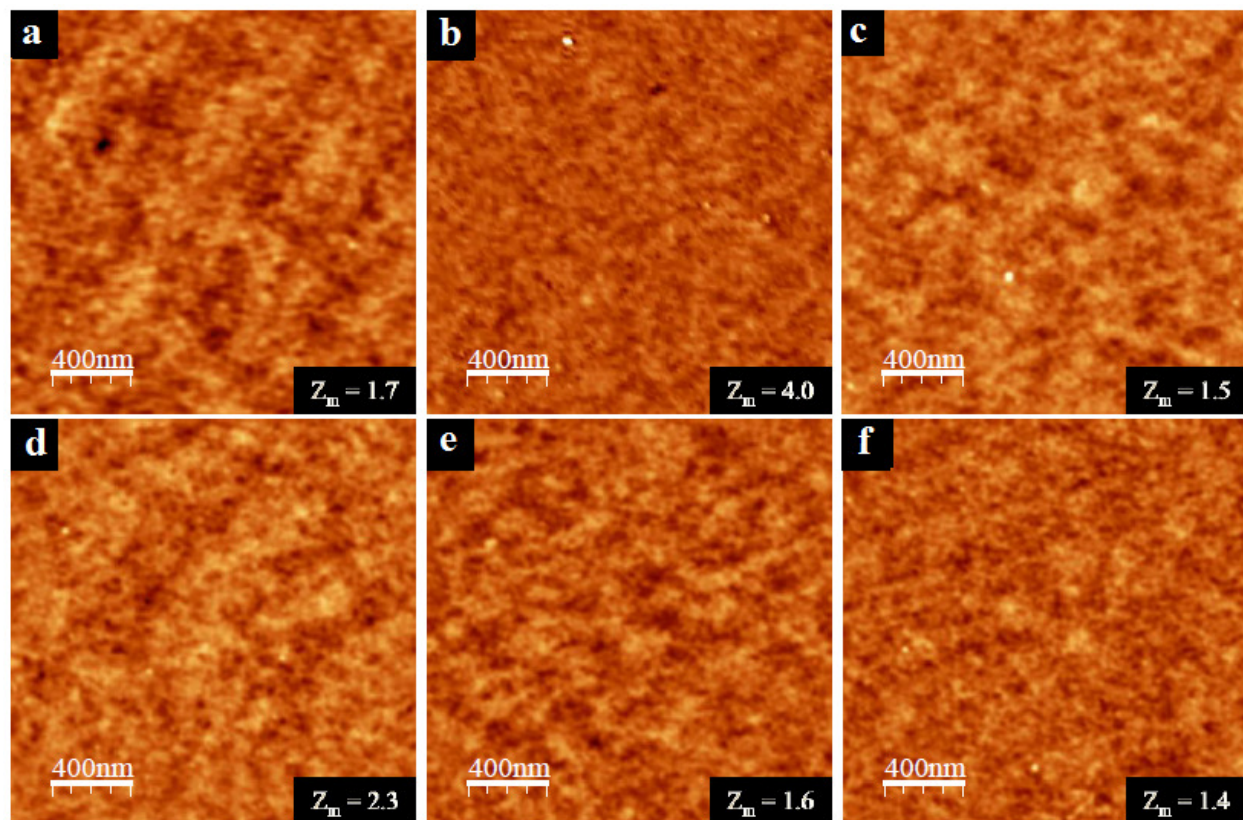


Figure 3-17: AFM topographic images (Scan size = $2 \times 2 \mu\text{m}^2$) show the morphologies of residual films of thicknesses h_{res} (a) ≈ 1.5 nm, (b) ≈ 2.5 nm, (c) ≈ 4.0 nm, (d) ≈ 4.6 nm, (e) ≈ 5.0 nm and (f) ≈ 6.0 nm on H-Si substrates without post annealing. Z_m represents the maximum height in nm.

Hence, one can infer that the toluene rinsing induces a chain relaxation or allows some rearrangements of PS molecules in the residual layer. This assumption is in agreement with the results of Gin *et al.* [32] who reported that the inner flattened layer has no thermal expansion when the loosely attached layer is thick whereas after removing the outer loosely adsorbed chains, the flattened layer can reorganize due to the resultant empty spaces (*i.e.*, more free volume). Toluene diffuses easily into the flattened layer during rinsing. It acts as a plasticizer lowering the T_g below room temperature. [9], [49] Hence the molecular mobility of the PS chains increases by minimizing the cumulative intermolecular forces along the chains leading to a reduction in the cohesion. Thus PS chains can glide over another in presence of toluene solvent to reach equilibrium by releasing the residual stress and/or erasing the density variations imposed during the spin-coating process.

3.6 Conclusion

In conclusion, our results show that a two-step top-down approach consisting (1) in the preparation of homogeneous thick films by spin-coating and (2) in thinning them by rinsing in a good solvent (*e.g.* toluene), could solve one of the most mysterious unanswered question encountered in the physics of extremely confined polymer films: why ultrathin films of PS are unstable on oxide-free silicon surfaces? We first demonstrated that the leaching procedure was perfectly adapted to obtain thin and smooth residual films without any hole even after post-annealing above T_g . By playing on two parameters, such as rinsing time (t_{rins}) and pre-annealing treatment (t_{an}), several desired thicknesses were obtained below 7 nm. After post-annealing above T_g , we observed that residual films deposited on oxide-free H-Si surfaces do not dewet as expected from the van der Waals theory. On the contrary, films deposited on SiO_x-Si substrates with SiO_x layer thickness around 2nm were showing a spinodal dewetting below a critical film thickness h_{trans} of about ≈ 2.9 nm. Above this value films are in a metastable state and were found to be uniform on a time scale of a few months. This transition between the two regimes unstable and metastable is in perfect agreement with the intermolecular van der Waals interactions theory. We attribute the stability of the films deposited on oxide-free silicon to the capability of toluene to remove either the residual stresses of the film or the density variations inside the film.

REFERENCES

- [1] B. Adhikari and S. Majumdar, “Polymers in sensor applications,” *Prog. Polym. Sci.*, vol. 29, no. 7, pp. 699–766, Jul. 2004.
- [2] Q. Huang, I. Yoon, J. Villanueva, K. Kim, and D. J. Sirbuly, “Quantitative mechanical analysis of thin compressible polymer monolayers on oxide surfaces,” *Soft Matter*, vol. 10, pp. 8001–8010, 2014.
- [3] L. H. Lee, *Adhesive Bonding*. Springer US, 2013.
- [4] A. L. Hook, C.-Y. Chang, J. Yang, J. Lockett, A. Cockayne, S. Atkinson, Y. Mei, R. Bayston, D. J. Irvine, R. Langer, D. G. Anderson, P. Williams, M. C. Davies, and M. R. Alexander, “Combinatorial discovery of polymers resistant to bacterial attachment,” *Nat. Biotechnol.*, vol. 30, no. 9, pp. 868–875, Sep. 2012.
- [5] S. Günes, H. Neugebauer, and N. S. Sariciftci, “Conjugated Polymer-Based Organic Solar Cells,” *Chem. Rev.*, vol. 107, no. 4, pp. 1324–1338, Apr. 2007.
- [6] G. Li, R. Zhu, and Y. Yang, “Polymer solar cells,” *Nat. Photonics*, vol. 6, no. 3, pp. 153–161, Mar. 2012.
- [7] C. Kim, A. Facchetti, and T. J. Marks, “Polymer Gate Dielectric Surface Viscoelasticity Modulates Pentacene Transistor Performance,” *Science (80-.)*, vol. 318, no. 5847, pp. 76–80, Oct. 2007.
- [8] C. Bollinne, S. Cuenot, B. Nysten, and a. M. Jonas, “Spinodal-like dewetting of thermodynamically-stable thin polymer films,” *Eur. Phys. J. E*, vol. 12, no. 3, pp. 389–396, 2003.
- [9] G. Reiter, M. Hamieh, P. Damman, S. Slavons, S. Gabriele, T. Vilmin, and E. Raphael, “Residual stresses in thin polymer films cause rupture and dominate early stages of dewetting,” *Nat. Mater.*, vol. 4, no. 10, pp. 754–758, Oct. 2005.

- [10] S. Napolitano and M. Wübbenhorst, “The lifetime of the deviations from bulk behaviour in polymers confined at the nanoscale,” *Nat. Commun.*, vol. 2, p. 260, Mar. 2011.
- [11] F. Wyart, J. Meglio, D. Quere, and P. Gennes, “Spreading of Nonvolatile Liquids in a Continuum Picture,” *Langmuir*, vol. 12, no. 8, pp. 335–338, 1991.
- [12] C. Redon, F. Brochard-Wyart, and F. Rondelez, “Dynamics of dewetting,” *Phys. Rev. Lett.*, vol. 66, no. 6, pp. 715–718, 1991.
- [13] P. G. de Gennes, F. B. Wyart, and Q. David, *Capillarity and Wetting Phenomena: Drops, Bubbles, Pearls, Waves*. Springer, 2004.
- [14] G. Reiter, “Probing Properties of Polymers in Thin Films Via Dewetting,” in *Glass Transition, Dynamics and Heterogeneity of Polymer Thin Films*, Springer, 2013.
- [15] G. Reiter, “Dewetting of thin polymer films,” *Phys. Rev. Lett.*, vol. 68, no. 1, pp. 75–78, Jan. 1992.
- [16] K. Jacobs, R. Seemann, and S. Herminghaus, “Stability and dewetting of thin liquid films,” in *Polymer thin films*, vol. 1, World Scientific, 2008, p. 243.
- [17] V. S. Mitlin, “Dewetting of Solid Surface: Analogy with Spinodal Decomposition,” *J. Colloid Interface Sci.*, vol. 156, no. 2, pp. 491–497, Mar. 1993.
- [18] A. Vrij, “Possible mechanism for the spontaneous rupture of thin, free liquid films,” *Discuss. Faraday Soc.*, vol. 42, no. 0, pp. 23–33, 1966.
- [19] R. Xie, A. Karim, J. Douglas, C. Han, and R. Weiss, “Spinodal Dewetting of Thin Polymer Films,” *Phys. Rev. Lett.*, vol. 81, no. 6, pp. 1251–1254, 1998.
- [20] J. N. Israelachvili, *Intermolecular and surface forces*. Academic Press London, 1991.
- [21] A. Sharma and G. Reiter, “Instability of Thin Polymer Films on Coated Substrates: Rupture, Dewetting, and Drop Formation,” *J. Colloid Interface Sci.*, vol. 178, no. 2, pp. 383–399, 1996.

- [22] J. Visser, "On Hamaker constants: A comparison between Hamaker constants and Lifshitz-van der Waals constants," *Adv. Colloid Interface Sci.*, vol. 3, no. 4, pp. 331–363, Dec. 1972.
- [23] D. B. Hough and L R. White, "The calculation of hamaker constants from liftshitz theory with applications to wetting phenomena," *Adv. Colloid Interface Sci.*, vol. 14, no. 1, pp. 3–41, 1980.
- [24] C. J. Van Oss, M. K. Chaudhury, and R. J. Good, "Interfacial Lifshitz-van der Waals and polar interactions in macroscopic systems," *Chem. Rev.*, vol. 88, no. 6, pp. 927–941, 1988.
- [25] T. Kerle, R. Yerushalmi-Rozen, J. Klein, and L. J. Fetters, "van der Waals stable thin liquid films : Correlated undulations and ultimate dewetting," *Eur. Lett.*, vol. 44, no. 4, pp. 484–490, 1998.
- [26] H. D. Ackler, R. H. French, and Y.-M. Chiang, "Comparisons of Hamaker constants for ceramic systems with intervening vacuum or water: From force laws and physical properties," *J. Colloid Interface Sci.*, vol. 179, pp. 460–469, 1996.
- [27] L. Bergström, "Hamaker constants of inorganic materials," *Adv. Colloid Interface Sci.*, vol. 70, pp. 125–169, 1997.
- [28] H. Zhao, Y. J. Wang, and O. K. C. Tsui, "Dewetting induced by complete versus nonretarded van der Waals forces.," *Langmuir*, vol. 21, no. 13, pp. 5817–24, Jun. 2005.
- [29] R. Seemann, S. Herminghaus, and K. Jacobs, "Dewetting Patterns and Molecular Forces: A Reconciliation," *Phys. Rev. Lett.*, vol. 86, no. 24, pp. 5534–5537, Jun. 2001.
- [30] A. Sharma, J. Mittal, and R. Verma, "Instability and Dewetting of Thin Films Induced by Density Variations," *Langmuir*, vol. 18, no. 26, pp. 10213–10220, Dec. 2002.
- [31] L. Xue and Y. Han, "Inhibition of dewetting of thin polymer films," *Prog. Mater. Sci.*, vol. 57, no. 6, pp. 947–979, 2012.

- [32] P. Gin, N. Jiang, C. Liang, T. Taniguchi, B. Akgun, S. K. Satija, M. K. Endoh, and T. Koga, “Revealed Architectures of Adsorbed Polymer Chains at Solid-Polymer Melt Interfaces,” *Phys. Rev. Lett.*, vol. 109, no. 26, p. 265501, Dec. 2012.
- [33] N. Jiang, J. Shang, X. Di, M. K. Endoh, and T. Koga, “Formation Mechanism of High-Density, Flattened Polymer Nanolayers Adsorbed on Planar Solids,” *Macromolecules*, vol. 47, pp. 2682–2689, 2014.
- [34] Y. Fujii, Z. Yang, J. Leach, H. Atarashi, K. Tanaka, and O. K. C. Tsui, “Affinity of Polystyrene Films to Hydrogen-Passivated Silicon and Its Relevance to the T_g of the Films,” *Macromolecules*, vol. 42, no. 19, pp. 7418–7422, Oct. 2009.
- [35] O. Guiselin, “Irreversible Adsorption of a Concentrated Polymer Solution,” *Europhys. Lett.*, vol. 17, pp. 225–230, 1992.
- [36] H. E. Johnson and S. Granick, “Granick_New mechanism for no equilibrium polymer adsorbtion.pdf.” *Science*, p. 966, 1992.
- [37] R. D. Priestley, C. J. Ellison, L. J. Broadbelt, and J. M. Torkelson, “Structural relaxation of polymer glasses at surfaces, interfaces, and in between.,” *Science*, vol. 309, no. 5733, pp. 456–9, Jul. 2005.
- [38] A. Van der Lee, L. Hamon, Y. Holl, and Y. Grohens, “Density profiles in thin PMMA supported films investigated by X-ray reflectometry,” *Langmuir*, vol. 17, no. 24, pp. 7664–7669, 2001.
- [39] G. Vignaud, M. S. Chebil, J. K. Bal, N. Delorme, T. Beuvier, Y. Grohens, and A. Gibaud, “Densification and Depression in Glass Transition Temperature in Polystyrene Thin Films,” *Langmuir*, vol. 30, pp. 11599–11608, 2014.
- [40] J. K. Bal, T. Beuvier, M. S. Chebil, G. Vignaud, Y. Grohens, M. K. Sanyal, and A. Gibaud, “Relaxation of Ultrathin Polystyrene Films Hyperswollen in Supercritical Carbon Dioxide,” *Macromolecules*, vol. 47, no. 24, pp. 8738–8747, Dec. 2014.

- [41] C. Housmans, M. Sferrazza, and S. Napolitano, “Kinetics of irreversible chain adsorption,” *Macromolecules*, vol. 47, pp. 3390–3393, 2014.
- [42] L. J. Fetters, N. Hadjichristidis, J. S. Lindner, and J. W. Mays, “Molecular Weight Dependence of Hydrodynamic and Thermodynamic Properties for Well-Defined Linear Polymers in Solution,” *Journal of Physical and Chemical Reference Data*, vol. 23, p. 619, 1994.
- [43] J. K. Bal, S. Kundu, and S. Hazra, “Growth and stability of Langmuir-Blodgett films on OH-, H-, or Br-terminated Si(001),” *Phys. Rev. B*, vol. 81, no. 4, p. 45404, Jan. 2010.
- [44] E. Jabbari and N. A. Peppas, “Use of ATR-FTIR to study interdiffusion in polystyrene and poly(vinyl methyl ether),” *Macromolecules*, vol. 26, no. 9, pp. 2175–2186, Apr. 1993.
- [45] J. Becker, G. Grun, R. Seemann, H. Mantz, K. Jacobs, K. R. Mecke, and R. Blossey, “Complex dewetting scenarios captured by thin-film models,” *Nat. Mater.*, vol. 2, no. 1, pp. 59–63, Jan. 2003.
- [46] R. Seemann, S. Herminghaus, and K. Jacobs, “Gaining control of pattern formation of dewetting liquid films,” *J. Phys. Condens. Matter*, vol. 13, no. 21, p. 4925, 2001.
- [47] G. Reiter, R. Khanna, and A. Sharma, “Enhanced Instability in Thin Liquid Films by Improved Compatibility,” *Phys. Rev. Lett.*, vol. 85, no. 7, pp. 1432–1435, Aug. 2000.
- [48] J. K. Bal, S. Kundu, and S. Hazra, “Hydrophobic to hydrophilic transition of HF-treated Si surface during Langmuir–Blodgett film deposition,” *Chem. Phys. Lett.*, vol. 500, no. 1–3, pp. 90–95, Nov. 2010.
- [49] L. Xu, A. Sharma, and S. W. Joo, “Dewetting of stable thin polymer films induced by a poor solvent: Role of polar interactions,” *Macromolecules*, vol. 45, pp. 6628–6633, 2012.

Chapter 4. Characteristic features of ultrathin polymer residual layer studied by rinsing with different solvents.

Parts of this chapter are extracted from:

“Solvent Assisted Rinsing: Stability/Instability of Ultrathin Polymer Residual Layer”

Adapted with permission from,

Beena Unni, A.; Vignaud, G.; Bal, J. K.; Delorme, N.; Beuvier, T.; Thomas, S.; Grohens, Y.; Gibaud, A. *Macromolecules* **2016**, *49*, 1807–1815.

Copyright © (2016) American Chemical Society

Summary

In the previous chapter, we have observed the formation of stable thin films by solvent rinsing method; hence it can be interesting to see in the following, what happens when different solvents are used for the rinsing process. The aim of this chapter is to study the effect of solvent selection while deconstructing PS thin films. Thin films of PS on silicon wafer with native oxide (PS/SiO_x-Si) were rinsed with four different solvents: toluene, chloroform, tetrahydrofuran (THF) and acetone to obtain the polymer residual layer. The thickness and morphology of the residual layer is measured, the experimentally observed stability/ instability of the residual layer is analyzed with Lifshitz van der Waals intermolecular theory with consideration to the specific interactions in the system.

4.1 Introduction

The characteristics of polymer thin films are greatly influenced by their interfaces. Due to the large surface to volume ratio, the influence of free surfaces and interfacial layers on the physical properties of films cannot be neglected for ultrathin films (thickness $h < 100$ nm). At the polymer/air interface, there exists a surface mobile layer which enhances the chain dynamics [1]–[3]. On the other hand, the substrate interface is known to reduce the dynamics because of an immobile polymer adsorbed layer [4]–[6]. However, our understanding of how the properties of thin films depend on the polymer structure at the polymer/substrate interface is still rudimentary. Several research groups have evidenced the formation of an irreversibly adsorbed polymer layers on the substrate with thickness of few nanometers, even without specific interactions of the polymer with the substrate [7]–[17]. Lot of studies shows that this irreversible layer plays a significant role on the physical properties of thin films, such as the enhancement of segmental mobility in proximity to this layer [10], [11], [18], [19], the control of the crystalline structure [20], [21], the impact on local viscosity [13], the long-range effects of this interface on the dynamics [22]–[25], the increase of the density at the polymer/substrate interface [14], [26] etc. Solvent rinsing is an effective method to obtain the details on this irreversibly adsorbed polymer on the substrate. Guiselin [7] was the first to propose a method of rinsing polymer thin films with good solvent. The underlying desorption mechanism of polymer thin films in contact with a solvent can be visualized as follows: When a supported polymer thin film is in contact with a good solvent, two distinct processes can occur: (i) the solvent diffuses in the polymer film and (ii) the polymer chains near the solid–liquid interface become solvated [27]. Due to the plasticization of the polymer by the solvent, a gel-like swollen layer is formed along with two separate interfaces, one between a glassy polymer and a gel layer and the other between the gel layer and the solvent [28], [29]. With the consequent formation of a swollen layer, chain disentanglement is favored and the solvated macromolecules are transported from the film into the solution.

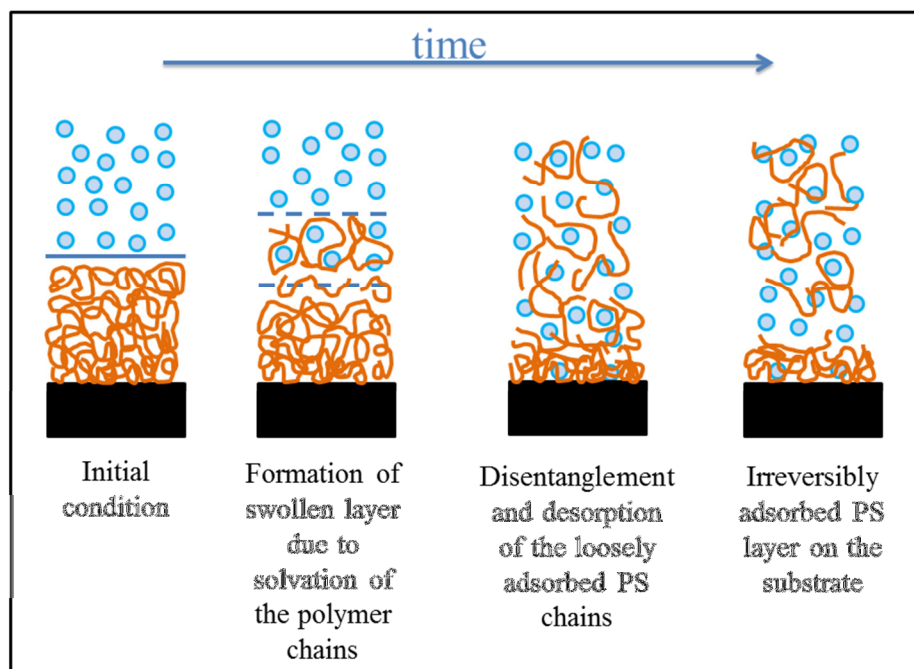


Figure 4-1: Sketch representing the desorption mechanism of PS/SiO_x-Si in contact with a good solvent. The substrate, the polymer and the solvent are shown in black, orange and blue respectively.

The non-adsorbed polymer chains dissolve after a specific induction time. These different steps of dissolution and desorption are illustrated in Figure 4-1. After the dissolution of non-adsorbed chains, the solvent is in direct contact with the irreversibly adsorbed polymer layer. Such an adsorbed polymer chain is attached to the surface by many segments with a very high adsorption energy per chain [30]. The removal of such adsorbed chain from the solid interface requires desorption of the fraction of polymer that is in contact with the surface overcoming its enthalpic barrier along with its disentanglement from neighboring chains (a diffusive process). Whereas dissolution with a good solvent of a thin PS film takes place in less than second and lasts only a few minutes [27], [31], partial desorption needs more time at low shear rates when there is no flow-enhanced desorption. In addition, the inter diffusive chain dynamics gets strongly hindered compared to the bulk when the distance from the substrate is less than $3Rg$, where Rg is the radius of polymer gyration of PS [32].

It is anticipated that the formation of loops in the adsorbed chains would provide a structure with which unadsorbed polymer chains can entangle effectively, thereby giving rise to this cohesion strength [33]. Thus by rinsing with good solvent, the unbound polymer is removed whereas the residual polymer which is physisorbed on the substrate is retained.

The study by Guiselin was to characterize the volume fraction profile of an irreversibly adsorbed polymer by removing the unbound polymer where the adsorbed layer is considered to be analogous to a poly disperse pseudo brush. Later Fuji *et al.* [9] and Durning *et al.* [8] successfully obtained a stable residual layer of polystyrene (PS) by the same method and showed that the thickness of the residual layer increased with increasing molecular weights. Despite rinsing with a good solvent, they also found that PS remains bound to a weakly attractive substrate by means of using hydrofluoric acid (HF) treated Si wafer. Recently Gin *et al.* [14] has shown that the equilibrium PS adsorbed layers have the two different density regions in the direction normal to the surface: the nearly identical inner higher density region regardless of molecular weights and the outer bulk like density region whose thickness increases with increasing molecular weights as shown below.

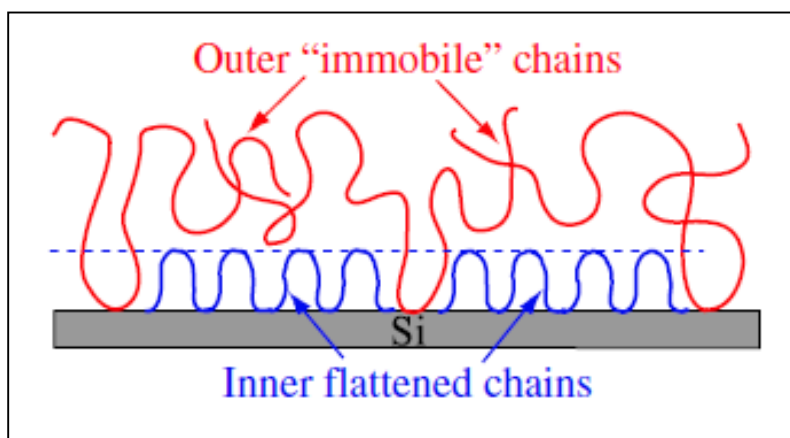


Figure 4-2: The schematic view of the two different chain conformations after the solvent rising supported PS thin film [14].

They were able to expose the flattened layer of thickness 2-3 nm to the air interface after prolonged (120 days) toluene rinsing. Jiang *et al.* [15] replaced toluene with chloroform to more effectively uncover the lone flattened layer.

They study the effect of the polymer/substrate interactions and the time of annealing on the flattened layer structure by using three different homopolymers: polystyrene, poly(2-vinylpyridine), and poly(methyl methacrylate). If the magnitude of the interactions controls the final thickness and the kinetics of the flattened layer formation, this study also reveals that the flattened layer has microscopic “textures” (partially covered surface) with characteristic lengths irrespective of the polymer used. It is not conclusive yet from this study whether the polymer/solid interaction is the main factor to control the size of the dimple structures. Yet another study from the same team (using toluene and chloroform for unleashing the unbound polymer) showed that the higher molecular weight polymer chains with a high chain length can “reel-in” the empty spaces of the flattened layer and develop the “loosely adsorbed polymer chains”, covering the flattened layer which makes the residual film stable compared to the low molecular weight polymers [34]. Xue *et al.* [35] also studied the effect of varying annealing time and molecular weight on the architecture of an irreversibly adsorbed layer of PMMA on quartz made by leaching with benzene. They found that the wettability of the PMMA film depends on the solvent properties. Recalling our previous study reported in Chapter 4, it brought out the possibility of obtaining stable ultrathin polymer films by solvent rinsing method. In short we introduced a two-step top-down approach comprising the preparation of homogeneous thick films by spin-coating and thinning them by rinsing in a good solvent that removes the residual stress and/or the density variation of the PS films inhibiting thermodynamically the dewetting on oxide-free silicon. Although a few studies have been made on solvent rinsing, the role of different solvents on the dissolution or desorption of polymer and thereby on the properties of the residual adsorbed layer remains largely unexplored. In order to understand the same, we perform solvent rinsing with four solvents such as toluene, chloroform, THF and acetone. These solvents selected for the experiments based on their Hansen solubility parameters. The aim is to understand the influence of solvents used for rinsing, on the characteristics of polymer residual layer such as remnant thickness, morphology, stability etc.

4.2 The film prior to solvent rinsing

The initial state of the spin-coated and annealed film (PS/SiO_x-Si) which is used for the later solvent rinsing study is shown in Figure 4-3.

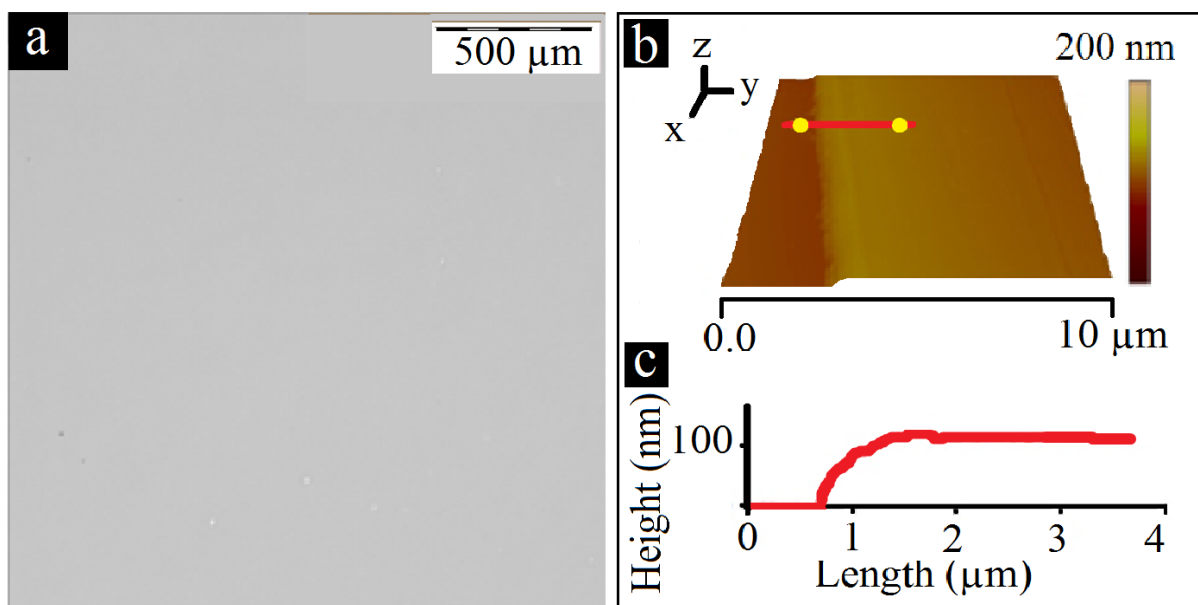


Figure 4-3: a) Optical microscope image of the PS/SiO_x-Si film after spin coating and pre-annealing. b) The 3D presentation of topographic image of PS/SiO_x-Si film obtained using AFM. c) The height profile along the drawn red line.

From the optical microscopic image, the film seems to be continuous without any signature of holes over a large scale. AFM imaging was done to characterize the surface at the nanoscale along with the height information. The AFM image shown in Figure 4-3, b provides the 3D perspective of PS/SiO_x-Si film after spin coating and pre-annealing (i.e. the annealing before solvent rinsing). The step observed in the profile is due to the scratch made on the left end of the film to obtain the thickness with AFM. The thickness is found to be 130 nm. A smooth continuous film is observed with an average roughness value ≈ 0.3 nm. All the experiments in this section are performed with such films. The rinsing is performed with toluene, chloroform, THF and acetone at different times from 5 seconds to 2 hours

4.3 Thickness of polymer residual layer after rinsing with various solvents

Figure 4-4 shows the evolution of the thickness of polymer residual layer after rinsing with toluene, chloroform, THF and acetone.

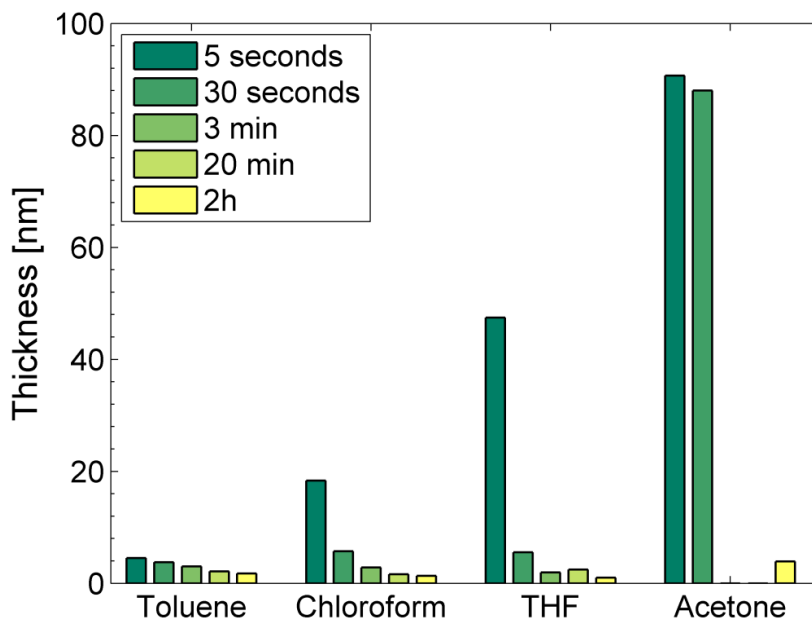


Figure 4-4: Residual thickness (h_{res}) of bound PS after rinsing with different solvents. h_{res} is measured by ellipsometry and complemented with XRR.

It can be seen that the residual film thickness decreases eventually with increased time of rinsing for all the solvents. i.e. as the time of rinsing increases, the residual thickness h_{res} decreases. After 5s of rinsing, the h_{res} value obtained for film rinsed with toluene is measured to be 4.51 nm. Whereas the h_{res} is measured as 18.33, 47.47 and 90.68 nm for films rinsed for 5s with chloroform, THF and acetone respectively. The variations observed in the h_{res} value obtained after rinsing with different solvents can be related to the quality of solvent. Where, the solvent quality is explained by means of the Relative energy difference of the solvents w.r.t. PS, which is acquired from the Hansen solubility parameters as given in Table 4-1.

Table 4-1: The HSP and relative energy difference values PS and some of its good solvents [37][38].

| Solvent | δ_d (MPa ^{0.5}) | δ_p (MPa ^{0.5}) | δ_h (MPa ^{0.5}) | R_d/R_o (Relative energy difference, <i>RED</i>) | Dipolar moment [36] (π/D) |
|-------------|-------------------------------------|----------------------------------|----------------------------------|--|------------------------------------|
| Polystyrene | 21.28 | 5.75 | 4.3 | - | |
| Toluene | 18 | 1.4 | 2 | 0.65 | 0.375 ± 0.010 |
| Chloroform | 17.3 | 3 | 5.6 | 0.67 | 1.04 ± 0.02 |
| THF | 16.8 | 5.7 | 8 | 0.76 | 1.75 ± 0.04 |
| Acetone | 15.5 | 10.5 | 7 | 1 | 2.88 ± 0.03 |

From Table 4-1, the compatibility of selected solvents with PS is in the increasing order from toluene>chloroform>THF>acetone. i.e. for example, due to their low *RED*, the interaction of toluene with PS is higher compared to the other solvents. Consequently toluene can easily remove polymer chains by promoting disentanglement. Thus, the lower the *RED*, the better the extraction of entangled chains from the adsorbed layer. Films having a smaller thickness are thus promoted. This explains why we observe different h_{res} for the same time of rinsing with different solvents.

4.4 The morphology of polymer residual layer after rinsing with various solvents

The morphology of residual films resulting from rinsing with three different solvents, whose residual film thickness (h_{res}) measured with ellipsometry as shown in Figure 4-4 is revealed by the images depicted in Figure 4-5.

For the films rinsed with acetone, there is a higher amount of polymer remaining in the substrate as it is comparatively a poor solvent. Hence the dewetting process is better displayed by optical microscopy as given in Figure 4-6.

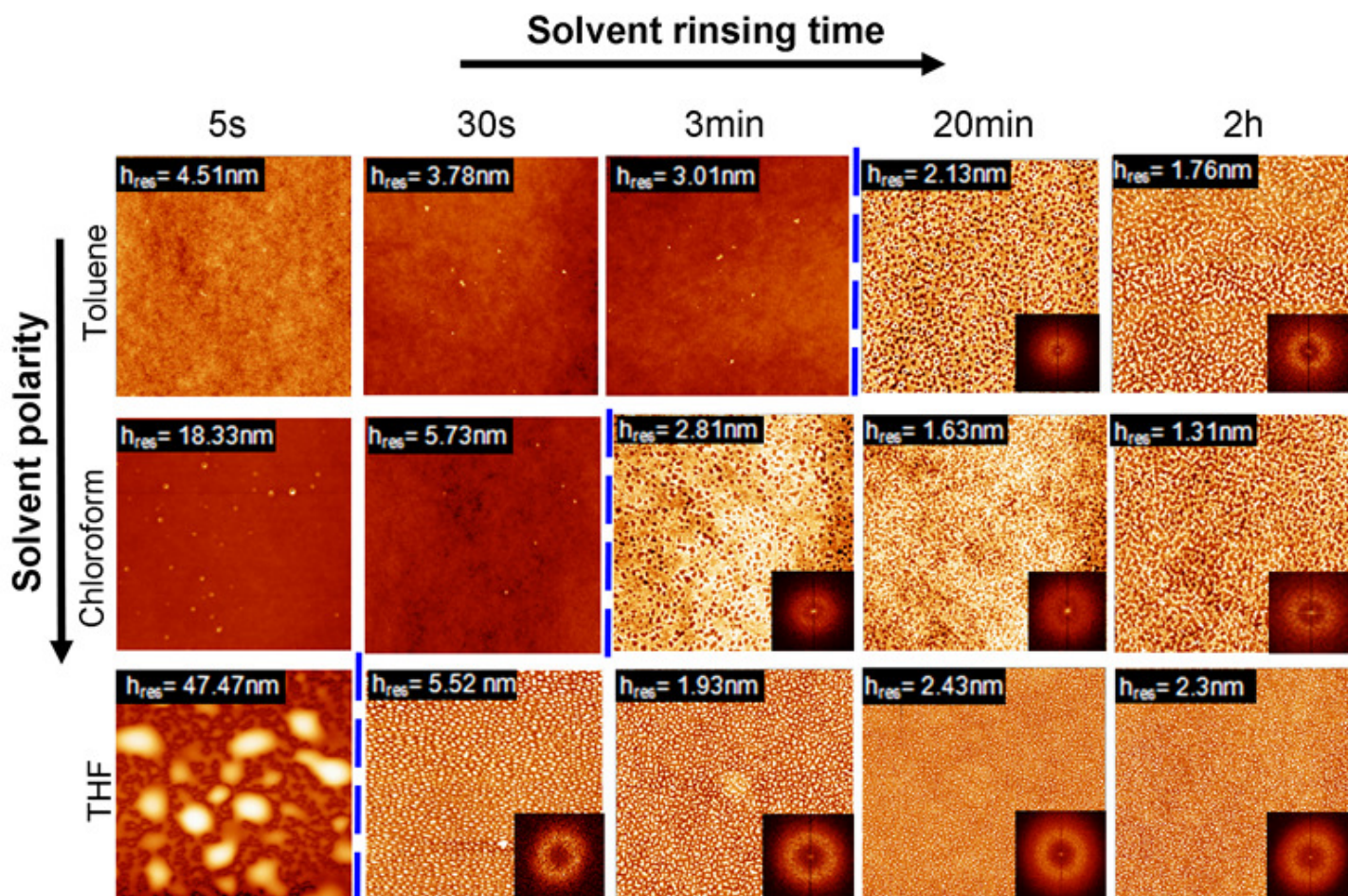


Figure 4-5: AFM topography (scan size = $5 \times 5 \mu\text{m}^2$) of residual film obtained after rinsing with different solvents: a) toluene, b) chloroform, c) THF and d) acetone. The dotted line represents the transition to spinodal dewetting.

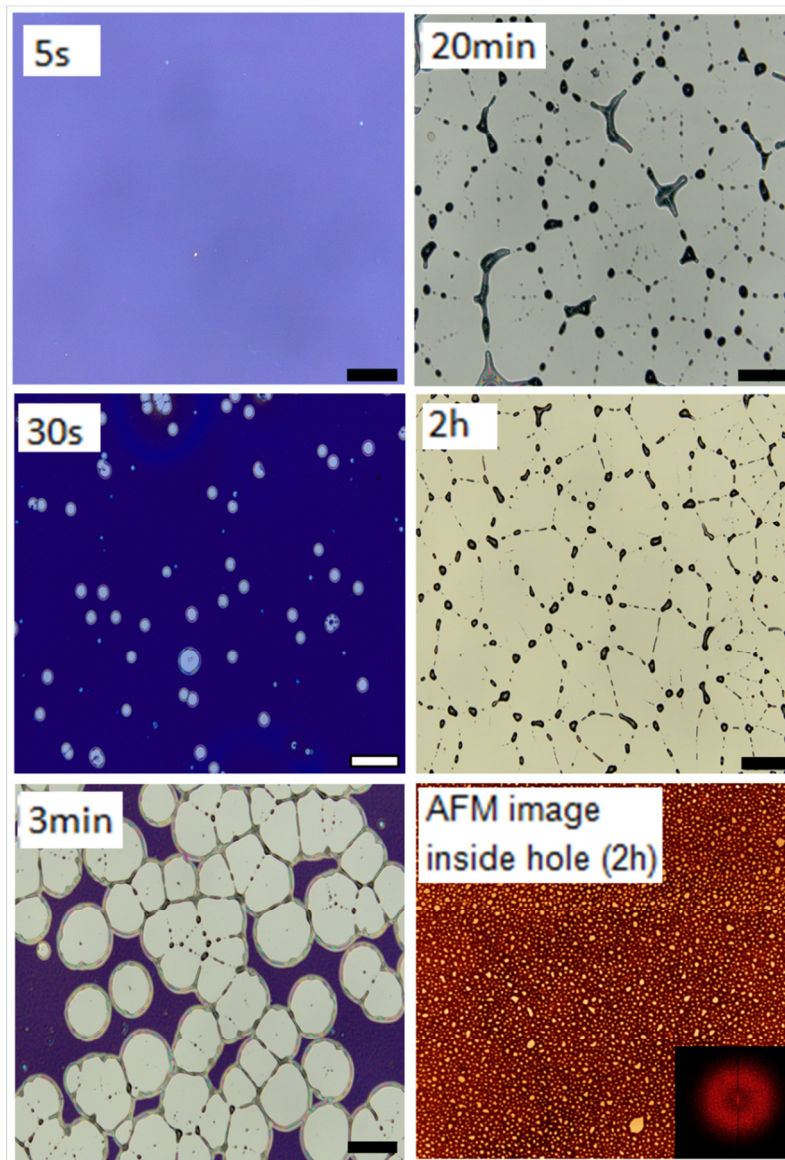


Figure 4-6: Optical images of PS films rinsed with acetone from 5s to 2h (scale bar 100 μm).
The scan size of AFM image = $5 \times 5 \mu\text{m}^2$

It clearly appears that the morphology of the residual films evolves with their thickness, h_{res} . With increased time of rinsing, the initially flat film turns non homogeneous revealing a bicontinuous surface pattern typically observed in spinodal dewetting [39]. All the fluctuations in film thickness are amplified under thermal stimulation even at room temperature (RT) and lead to spontaneous dewetting.

Solvent molecules are known to readily diffuse and saturate the PS film, reducing the glass transition temperature of the polymer below the room temperature and thereby rendering it mobile for reorganization [40], [41]. Thus, once the solvent has leached away the outer loosely attached polymer chains, a solvent-driven dewetting takes place [29], [42]. As depicted in the inset of Figure 4-5 and Figure 4-6, the Fast Fourier transform (FFT) of the images reveals a ring pattern indicating the existence of a preferred wavelength of the instabilities which is the signature of a spinodal dewetting. The blue dotted line points out the transition where the film undergoes a spinodal dewetting in Figure 4-5. Considering the particular case of the THF rinsing, the film is already no more uniform after 5 s of rinsing (thus before the marked dotted line), indicating that the film has started a dewetting process. Whereas we can observe in a larger scale, the smooth film breaks up by the creation of randomly distributed holes in acetone rinsed films also. However, within the experimental error, no correlations of hole sites can be detected from FFT after 5s of rinsing with THF and acetone, which rules out the possibility of a spinodal dewetting. Yet, the presence of a native oxide layer probably makes the film metastable, so that only nucleation (randomly distributed holes) can drive such a thicker films toward dewetting [43].

Yet another striking effect from the film morphology is that all the films after solvent rinsing undergo spinodal dewetting at different instants of rinsing time, i.e., at different values of h_{res} . In the case of toluene rinsed films, the spinodal dewetting is observed after 20 min of rinsing ($h_{res} = 2.1$ nm) while the films rinsed with chloroform exhibits spinodal dewetting after 3 min of rinsing ($h_{res} = 2.8$ nm) and after 30 s for THF rinsed films ($h_{res} = 5.5$ nm). The exact rinsing time at which acetone rinsed film undergo spinodal dewetting is not obtained as AFM imaging is not done inside very small holes observed in the initial stages, but the film from which we obtain the dewetting pattern inside the hole has a thickness of 8 nm. This raises the question: what property of the solvent influences the onset of spinodal dewetting at different h_{res} ?

The dewetting can be influenced by a lot of factors such as composition of polymer [44], film thickness [45], type of substrate used [46], disjoining pressure involved [47] etc. Among the underlying causes of dewetting, Sharma [48] pointed out the fact that the polar interactions cannot be neglected for a thin film sandwiched between a substrate and a semi-infinite fluid.

In a similar way, Lee *et al.* [40] differentiate between thermal dewetting and solutal dewetting where in the former case the instability is caused due to the long-range force of Lifshitz–van der Waals interactions, and in the latter one it can be attributed to the short-range force of polar interactions. Recently, Xu *et al.* [41] demonstrated that PS films which are stable under thermal annealing are rendered unstable to dewetting when contacted by acetone. They explained by the introduction of destabilizing polar interactions, notwithstanding the stabilizing apolar Lifshitz–van der Waals interactions. The work by Verma and Sharma [49] is another good example where they found that strong polar solvents play a significant role in the dewetting process. They were able to fabricate submicron droplets and arrays by the dewetting of ultrathin PS using optimal mixture of water, acetone, and methyl ethyl ketone overcoming the weak destabilizing Lifshitz–van der Waals forces and the high surface energy penalty required for deformations on small scales. Thus from these studies, two key factors that can influence the instability of films which are in contact with a solvent are the solvent polarity and the Lifshitz–van der Waals interactions in the system. In our case, the solvents we used present a significant difference in their dipole moment (tabulated in Table 4-1). From our experimental observations (Figure 4-5 and Figure 4-6) we can surmise that the films rinsed with a solvent having higher polarity dewet faster than the ones rinsed with weakly polar solvents. Hence, the acetone rinsed film dewets before the one rinsed with THF and chloroform respectively. The film rinsed with toluene which has the weakest polarity value undergoes dewetting at a later stage. Our observations are in line with the results of Lee *et al.*, [40] who observed that the acetone-laden film would become unstable first followed by the toluene-laden film. With increased time of rinsing the continued coalescence of holes finally leads to the formation of PS droplets generating a regular pattern of polygons as characteristics of thermal annealing. [50] The use of a poor solvent like acetone prevents a rapid dissolution of the polymer during the first 30s of rinsing. Consequently, the film which is still thick initiates a dewetting by hole nucleation. However, numerical simulations [51] have highlighted that different morphologies (isolated circular holes, droplets, bicontinuous) and their combinations can all be produced by the spinodal decomposition mechanism depending on the form of the intermolecular potential in an extended neighborhood of the film thickness. Thus it is clear from the experimental measurements that when the polarity of the solvents increases, the film is able to dewet earlier, i.e., at a higher residual thickness.

4.5 The stability/instability of polymer residual layer analyzed with Van der Waals - intermolecular theory

In order to predict the stability of the polymer residual layer obtained after rinsing with different solvents, we have to recall the free energy $\Delta F(h)$ and its second derivative $\Delta F''(h)$ which can determine the stability or instability of polymer films as already discussed in chapters 1 and 4. Looking back to the concept, $\Delta F(h)$ is defined as the excess free energy per unit area necessary to bring two interfaces (the substrate–polymer and the polymer–solvent interfaces) from infinity to a certain distance h . The distance h defines the thickness of the polymer layer separating the two interfaces. The sign of the second derivative of the free energy indicates whether the film is stable ($\Delta F''(h) > 0$) or dewets spontaneously ($\Delta F''(h) < 0$). [43] Thus the effective free energy of a system can be represented as follows,

$$\Delta F(h) = \Delta F_{LW}(h) + \Delta F_{AB}(h) + c/h^8 \quad 4-1$$

where $\Delta F_{LW}(h)$ represents the long-range interactions by the Lifshitz-van der Waals potential and $\Delta F_{AB}(h)$ represents the polar contribution by the acid-base interactions in the system. The last term includes short-range electrostatic repulsion of strength c whose value is $1.8 \pm 1 \times 10^{-77} \text{ Jm}^6$ for a silicon wafer with 1.7 nm of native oxide. [43], [46]

We first consider the Lifshitz-van der Waals component, $\Delta F_{LW}(h)$. As the film is totally immersed in the solvent during the time of rinsing, the system can be thought of a 4-layered system like Si/SiO_x/PS/Solvent in which the last layer is the solvent itself. Accordingly, $\Delta F_{LW}(h)$ can be expressed as

$$\Delta F_{LW}(h) = \left(\frac{-A_{Si/PS/Solvent}}{12\pi(h + d_{SiO_x})^2} \right) + \left(\frac{-A_{SiO_x/PS/Solvent}}{12\pi h^2} \right) - \left(\frac{-A_{SiO_x/PS/Solvent}}{12\pi(h + d_{SiO_x})^2} \right) \quad 4-2$$

where $A_{Si/PS/Solvent}$ and $A_{SiO_x/PS/Solvent}$ are the effective Hamaker constants of the Si/PS/Solvent and SiO_x/Ps/Solvent 3 layer systems, respectively. The effective Hamaker constant (A_{132}) of a 3 layer system is calculated using the relation:

$$A_{123} = (\sqrt{A_{11}} - \sqrt{A_{22}})(\sqrt{A_{33}} - \sqrt{A_{22}}) \quad 4-3$$

In our case, equation 4-3 can be written as

$$A_{SiO_2/PS/solvent} = (\sqrt{A_{SiO_2/SiO_2}} - \sqrt{A_{PS/PS}})(\sqrt{A_{solvent/solvent}} - \sqrt{A_{PS/PS}}) \quad 4-4. (a)$$

and

$$A_{Si/PS/solvent} = (\sqrt{A_{Si/Si}} - \sqrt{A_{PS/PS}})(\sqrt{A_{solvent/solvent}} - \sqrt{A_{PS/PS}}) \quad (b)$$

To calculate the effective Hamaker constants of the system, Hamaker constants of each interface (

Table 4-2) were chosen as the average value of values reported in the literature. [52]–[59]

Table 4-2: The Hamaker constants reported in the literature [52]–[59] and their average value used in our calculations.

| | Hamaker constants values reported in literature(J) | Average Hamaker constant value(J) |
|-------------------|--|-----------------------------------|
| $A_{Si/Si}$ | 19 - 24 × 10 ⁻²⁰ | 22.3 × 10 ⁻²⁰ |
| A_{SiO_2/SiO_2} | 5.0 - 6.6 × 10 ⁻²⁰ | 5.8 × 10 ⁻²⁰ |
| $A_{PS/PS}$ | 6.15 - 7.9 × 10 ⁻²⁰ | 7.56 × 10 ⁻²⁰ |

The Hamaker constants of solvents were calculated from their surface tension using the relation [51], [54]:

$$\gamma_i = \frac{A_{ii}}{24 \pi l_0^2} \quad 4-5$$

where γ_i is the surface tension of a solvent i , ' A_{ii} ' is the Hamaker constant (solvent/solvent) and l_o corresponds to the cut-off distance which can be taken equal to 1.57 Å. [54] The calculated values are given in Table 4-3

Table 4-3: Correlation between the surface tension of pure solvents and the effective Hamaker constants of the three layer systems. $\gamma_{Solvent}$ is the surface tension of the pure solvents. $A_{Solvent/Solvent}$ is the Hamaker constant of the solvent, $A_{SiO_2/PS/Solvent}$ and $A_{Si/PS/Solvent}$ are the effective Hamaker constants of $SiO_2/PS/Solvent$ and $Si/PS/Solvent$ three layer systems, respectively. The values are calculated from the average Hamaker constant values in Table 4-2 The Hamaker constants reported in the literature [52]–[59] and their average value used in our calculations.

| | $\gamma_{Solvent}$ (mN/m) | $A_{Solvent/Solvent}$ (10^{-20} J) | $A_{SiO_2/PS/Solvent}$ (10^{-20} J) | $A_{Si/PS/Solvent}$ (10^{-20} J) |
|------------|------------------------------|--|---|--|
| Toluene | 28.40 | 5.28 | -0.89 | 0.15 |
| Chloroform | 27.50 | 5.11 | -0.96 | 0.17 |
| THF | 26.40 | 4.90 | -1.05 | 0.18 |
| Acetone | 25.20 | 4.68 | -1.15 | 0.20 |

The substitution of the tabulated values in equation 4-2 gives the expression for Lifshitz-van der Waals component of the free energy and of its second derivative as a function of the film thickness. The results are represented as in Figure 4-7 for the 4 solvents.

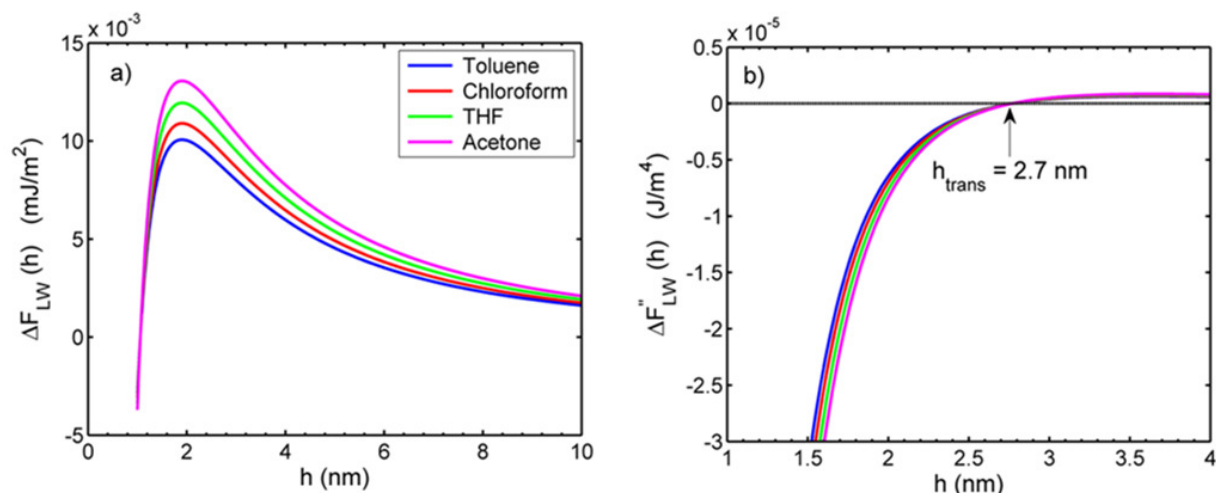


Figure 4-7: (a) Simulation of the Lifshitz-van der Waals component of the free energy ΔF_{LW} and (b) its second derivative $\Delta F''_{LW}(h)$ as a function of film thickness h for PS films for the four layer system $Si/SiO_x/PS/Solvent$ under different solvent media. The effective Hamaker constants are the ones given in Table 4-3 and the thickness of the SiO_x layer was taken to be equal to 1.7 nm.

From Figure 4-7.a, for all the solvents, the excess free energy per unit area, $\Delta F_{LW}(h)$ possess both positive and negative values which points to the fact that the system is unstable for small film thicknesses whereas metastable for larger film thicknesses. [60], [61] The system has to overcome a potential barrier to reach the lowest energy state which is slightly different according to the solvent used. The potential barrier is a bit higher for a film rinsed in acetone and decreases in order for the films rinsed with THF, chloroform and then toluene respectively. It is readily shown that spinodal dewetting can take place only if the second derivative of $\Delta F_{LW}(h)$ with respect to film thickness is negative. From Figure 4-7.b, it is quite amazing to observe that the transition thickness at which the film undergoes spinodal dewetting, h_{trans} is equal to 2.7 ± 1 nm and is the same for all the solvents. Yet from the experimental results, only the toluene-rinsed film shows a spinodal dewetting for a thickness $h_{res} = 2.1$ nm less than $h_{trans} = 2.7$ nm while all other films rinsed with polar solvents experimentally dewet at a thickness which is higher than the calculated value h_{trans} . Since the polarity of toluene is almost negligible, one can logically infer that the difference in these behaviors can be attributed to the contribution of polar interactions. It is thus important to quantify the contribution of the polar component $\Delta F_{AB}(h)$ to the total free energy of the system.

4.6 The stability/instability of polymer residual layer analyzed with effective free energy of the system

The acid-base (*AB*) interactions occur between molecules that display conjugate polarities as measured by their electron (proton) donor and acceptor capabilities. PS is a weakly electron-donor monopolar material but when the polar solvent molecules enter into the PS film, the polar interactions have to be considered. The contribution by short range polar interactions, can be expressed as

$$\Delta F_{AB}(h) = S_p \exp((d_{min} - h)/l) \quad 4-6$$

where S_p is the polar component of spreading coefficient and $\exp((d_{min} - h)/l)$ stands for the decay function describing the short range of the polar interactions with the correlation length l . The decay function for the polar interactions satisfies the relation $\exp((d_{min} - h)/l) = 1$ at a cutoff d_{min} and is 0 at large distances. For water, an estimation of the correlation length is about $l = 0.6$ nm [48] whereas for polymer l can be taken as 2.5 nm. [51] The value of S_p can be evaluated from contact angle measurements. [62]

$$S = S_{LW} + S_p = \gamma_{23} (\cos\theta - 1) \quad 4-7$$

where the spreading coefficient, S is the sum of two terms: the long range Lifshitz-van der Waals dispersive surface energy S_{LW} and the contribution by short range polar interactions S_p . Hence it is possible to estimate the spreading coefficient S by knowing the values of the contact angle θ and of the surface tension. The surface tension γ between PS and the solvent is calculated by the following relation with $\gamma_{PS} = 40.7$ mN/m

$$\gamma_{PS,Solvent} = \gamma_{PS} + \gamma_{Solvent} - 2(\gamma_{PS} * \gamma_{Solvent})^{1/2} \quad 4-8$$

where $\gamma_{Solvent}$ is taken from Table 4-3.

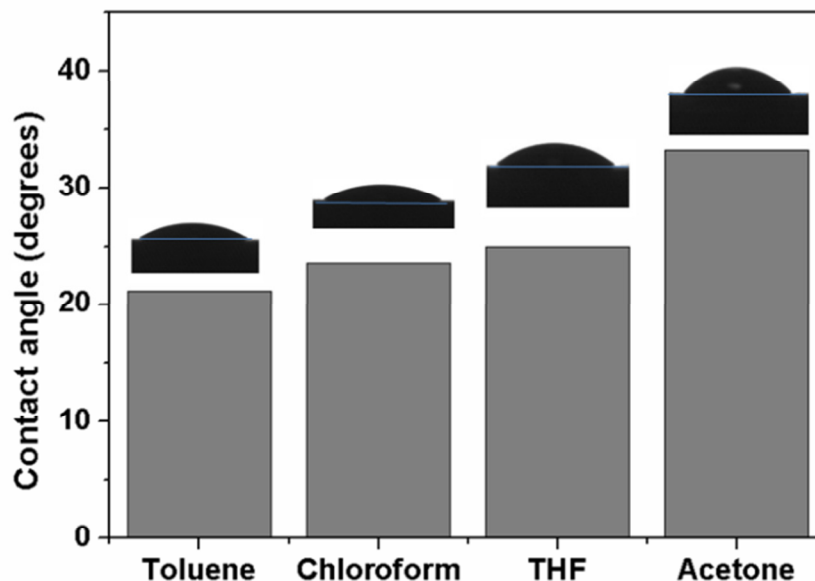


Figure 4-8 : The contact angle values between a bulk PS substrate and various solvents measured by contact angle goniometry. Photographs corresponding to the measurements are given above the bars.

The measurement of the contact angle between PS and various solvents is carried out by means of contact angle goniometry (Figure 4-8). It gives the spreading coefficient values calculated using Eq. 4-7. One can then derive S_p by subtracting the long range Lifshitz-van der Waals dispersive forces S_{LW} to S . For calculating the dispersive forces S_{LW} , we consider the film thickness at d_{min} , which is the equilibrium film thickness of our system at which the free energy $\Delta F_{LW}(h)$ possesses the minimum value. This distance d_{min} is due to equilibrium between the extremely short range repulsion and the attractive LW interactions. At d_{min} , the free energy per unit area and the dispersive forces are related as follows, [48]

$$\Delta F_{LW}(d_{min}) = S_{LW} \quad 4-9$$

Knowing the dependence of each term of Eq. 4-1 with the film thickness h , we have numerically simulated the total free energy $\Delta F(h)$. We fixed the correlation length l to 1.1 nm and the power α to 7.83 in the short-range interaction c/d_{min}^α in order to match the experimental results to the theoretical value $h_{trans.}$. Then the values of S_{LW} calculated from equation 4-9 with $d_{min} = 6 \text{ \AA}$

obtained from the simulation (which is matching with the results of Seeman *et al.* [43], $d_{min} = 8 \text{ \AA}$ for a 1.7 nm thick native oxide layer) are given in the Table 4-4 along with the S_p values obtained thereby. In the numerical simulation, it is interesting to note that the power α plays a role on d_{min} , the location of the minimum of energy (thus affecting the calculation of S_{LW} and S_p) and the correlation length l impacts directly the values of h_{trans} . From Table 4-4, it can be seen that the spreading parameter S_p which represents the contribution of the short range polar interactions to the total free energy of the system increases with increasing polarity of the solvents. Hence it is now clear that the instability is accelerated by the polarity of solvents, which increases in the order $S_{p\text{toluene}} < S_{p\text{Chloroform}} < S_{p\text{THF}} < S_{p\text{acetone}}$.

Table 4-4: Correlation between the surface tension $\gamma_{PS/Solvent}$, the total S , the Lifshitz-van der Waals S_{LW} and the polar S_p spreading coefficients.

| | $\gamma_{PS/Solvent}$ (mN/m) | S (mN/m) | S_{LW} (N/m) x 10^{-5} | S_p (N/m) x 10^{-5} |
|------------|---------------------------------|---------------|-------------------------------|----------------------------|
| Toluene | 1.10 | -0.07 | - 5.92 | -1.53 |
| Chloroform | 1.29 | -0.11 | -6.69 | -4.06 |
| THF | 1.54 | -0.14 | -7.75 | -6.69 |
| Acetone | 1.85 | -0.3 | -8.90 | -21.35 |

Thus by considering the 3 contributions, i.e. the effective contribution of Lifshitz-van der Waals ΔF_{LW} , the polar contribution ΔF_P along with the steric repulsion energy c/h^α , the excess free energy per unit of area ΔF and its second derivative $\Delta F''$ as a function of film thickness h for PS films on native oxide covered Si substrate under different solvent exposures could be simulated. They are plotted in Figure 4-9.

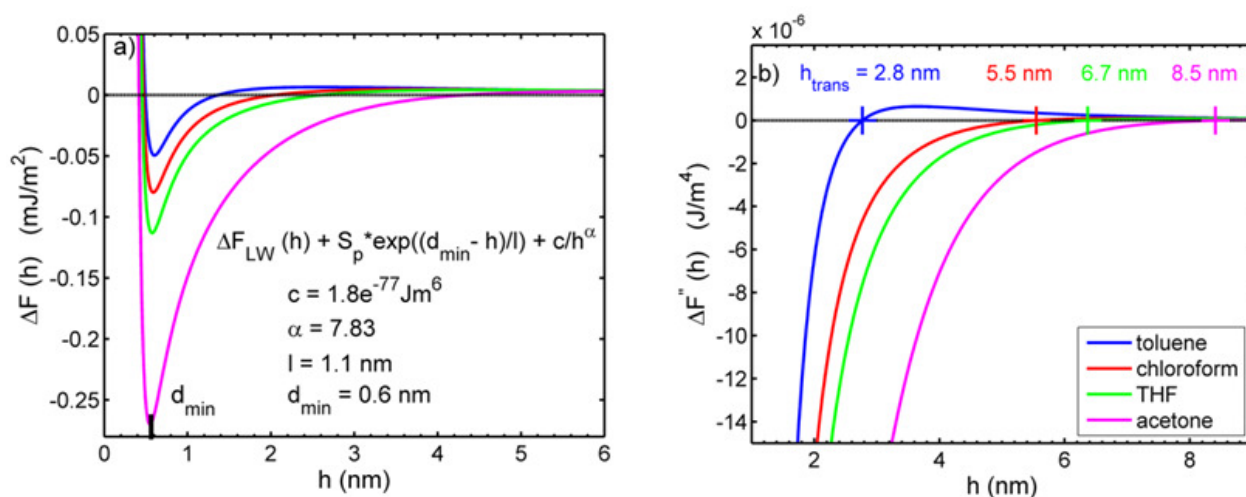


Figure 4-9: Simulation of (a) the effective free energy ΔF and (b) its second derivative $\Delta F''$ as a function of PS film thickness h for a four layer Si/SiO_x/PS/Solvent system. In these simulations, 4 solvents are considered: toluene, chloroform, THF and acetone. The effective free energy takes into account the effective contribution of the Lifshitz-van der Waals ΔF_{LW} and of the polar ΔF_P components as well as the steric repulsion energy c/h^α .

The consideration of polar contributions along with the effect of steric repulsion paves the way to a drastic change in the resulting free energy curves as shown in Figure 4-9. In comparison to toluene rinsed samples (Figure 4-9.a), the acetone laden samples depicts an increase in its negative value of free energy for a smaller thickness, which clearly points out the amplification of instability with increasing polar interactions in the system. From the second derivative of the effective free energy (Figure 4-9.b), h_{trans} is found to be increased with the polarity of the solvent. Consequently the films undergo spinodal dewetting at different thicknesses w.r.t. the type of solvent used. The h_{trans} value of toluene is found to be around 2.8 nm, where we could experimentally observe the spinodal dewetting pattern when its thickness fall below 3 nm i.e. at 2.1 nm. In case of chloroform and THF, h_{trans} is observed at 5.5 nm and 6.7 nm, respectively whose experimental dewetted results estimate h_{trans} to be in the 2.8 – 5.7 nm range and 5.5 – 47.5 nm range, respectively (Figure 4-5). The AFM images inside the hole of the films dewetted by acetone rinsing also exhibits a dewetted pattern at a thickness of 8 nm which is less than its h_{trans} of 8.5 nm. Thus in case of solvents owing to the low polarity (case of toluene), the transition thickness h_{trans} below which the film spinodally dewets can be directly obtained by the Lifshitz-van der Waals theory,

whereas the contribution of the acid base interactions has to be taken in account for the polar solvents. If our numerical simulation undeniably shows the influence of the polar interactions on the transition h_{trans} , we must stress that it is not an absolute calculation but can be considered as a comparative calculation. An example of complexity is the polar AB interactions which decay exponentially for simple liquids, but till date their decay behavior for the polymer–solvent mixtures is not really known.

4.7 Conclusion

Polystyrene thin films supported on SiO_x -Si substrates were rinsed with four different solvents: toluene, chloroform, THF and acetone. These solvents can be defined by their Hansen solubility parameter HSP. We observed that the closer their HSP to the one of PS and the faster the dissolution and desorption of the polymer chains. This is in good agreement with the Relative Energy Difference theory. In addition, we observed for this four layer Si/SiO_x/PS/Solvent system, that the films exhibited two different morphologies depending on their thicknesses h . For $h > h_{trans}$, the films were flat whereas they exhibited spinodal dewetting for $h < h_{trans}$. When toluene was used as solvent, the experimental transition thickness h_{trans} was equal to about 2.8 nm. This value can be explained theoretically by determining the apolar Lifshitz-van der Waals free energy ΔF_{LW} . However, as soon as the other solvents were used for rinsing, h_{trans} was clearly shifting to higher value. In particular, we highlighted a correlation between h_{trans} and the polarity of the solvent. To go deeper into the analyses, the polar acid-base free energy ΔF_{AB} was determined and we demonstrated that the addition of this polar term ΔF_{AB} to the LW free energy can perfectly explain the unstable and metastable domains for the 4 different solvents. Thus from these results, it is interesting to note that we can tune the thickness, morphology, amount of polymer bound to the substrate etc., by employing a solvent specific rinsing.

REFERENCES

- [1] Z. Fakhraai and J. A. Forrest, "Measuring the surface dynamics of glassy polymers.," *Science*, vol. 319, no. 5863, pp. 600–604, 2008.
- [2] N. Delorme, M. S. Chebil, G. Vignaud, V. Le Houerou, J.-F. Bardeau, R. Busselez, A. Gibaud, and Y. Grohens, "Experimental evidence of ultrathin polymer film stratification by AFM force spectroscopy," *Eur. Phys. J. E*, vol. 38, no. 6, p. 56, 2015.
- [3] Z. Yang, Y. Fujii, F. K. Lee, C.-H. Lam, and O. K. C. Tsui, "Glass transition dynamics and surface layer mobility in unentangled polystyrene films.," *Science*, vol. 328, no. 5986, pp. 1676–9, Jul. 2010.
- [4] X. Jie, L. Ding, J. Chen, S. Gao, L. Li, D. Zhou, X. Li, and G. Xue, "Sensitive Characterization of the Influence of Substrate Interfaces on Supported Thin Films," *Macromolecules*, vol. 47, no. 18, pp. 6365–6372, 2014.
- [5] R. P. White, C. C. Price, and J. E. G. Lipson, "Effect of Interfaces on the Glass Transition of Supported and Freestanding Polymer Thin Films," *Macromolecules*, vol. 48, pp. 4132–4141, 2015.
- [6] F. Chen, D. Peng, C.-H. Lam, and O. K. C. Tsui, "Viscosity and Surface-Promoted Slippage of Thin Polymer Films Supported by a Solid Substrate," *Macromolecules*, vol. 48, no. 14, pp. 5034–5039, Jul. 2015.
- [7] O. Guiselin, "Irreversible Adsorption of a Concentrated Polymer Solution," *Europhys. Lett.*, vol. 17, pp. 225–230, 1992.
- [8] C. J. Durning, B. O'Shaughnessy, U. Sawhney, D. Nguyen, J. Majewski, and G. S. Smith, "Adsorption of poly(methyl methacrylate) melts on quartz," *Macromolecules*, vol. 32, pp. 6772–6781, 1999.
- [9] Y. Fujii, Z. Yang, J. Leach, H. Atarashi, K. Tanaka, and O. K. C. Tsui, "Affinity of Polystyrene Films to Hydrogen-Passivated Silicon and Its Relevance to the T_g of the Films," *Macromolecules*, vol. 42, no. 19, pp. 7418–7422, Oct. 2009.

- [10] S. Napolitano, C. Rotella, and M. Wübbenhorst, “Can Thickness and Interfacial Interactions Univocally Determine the Behavior of Polymers Confined at the Nanoscale?,” *ACS Macro Lett.*, vol. 1, no. 10, pp. 1189–1193, Oct. 2012.
- [11] S. Napolitano, A. Pilleri, P. Rolla, and M. Wübbenhorst, “Unusual Deviations from Bulk Behavior in Ultrathin Films of Poly(tert-butylstyrene): Can Dead Layers Induce a Reduction of T_g?,” *ACS Nano*, vol. 4, no. 2, pp. 841–848, Feb. 2010.
- [12] S. Napolitano and M. Wübbenhorst, “The lifetime of the deviations from bulk behaviour in polymers confined at the nanoscale,” *Nat. Commun.*, vol. 2, p. 260, Mar. 2011.
- [13] T. Koga, N. Jiang, P. Gin, M. K. Endoh, S. Narayanan, L. B. Lurio, and S. K. Sinha, “Impact of an irreversibly adsorbed layer on local viscosity of nanoconfined polymer melts,” *Phys. Rev. Lett.*, vol. 107, no. 22, pp. 1–5, 2011.
- [14] P. Gin, N. Jiang, C. Liang, T. Taniguchi, B. Akgun, S. K. Satija, M. K. Endoh, and T. Koga, “Revealed Architectures of Adsorbed Polymer Chains at Solid-Polymer Melt Interfaces,” *Phys. Rev. Lett.*, vol. 109, no. 26, p. 265501, Dec. 2012.
- [15] N. Jiang, J. Shang, X. Di, M. K. Endoh, and T. Koga, “Formation Mechanism of High-Density, Flattened Polymer Nanolayers Adsorbed on Planar Solids,” *Macromolecules*, vol. 47, pp. 2682–2689, 2014.
- [16] J. K. Bal, T. Beuvier, A. B. Unni, E. A. Chavez Panduro, G. Vignaud, N. Delorme, M. S. Chebil, Y. Grohens, and A. Gibaud, “Stability of Polymer Ultrathin Films (<7 nm) Made by a Top-Down Approach,” *ACS Nano*, vol. 9, no. 8, pp. 8184–8193, Aug. 2015.
- [17] S. Napolitano, *Non-equilibrium Phenomena in Confined Soft Matter: Irreversible Adsorption, Physical Aging and Glass Transition at the Nanoscale*. Springer, 2015.
- [18] S. Napolitano and D. Cangialosi, “Interfacial Free Volume and Vitrification: Reduction in T,” *Macromolecules*, vol. 46, pp. 8051–8053, 2013.
- [19] D. Cangialosi, “Effect of Confinement Geometry on Out-of-Equilibrium Glassy Dynamics,” in *Non-equilibrium Phenomena in Confined Soft Matter*, Springer, 2015, pp. 265–298.

- [20] M. Asada, N. Jiang, L. Sendogdular, P. Gin, Y. Wang, M. K. Endoh, T. Koga, M. Fukuto, D. Schultz, M. Lee, X. Li, J. Wang, M. Kikuchi, and A. Takahara, "Heterogeneous Lamellar Structures Near the Polymer/Substrate Interface," *Macromolecules*, vol. 45, no. 17, pp. 7098–7106, Sep. 2012.
- [21] B. Vanroy, M. Wübbenhorst, and S. Napolitano, "Crystallization of thin polymer layers confined between two adsorbing walls," *ACS Macro Lett.*, vol. 2, no. 2, pp. 168–172, Feb. 2013.
- [22] X. Zheng, M. H. Rafailovich, J. Sokolov, Y. Strzhemechny, S. A. Schwarz, B. B. Sauer, and M. Rubinstein, "Long-Range Effects on Polymer Diffusion Induced by a Bounding Interface," *Phys. Rev. Lett.*, vol. 79, no. 2, pp. 241–244, 1997.
- [23] G. Vignaud, J. F. Bardeau, A. Gibaud, and Y. Grohens, "Multiple glass-transition temperatures in thin supported films of isotactic PMMA as revealed by enhanced raman scattering," *Langmuir*, vol. 21, no. 19, pp. 8601–8604, 2005.
- [24] S. Ata, K. Ito, Y. Kobayashi, and T. Ougizawa, "Possible origin of reduced glass transition temperatures of spin-cast ultrathin polystyrene films," *Chem. Phys. Lett.*, vol. 517, no. 1–3, pp. 68–70, Nov. 2011.
- [25] D. Qi, Z. Fakhraai, and J. A. Forrest, "Substrate and chain size dependence of near surface dynamics of glassy polymers," *Phys. Rev. Lett.*, vol. 101, no. 9, pp. 1–4, 2008.
- [26] G. Vignaud, M. S. Chebil, J. K. Bal, N. Delorme, T. Beuvier, Y. Grohens, and A. Gibaud, "Densification and Depression in Glass Transition Temperature in Polystyrene Thin Films," *Langmuir*, vol. 30, pp. 11599–11608, 2014.
- [27] V. Marcon and N. F. A. van der Vegt, "How does low-molecular-weight polystyrene dissolve: osmotic swelling vs. surface dissolution," *Soft Matter*, vol. 10, pp. 9059–9064, 2014.
- [28] B. A. Miller-Chou and J. L. Koenig, "A review of polymer dissolution," *Prog. Polym. Sci.*, vol. 28, pp. 1223–1270, Aug. 2003.

- [29] J. You, S. Zhang, G. Huang, T. Shi, and Y. Li, "Solvent annealing induced phase separation and dewetting in PMMA/SAN blend film: Film thickness and solvent dependence," *J. Chem. Phys.*, vol. 138, no. 24, pp. 3943–3948, 2013.
- [30] C. Yu and S. Granick, "Revisiting Polymer Surface Diffusion in the Extreme Case of Strong Adsorption," *Langmuir*, vol. 30, no. 48, pp. 14538–14544, Dec. 2014.
- [31] I. Devotta, V. D. Ambeskar, A. B. Mandhare, and R. A. Mashelkar, "The life time of a dissolving polymeric particle," *Chem. Eng. Sci.*, vol. 49, no. 5, pp. 645–654, 1994.
- [32] N. Jiang, L. Sendogdular, X. Di, M. Sen, P. Gin, M. K. Endoh, T. Koga, B. Akgun, M. Dimitriou, and S. Satija, "Effect of CO₂ on a Mobility Gradient of Polymer Chains near an Impenetrable Solid," *Macromolecules*, vol. 48, pp. 1795–1803, 2015.
- [33] Z. Huang, H. Ji, J. W. Mays, and M. D. Dadmun, "Understanding the grafting of telechelic polymers on a solid substrate to form loops," *Macromolecules*, vol. 41, no. 3, pp. 1009–1018, 2008.
- [34] N. Jiang, J. Wang, X. Di, J. Cheung, W. Zeng, M. K. Endoh, T. Koga, and S. K. Satija, "Nanoscale adsorbed structures as a robust approach for tailoring polymer film stability," *Soft Matter*, vol. 12, no. 6, pp. 1801–1809, 2016.
- [35] L. Xue and Y. Han, "Autophobic dewetting of a poly(methyl methacrylate) thin film on a silicon wafer treated in good solvent vapor," *Langmuir*, vol. 25, no. 24, pp. 5135–5140, 2009.
- [36] D. R. Lide, *CRC Handbook of Chemistry and Physics*. 2003.
- [37] D. C. Sherrington, "Preparation, structure and morphology of polymer supports," *Chem. Commun.*, no. 21, pp. 2275–2286, 1998.
- [38] D. Kim, S. Park, Y. Choi, and S. K. Lee, "Optimization of Solvent for the Determination of Polybrominated Diphenyl Ethers in High-Impact Polystyrene by GC / ECD," *Bull. Korean Chem. Soc.*, vol. 33, no. 10, pp. 3485–3488, 2012.
- [39] R. Xie, A. Karim, J. Douglas, C. Han, and R. Weiss, "Spinodal Dewetting of Thin Polymer Films," *Phys. Rev. Lett.*, vol. 81, no. 6, pp. 1251–1254, 1998.

- [40] S. H. Lee, P. J. Yoo, S. J. Kwon, and H. H. Lee, "Solvent-driven dewetting and rim instability," *J. Chem. Phys.*, vol. 121, no. 2004, pp. 4346–4351, 2004.
- [41] L. Xu, A. Sharma, and S. W. Joo, "Dewetting of stable thin polymer films induced by a poor solvent: Role of polar interactions," *Macromolecules*, vol. 45, pp. 6628–6633, 2012.
- [42] S. Zhang, T. Shi, J. You, and Y. Li, "Solvent annealing induced phase separation and dewetting in PMMA/SAN blend films: composition dependence," *Polym. Chem.*, vol. 4, no. 14, pp. 3943–3948, 2013.
- [43] R. Seemann, S. Herminghaus, and K. Jacobs, "Dewetting Patterns and Molecular Forces: A Reconciliation," *Phys. Rev. Lett.*, vol. 86, no. 24, pp. 5534–5537, Jun. 2001.
- [44] J. You, S. Hu, Y. Liao, K. Song, Y. Men, T. Shi, and L. An, "Composition effect on dewetting of ultrathin films of miscible polymer blend," *Polymer.*, vol. 50, no. 19, pp. 4745–4752, 2009.
- [45] J. You, Y. Liao, Y. Men, T. Shi, and L. An, "Film Thickness Dependence of Phase Separation and Dewetting Behaviors in PMMA/SAN Blend Films," *Langmuir*, vol. 26, no. 18, pp. 14530–14534, 2010.
- [46] R. Seemann, S. Herminghaus, and K. Jacobs, "Gaining control of pattern formation of dewetting liquid films," *J. Phys. Condens. Matter*, vol. 13, no. 21, p. 4925, 2001.
- [47] H. I. Kim, C. M. Mate, K. A. Hannibal, and S. S. Perry, "How Disjoining Pressure Drives the Dewetting of a Polymer Film on a Silicon Surface," *Phys. Rev. Lett.*, vol. 82, no. 17, pp. 3496–3499, 1999.
- [48] A. Sharma, "Relationship of Thin Film Stability and Morphology to Macroscopic Parameters of Wetting in the Apolar and Polar Systems," *Langmuir*, vol. 28, no. 23, pp. 861–869, 1993.
- [49] A. Verma and A. Sharma, "Submicrometer pattern fabrication by intensification of instability in ultrathin polymer films under a water-solvent mix," *Macromolecules*, vol. 44, no. 12, pp. 4928–4935, 2011.

- [50] G. Reiter, "Dewetting of thin polymer films," *Phys. Rev. Lett.*, vol. 68, no. 1, pp. 75–78, Jan. 1992.
- [51] A. Sharma and R. Khanna, "Pattern Formation in Unstable Thin Liquid Films," *Phys. Rev. Lett.*, vol. 81, no. 16, pp. 3463–3466, 1998.
- [52] H. D. Ackler, R. H. French, and Y.-M. Chiang, "Comparisons of Hamaker constants for ceramic systems with intervening vacuum or water: From force laws and physical properties," *J. Colloid Interface Sci.*, vol. 179, pp. 460–469, 1996.
- [53] L. Bergström, "Hamaker constants of inorganic materials," *Adv. Colloid Interface Sci.*, vol. 70, pp. 125–169, 1997.
- [54] J. N. Israelachvili, *Intermolecular and surface forces*. Academic Press London, 1991.
- [55] H. Zhao, Y. J. Wang, and O. K. C. Tsui, "Dewetting induced by complete versus nonretarded van der Waals forces.," *Langmuir*, vol. 21, no. 13, pp. 5817–24, Jun. 2005.
- [56] D. B. Hough and L R. White, "The calculation of hamaker constants from liftshitz theory with applications to wetting phenomena," *Adv. Colloid Interface Sci.*, vol. 14, no. 1, pp. 3–41, 1980.
- [57] T. Kerle, R. Yerushalmi-Rozen, J. Klein, and L. J. Fetters, "van der Waals stable thin liquid films : Correlated undulations and ultimate dewetting," *Eur. Lett.*, vol. 44, no. 4, pp. 484–490, 1998.
- [58] A. Sharma and G. Reiter, "Instability of Thin Polymer Films on Coated Substrates: Rupture, Dewetting, and Drop Formation," *J. Colloid Interface Sci.*, vol. 178, no. 2, pp. 383–399, 1996.
- [59] C. J. Van Oss, M. K. Chaudhury, and R. J. Good, "Interfacial Lifshitz-van der Waals and polar interactions in macroscopic systems," *Chem. Rev.*, vol. 88, no. 6, pp. 927–941, 1988.
- [60] A. Sharma and R. Khanna, "Pattern formation in unstable thin liquid films under the influence of antagonistic short- and long-range forces.," *J. Chem. Phys.*, vol. 110, no. 10, pp. 4929–4936, 1999.

- [61] L. Xue and Y. Han, “Pattern formation by dewetting of polymer thin film,” *Prog. Polym. Sci.*, vol. 36, no. 2, pp. 269–293, 2011.
- [62] Y. Li, J. Q. Pham, K. P. Johnston, and P. F. Green, “Contact Angle of Water on Polystyrene Thin Films : Effects of CO 2 Environment and Film Thickness,” *Langmuir*, vol. 23, pp. 9785–9793, 2007.

Chapter 5. Stability and glass transition temperature of residual films on H-Si wafers

Summary

After the discussions about the polymer residual layer and its extraction in the previous chapters, this chapter is mainly dedicated to the study of glass transition behavior of the polymer residual layers. The thickness, morphology, stability etc. of the residual layers which are obtained by means of rinsing with four different solvents are analyzed, which is then followed by the analysis of glass transition properties by means of spectroscopic ellipsometry.

5.1 Introduction

The glass transition temperature is a particularly important physical property for thin film applications since it marks the temperature at which a number of physical properties of the polymer change such as the coefficient of thermal expansion, mechanical modulus and loss (and their dielectric and acoustical equivalents), rate of diffusion through the polymer and many other properties. [1] Moving towards its concept, the polymers which are semi-crystalline possess both amorphous and crystalline regions. Depending on the temperature, the region which is amorphous can be either in the glassy or rubbery state. The temperature at which the transition in the amorphous regions between the glassy and rubbery state occurs is called the glass transition temperature, T_g . Considering a more quantitative characterization of T_g , in cooling an amorphous material from the liquid state, at the glass transition temperature, there is a change in slope of the curve of specific volume vs. temperature, moving from a low value in the glassy state to a higher value in the rubbery state over a range of temperatures. This is illustrated in Figure 5-1. From this figure, the intersection of the two straight line segments of curve for the amorphous material defines the glass transition temperature, T_g .

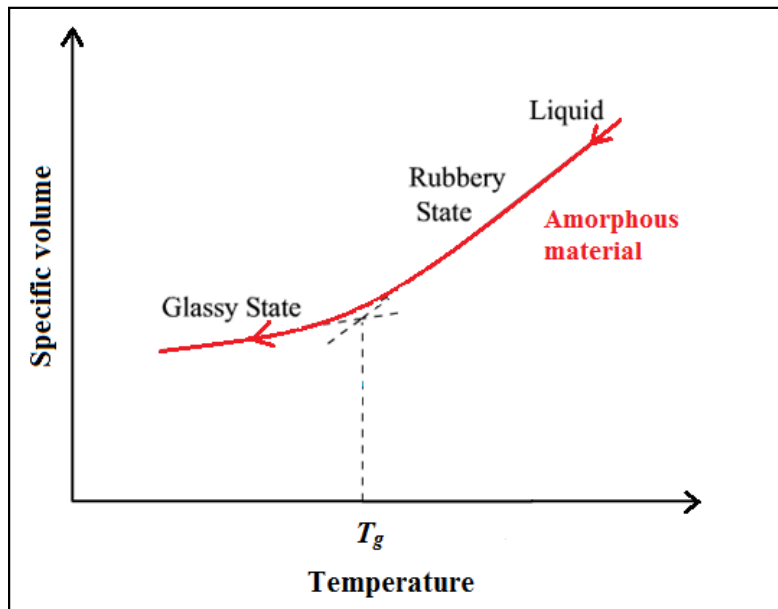


Figure 5-1: Schematic representation for the temperature transitions observed in an amorphous material

Here we study polymer residual layers, which are supported thin films confined by their thickness. When the polymer films are confined by their thickness, their glass transition temperature nature remains elusive. In presence of a substrate, the film is considered to have a gradient of mobility along the confinement dimension, which is well explained by a trilayer model which consists of a liquid like free surface region, a reduced mobility layer near the substrate and a bulk like layer in between. [2], [3] Various studies reported that the T_g is reduced in the proximity of the free surface, whereas an increased T_g is reported near the adsorbing interface due to the slow molecular motion.[4]–[6] So the T_g shifts observed in thin films can be generally interpreted in terms of the combined influences of the substrate and free surface. [7], [8] Focusing on the residual polymer adsorbed to the substrate, it is found to have a significant influence in the film T_g . An increase in T_g is widely reported for polymers exhibiting strong attractive interactions with the substrate when film thickness decreases below a critical value. [4], [9]–[17] On the other hand, decrease in T_g is observed for polymers lacking such attractive interactions with the substrate. [18]–[22] The neutron reflectivity studies on polycarbonate films less than 20 nm resulted in elevated T_g , which points to the fact that the dynamics of the adsorbed polymer chains in the direction normal to the film surface is strongly hindered even above temperature greater than T_g . [23] Apart from this, the residual layer is found to be the reason for the existence of an increase in the local viscosity while approaching the substrate. Various studies showed that the segmental mobility is enhanced near the proximity of the irreversibly adsorbed polymer layer.[24]–[28] An increased film density was reported near the substrate polymer interface in recent simulations,[29] which is matching with the results obtained by ellipsometry [30] and X ray reflectivity. [31] It is also evidenced that the crystalline structure of film is controlled by the polymer substrate interface. [32], [33] So, as the study about the polymer residual layer being significant, it is interesting to know how one can obtain the details of the same. Along with many studies that probed the substrate interface effects within the supported polymer thin film based on the concept of multi-layer structuration, [2]–[4], [13], [18], [34] many studies were done exclusively on the residual layer by removing the bulk and surface layer of film, which revealed various properties and influence of residual layer in the system. In such cases, usually the residual layer is revealed (removing bulk and surface layers) by means of rinsing with a good solvent as proposed by Guiselin, who found that the polymer chains adsorbed on the substrate are retained after rinsing supported thin film with a good solvent. [35]–[39]

The significance of selecting the solvents for such extraction of residual layer is discussed in the previous chapter. [40] A recent study by Gin *et. al* throws light on the fact that the adsorbed layers are composed of the two different nano architectures: flattened chains that constitute the inner higher density region of the adsorbed layers and loosely adsorbed polymer chains that form the outer bulk like density region. [31] A later study from the same group on the flattening process of polymer chains postulated that increasing the number of surface-segmental contacts (i.e., enthalpic gain) is the driving force for the flattening process of the polymer chains, even onto a weakly interactive solid to overcome the conformational entropy loss in the total free energy. [41] Studies done on the kinetics of irreversible adsorption showed two adsorption regimes based on the time evolution of adsorbed layer thickness that is linear at short times and logarithmic at longer times, separated by a temperature independent crossover thickness and a molecular weight independent crossover time. [42] The study on the distribution of glass transition temperatures and dielectric relaxation strength inside ultrathin polymer films based on the residual layer proved that the chain organization and its evolution upon annealing are key parameters in rationalizing the thermal properties of polymer layers at interface. [43] Even if numerous studies that investigated the details of polymer residual layer exist, a pivotal parameter which is less understood from literature is the glass transition behavior of the polymer residual layer. Among the existing reports, no significant changes in the thickness of flattened layer were observed with the temperature XR experiments up to 200 °C for polymers such as P2VP, PS and PMMA. [38] On contrary, modulated thermal gravimetric analysis of PMMA films resulted in a single transition for bulk and broader two-component transitions for the adsorbed polymer layer. [44] A recent study by the fluorescence bilayer method also found a substantial reduction in T_g as compared to bulk due to the influence of the free surface. They could recover the bulk T_g on a time scale reflecting the degree of adsorption, by submerging the adsorbed layer by the deposition of an additional layer above the residual layer. [45] Considering the existing disparity in the reported residual layer T_g , the prime objective of this chapter is to investigate the glass transition behavior of polystyrene residual layers on silicon (Si) wafer, addressing the uncertainty, whether the residual layer is mobile or not ?

5.2 Thickness and morphology of polymer residual layer after rinsing with various solvents

When the PS on H terminated Si wafer (PS-H/Si) thin films with an initial thickness of around 130 nm are rinsed with various solvents for 20 mins, we obtain the residual layers with the thicknesses as shown in Figure 5-2 after the post annealing. It is clear from the figure that the residual polymer thickness is influenced by the type of the solvent. The residual polymer thickness increases in order after rinsing with toluene, chloroform, THF and acetone. This can be explained by the relative energy difference (*RED*) between the polymer and the solvent used for rinsing which is calculated by means of the Hansen solubility parameters. [46] The details of which is given in Chapter 4. [40] It is important to consider this thermodynamic parameter as a solvent is said to be compatible (good solvent) for the polymer, if they possess similar solubility parameters [47]. According to Hansen's theory, lesser the relative energy difference between the polymer and solvent, better is the solubility. Considering the solvents we used here, their compatibility with PS is in the increasing order from toluene > chloroform > THF > acetone. (The relative energy difference between each solvent and PS is already discussed in chapter 4. Table 4-1)

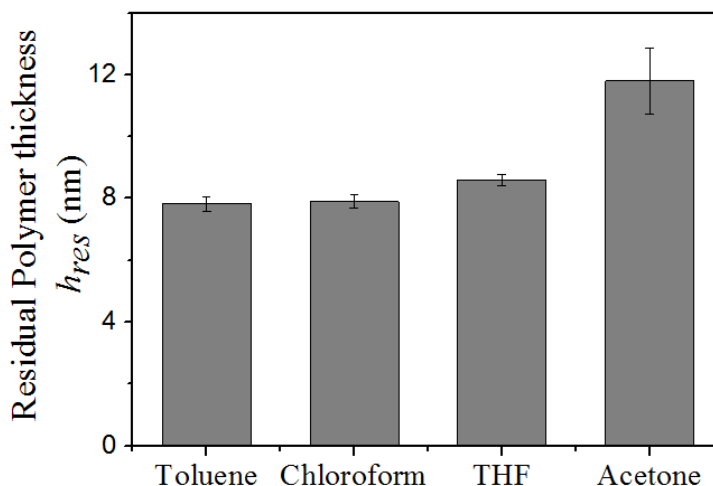


Figure 5-2. Residual thickness (h_{res}) of PS obtained by ellipsometry after rinsing with various solvents and post annealing (Acetone PS-HF is approximate value)

That is, toluene possesses the lowest *RED* value and acetone the highest. Hence considering its low *RED* value, the interaction of toluene with PS is higher compared to the other solvents. So toluene can easily remove polymer chains by boosting chain disentanglement. That is, lower the *RED* value, the better the extraction of entangled chains from the adsorbed layer which can explain the increase in residual layer thickness with increasing relative energy difference.

Considering the morphology of the residual layer, there was no detectable details obtained with optical microscope except for acetone rinsed samples, which is shown in Figure 5-3. Here the polymer agglomerates are oriented in the form of polygonal structure, leaving holes in the film resembling a dewetting pattern.

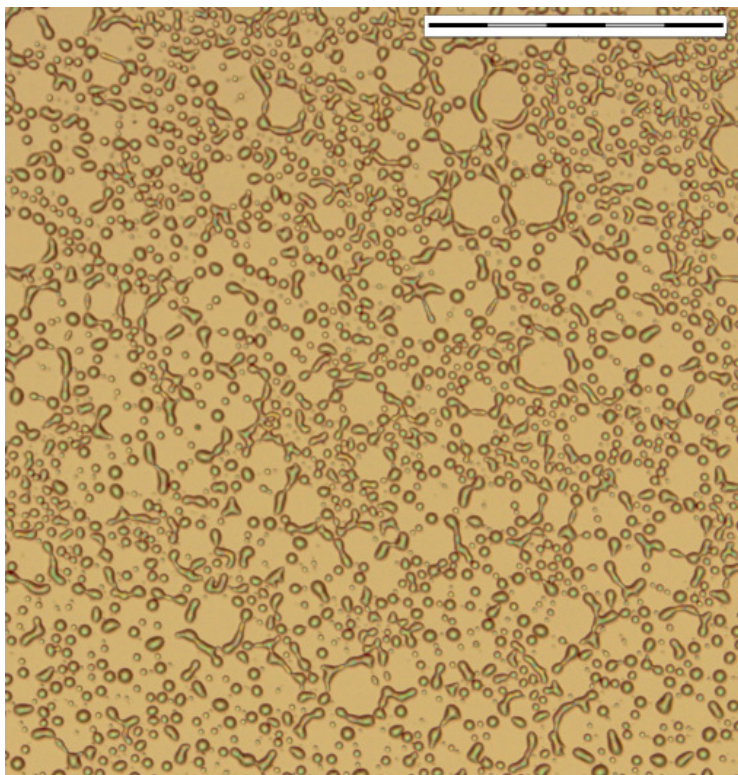


Figure 5-3. Optical microscope images showing the PS/H-Si after rinsing with acetone and post annealing (Scale bar: 500 μm)

The measured height of the agglomerated polymer is in the range of 400 nm to 1 μ m. In this case, the acetone molecules readily diffuses and saturates the PS film, reducing the glass transition temperature of the polymer below the room temperature and thereby rendering it mobile for reorganization. [48] Being a polar solvent, acetone can additionally induce a strong destabilizing electrostatic force. [49] The rapid polymer dissolution favoured by good solvents make the polymer reorganization undetectable by the optical microscope.

As highlighted by Lee *et al* [50] in a similar system, this kind of rim instability is the sign of dewetting induced mainly by the solvent polarity which is a type II rim instability in which the rim undulation leads to finger formation followed by breaking of these fingers into droplets. It is also pertinent that the thermally annealed thin polymer films that are stable on higher energy substrates owing to stabilizing repulsive van der Waals force can be made unstable at room temperature by contact with vapor of a poor solvent and to a much greater extent, by immersing them in the same liquid solvent. [48], [51] A recent study by Al-Khayat *et. al.* also reported that the PS films dewetted readily in a mixture of the vapor of a good solvent and a nonsolvent compared to a dewetting solely by good solvent. [52] Similar studies could even find some practical application, for example, to fabricate submicron droplets and arrays by the dewetting of ultrathin PS using strong polar solvents, overcoming the weak destabilizing Lifshitz–van der Waals forces and the high surface energy penalty required for deformations on small scales. [53] Thus the unique dewetting pattern observed for the sample rinsed with acetone is due to the solvent polarity and the low dissolution of polymer.

In order to characterize the residual layer remaining after rinsing with other solvents, we employed AFM imaging. In case of acetone, (Figure 5-4, d) the AFM image represents the topography inside the hole of dewetted PS film. (That is the bound polymer inside the hole, which is obtained by means of rinsing with a poor solvent is investigated) The polystyrene remaining on H-Si substrate is devoid of any specific features. It seems to be stable irrespective of the solvent used for rinsing.

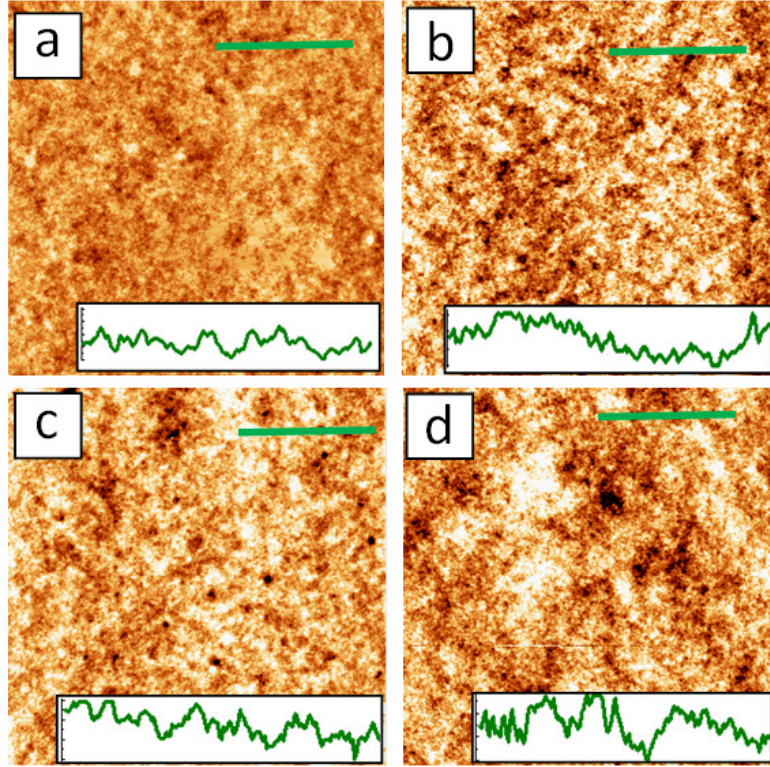


Figure 5-4. AFM images of PS/H-Si after rinsing with solvents a) toluene, b) chloroform, c) THF and d) acetone and post annealing. Scan size ($5 \times 5 \mu\text{m}^2$). Inset shows the surface profiles which scales from 0-1.4 nm.

5.3 The stability/instability of polymer residual layer analyzed with Van der Waals - intermolecular theory

The stability of films is often discussed in terms of the effective interfacial potential of the system, which is the excess free energy per unit area to bring two interfaces from infinity to a specific distance, h . The distance h defines the thickness of the liquid layer separating the two interfaces. The sign of second derivative of the interfacial potential indicates whether the film is stable ($\Delta F''(h) > 0$) or dewets spontaneously ($\Delta F''(h) < 0$). [54] That effective free energy of a system can be represented as follows,

$$\Delta F(h) = \Delta F_{LW}(h) + \Delta F_{AB}(h) + c/h^8 \quad 5-1$$

where $\Delta F_{LW}(h)$ represents the long-range interactions by the Lifshitz-van der Waals potential, $\Delta F_{AB}(h)$ represents the polar contribution by the acid-base interactions in the system and the last term includes short-range electrostatic repulsion of strength 'c'. The Lifshitz-van der Waals component, $\Delta F_{LW}(h)$ can be written as follows,

$$\Delta F_{LW}(h) = \left(\frac{-A_{Si/PS/Solvent}}{12\pi(h)^2} \right) \quad 5-2$$

where $A_{Si/PS/Solvent}$ is the effective Hamaker constants of the Si/PS/Solvent and 3 layer system. The contribution by short range polar interactions, can be expressed as

$$\Delta F_{AB}(h) = S_p \exp((d_{min} - h)/l) \quad 5-3$$

where S_p is the polar component of spreading coefficient and $\exp((d_{min} - h)/l)$ stands for the decay function describing the short range of the polar interactions with the correlation length l . The decay function for the polar interactions satisfies the relation $\exp((d_{min} - h)/l) = 1$ at a cutoff d_{min} and is 0 at large distances. For polymer l can be taken as 2.5 nm. [55]

In our case, the films are immersed in solvents which is capable of removing the non-adsorbed chains and thus reducing the film thickness and thereby stability. i.e. the film instability is accelerated compared to condition when the film is situated in air medium. From our previous study in chapter 4, the PS/SiOx-Si is unstable and it spinodally dewets at different thicknesses with respect to the type of solvent used. [40] Hence it is interesting to see what happens when the PS/H-Si is in contact with various solvents. Figure 5-5 shows the effective interfacial potential and its second derivative as a function of the film thickness which is plotted using the parameters listed in Table 5-1. From the $\Delta F(h)$ curve, it possess both positive and negative values which points to the fact that the system is unstable for small film thicknesses whereas metastable for larger film thicknesses. [56], [57] Apart from the film rinsed with toluene, from the second derivative of interfacial potential, the films undergo spinodal dewetting under a thickness of ~7nm. (For PS/H-Si, the residual thickness values we obtained are 7.83, 7.9, 8.62 and 11.8 nm respectively. That is none of the films are supposed to dewet spinodally above 7 nm, which is in line with our experimental observation.

Another point to be noted in theoretical simulation is that, irrespective of the thickness, the toluene rinsed films are stable and the instability is accelerated by the increasing polarity of solvents. This is also in agreement with the topography of the toluene rinsed PS/H-Si (Figure 5-4, ii, a). Even if there is no spinodal dewetting pattern observed for rest of samples (Figure 5-4, ii, b, c and d), some random hole initiations can be observed, which is not surprising as their thickness lies in the border line of transition from positive to negative considering the second derivative of interfacial potential. At this stage, it is also to be remembered that the solvent polarity can accelerate the instability. [58]

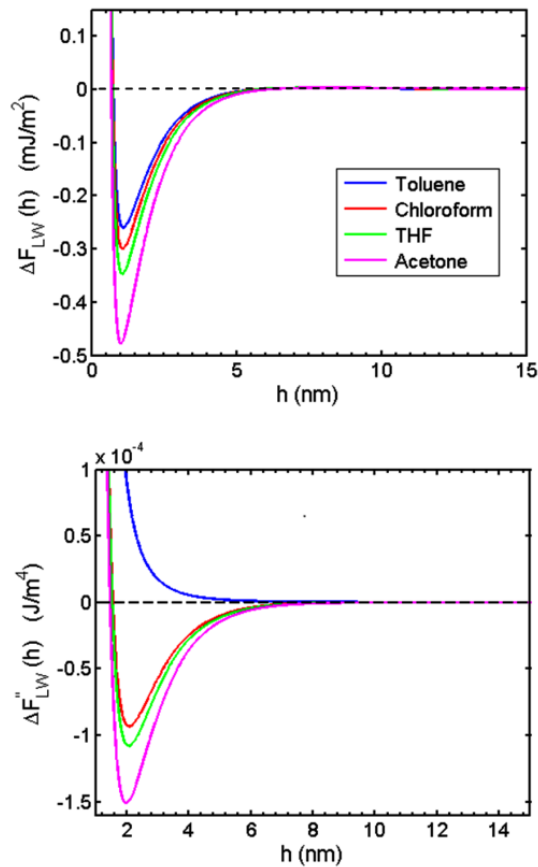


Figure 5-5. Simulation of (a) the effective interfacial potential ΔF and (b) its second derivative $\Delta F''$ as a function of PS film thickness 'h' for PS/H-Si. The effective free energy takes into account the effective contribution of the Lifshitz-van der Waals ΔF_{LW} and of the polar ΔF_P components as well as the steric repulsion energy c/h^α .

Table 5-1. Parameters for the simulation of interfacial potential curve. $A_{SiO_2/PS/Solvent}$ and $A_{Si/PS/Solvent}$ are the effective Hamaker constants of $SiO_2/PS/Solvent$ and $Si/PS/Solvent$ three layer systems. S_p , the polar spreading coefficient. RED, relative energy difference values PS and some of its good solvents. [40]

| | $A_{Si/PS/Solvent}$ (10^{-20} J) | S_p (N/m) $\times 10^{-5}$ | Dipolar moment[59] (π/D) |
|------------|--|---------------------------------|-----------------------------------|
| Toluene | 0.15 | -1.53 | 0.375 ± 0.01 |
| Chloroform | 0.167 | -4.06 | 1.04 ± 0.02 |
| THF | 0.18 | -6.69 | 1.75 ± 0.04 |
| Acetone | 0.2 | -21.35 | 2.88 ± 0.03 |

5.4 Glass transition properties of polymer residual layer

The change in the ellipsometric angle with respect to the variation in film thickness/ refractive index is measured where the temperature corresponding to the change in the slope represents the glass transition temperature. For example, Figure 5-6. a represents the transition temperature measured for 100 nm PS/H-Si. (before rinsing) which is equal to the bulk glass transition temperature of polystyrene which is 100°C. Figure 5-6 b. represents the transition temperatures measured for the samples rinsed with chloroform, with a final thickness of ~ 7.9 nm. Multiple temperature transitions are observed for the films after rinsing, one near 90°C and the second transition is observed at 132°C with no bulk value of T_g . All samples after solvent rinsing possessed two temperature transitions similar to Figure 5-6 b, where the transition above the bulk T_g is denoted as T+ and below T_g is notated as T-, following T- and T+ notation for the T_g of surface layer and polymer bound to substrate by various authors. [60]–[62] The multiple transition temperatures observed for all the samples that are rinsed with various solvents are shown in Figure 5-6.

Considering the T_g of entire films (films without rinsing), various experimental techniques already provided evidence for the existence of uneven distribution of glass transition upon confinement. Deviating from the bulk, regions with enhanced mobility near the free surface was reported by many studies. [5], [63]–[66] This enhanced mobility leading to a reduced T_g near the surface was reported with the ellipsometric studies in thin supported glassy polystyrene films.[67]

The segmental motion at the substrate interface is reported to follow a slower dynamics compared to the bulk [23], [24], [36], [68], [69] and the study on the long range effects on the polymer diffusion induced by a bounding interface found that the T_g is increased near such walls. [70] The interface and surface effects on the glass transition in thin polystyrene films studied by PALS measurement in a three layer model found that the entire film may not be characterized as having only one value of T_g which later lead to the proposal of a three-layer model in which, within thin films there are three layers with different mobilities and glass transition temperatures. [2]

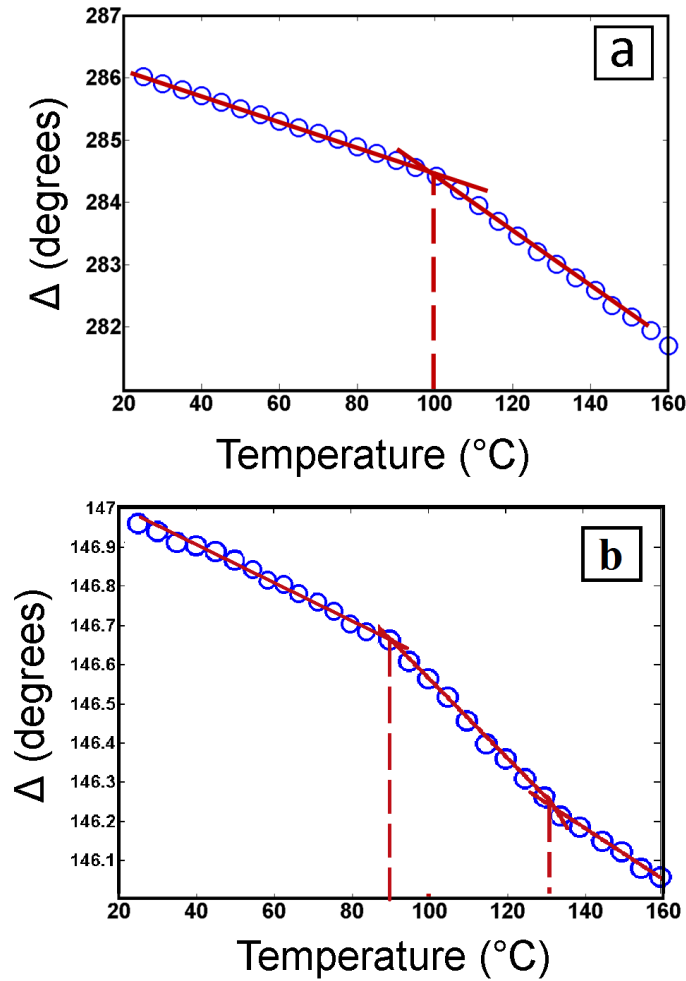


Figure 5-6. Raw ellipsometric curves showing Δ as function of temperature for a) PS/H-Si (100 nm) measured at 2.75 eV b) PS/H-Si (~ 7.9 nm) after chloroform rinsing and post annealing.

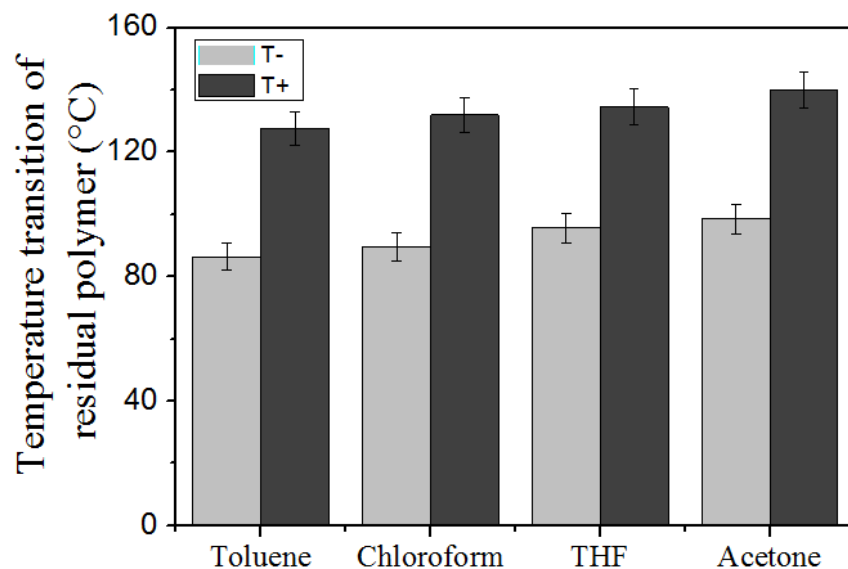


Figure 5-7. Temperature transition of PS/H-Si after rinsing with various solvents.

Considering the structure of the polymer residual layer, it is considered as a Guiselin brush which is composed of, part of the polymer chain that are attached to the substrate (strongly adsorbed chains), and the parts that starts from the substrate and returns back or parts that dangles (loosely adsorbed chains). In fact the loosely adsorbed chains are in contact with the free surface. From the ellipsometric measurements, we obtain two temperature transitions, one above and one below the bulk T_g value of PS. This is matching very well with the observations of Blum *et al.* who found a two component transition for the adsorbed polymer with a bulk like transition for the loosely bound polymer and an elevated glass transition for the tightly bound polymer. [44] The adsorbed residual layer T_g measured fluorescence bilayer method found a substantial reduction in T_g as compared to bulk. [45] By submerging the adsorbed layer by the deposition of an additional layer above the residual layer, they recovered of the bulk T_g on a time scale reflecting the degree of adsorption. This point to the significant influence of free surface that causes a decreased T_g of residual layer. Various studies reported that the flattened chains and loosely adsorbed chains are able to move or slide in the lateral direction. [38], [71], [72] The segmental dynamics measurement of semi-isolate and isolate chains in contact with an attractive solid substrate reported that, 12% of the segments showed the slower relaxation dynamics compared to the bulk while the rest still exhibited a bulk-like dynamic T_g .

The molecular dynamics simulations showed that the segmental dynamics is slower for the stiffer chains that are bound to the substrate (trains), compared to the unadsorbed segments that includes the loops and tails. [73] Hence one can conclude that the elevated T_g observed for the chains pinned to the substrate and T^- is from the unadsorbed polymer segments. This observation can be schematically represented as shown in Figure 5-8. Here a supported thin film with a multi-layer T_g distribution after rinsing with a good solvent is found to have the temperature transitions below and above the bulk T_g value.

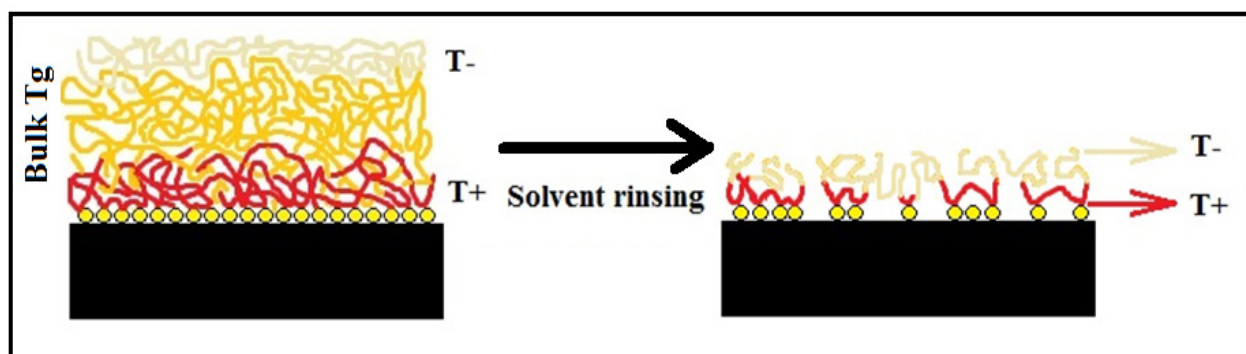


Figure 5-8. Schematic representation of the effect of solvent rinsing on the supported thin film and transition temperature

Considering the effect of solvent in the T_g of the residual layer, It can be seen that both T^- and T^+ of the residual layer increases slightly, in order from toluene to acetone as shown in Figure 5-7. We hypothesize this observation with respect to the *RED*. That is the T_g increases with the increasing relative energy difference between the polymer and the solvent. As the relative energy difference increases, the ability of the solvent to extract the adsorbed polymer chains decreases resulting in the increased thickness of the residual layer due to presence of more non-desorbed chains. In case of PS, a number of experiments already showed that the T_g increases with the film thickness. [74] Apart from this, the increased T_g can also have a contribution from the increased polymer substrate interaction. [11], [75], [76] Thus the thickness of residual layer which is dependent on the quality of solvent used for its extraction is found have spectacular influence on the glass transition properties of polymer residual layer.

5.5 Conclusion

The residual layers of polystyrene on the H-terminated wafers, after rinsing with various solvents are devoid of spinodal dewetting at a thickness above 7 nm. In case of rinsing with a polar solvent like acetone, the residual layer undergoes dewetting at a microscopic scale. Unlike the glass transition behavior of bulk polymer, two temperature transitions were observed for the residual polymer layer, one above and one below the bulk T_g value of polymer. This elevated temperature transition observed can be attributed to the chains pinned to the substrate whereas the temperature transition observed below the bulk T_g can have its origin from the unadsorbed polymer segments in contact with the free surface.

REFERENCES

- [1] L. Singh, “Effect of nanoscale confinement on the physical properties of polymer thin films,” Georgia Institute of Technology, 2004.
- [2] G. DeMaggio, W. Frieze, D. Gidley, M. Zhu, H. Hristov, and a. Yee, “Interface and Surface Effects on the Glass Transition in Thin Polystyrene Films,” *Phys. Rev. Lett.*, vol. 78, no. 8, pp. 1524–1527, Feb. 1997.
- [3] K. Fukao and Y. Miyamoto, “Glass transitions and dynamics in thin polymer films: dielectric relaxation of thin films of polystyrene,” *Phys. Rev. E. Stat. Phys. Plasmas. Fluids. Relat. Interdiscip. Topics*, vol. 61, no. 2, pp. 1743–54, Feb. 2000.
- [4] R. D. Priestley, C. J. Ellison, L. J. Broadbelt, and J. M. Torkelson, “Structural relaxation of polymer glasses at surfaces, interfaces, and in between.,” *Science*, vol. 309, no. 5733, pp. 456–9, Jul. 2005.
- [5] Z. Fakhraai and J. A. Forrest, “Measuring the surface dynamics of glassy polymers.,” *Science*, vol. 319, pp. 600–604, 2008.
- [6] M. D. Ediger and J. A. Forrest, “Dynamics near Free Surfaces and the Glass Transition in Thin Polymer Films: A View to the Future,” *Macromolecules*, vol. 47, pp. 471–478, 2014.
- [7] J. A. Forrest and K. Dalnoki-Veress, “The glass transition in thin polymer films,” *Adv. Colloid Interface Sci.*, vol. 94, pp. 167–196, 2001.
- [8] R. P. White, C. C. Price, and J. E. G. Lipson, “Effect of Interfaces on the Glass Transition of Supported and Freestanding Polymer Thin Films,” *Macromolecules*, vol. 48, no. 12, pp. 4132–4141, Jun. 2015.
- [9] C. J. Ellison and J. M. Torkelson, “Sensing the glass transition in thin and ultrathin polymer films via fluorescence probes and labels,” *J. Polym. Sci. Part B Polym. Phys.*, vol. 40, no. 24, pp. 2745–2758, Dec. 2002.

- [10] J. L. Keddie, R. A. L. Jones, and R. A. Cory, “Interface and surface effects on the glass-transition temperature in thin polymer films,” *Faraday Discuss.*, vol. 98, pp. 219–230, 1994.
- [11] J. van Zanten, W. Wallace, and W. Wu, “Effect of strongly favorable substrate interactions on the thermal properties of ultrathin polymer films,” *Physical Review E*, vol. 53. pp. R2053–R2056, 1996.
- [12] Y. Grohens, L. Hamon, G. Reiter, a. Soldera, and Y. Holl, “Some relevant parameters affecting the glass transition of supported ultra-thin polymer films,” *Eur. Phys. J. E*, vol. 8, no. 2, pp. 217–224, May 2002.
- [13] D. S. Fryer, R. D. Peters, E. J. Kim, J. E. Tomaszewski, J. J. de Pablo, P. F. Nealey, C. C. White, and W. Wu, “Dependence of the Glass Transition Temperature of Polymer Films on Interfacial Energy and Thickness,” *Macromolecules*, vol. 34, no. 16, pp. 5627–5634, Jul. 2001.
- [14] C. H. Park, J. H. Kim, M. Ree, B.-H. Sohn, J. C. Jung, and W.-C. Zin, “Thickness and composition dependence of the glass transition temperature in thin random copolymer films,” *Polymer.*, vol. 45, no. 13, pp. 4507–4513, Jun. 2004.
- [15] M. K. Mundra, C. J. Ellison, P. Rittigstein, and J. M. Torkelson, “Fluorescence studies of confinement in polymer films and nanocomposites: Glass transition temperature, plasticizer effects, and sensitivity to stress relaxation and local polarity,” *Eur. Phys. J. Spec. Top.*, vol. 141, no. 1, p. 143, 2007.
- [16] C. J. Ellison, S. D. Kim, D. B. Hall, and J. M. Torkelson, “Confinement and processing effects on glass transition temperature and physical aging in ultrathin polymer films: novel fluorescence measurements.,” *Eur. Phys. J. E. Soft Matter*, vol. 8, no. 2, pp. 155–66, May 2002.

- [17] R. D. Priestley, L. J. Broadbelt, and J. M. Torkelson, “Physical Aging of Ultrathin Polymer Films above and below the Bulk Glass Transition Temperature: Effects of Attractive vs Neutral Polymer–Substrate Interactions Measured by Fluorescence,” *Macromolecules*, vol. 38, no. 3, pp. 654–657, Feb. 2005.
- [18] C. J. Ellison and J. M. Torkelson, “The distribution of glass-transition temperatures in nanoscopically confined glass formers.,” *Nat. Mater.*, vol. 2, no. 10, pp. 695–700, Oct. 2003.
- [19] J. L. Keddie, R. A. L. Jones, and R. A. Cory, “Size-Dependent Depression of the Glass Transition Temperature in Polymer Films .,” *Europhys. Lett.*, vol. 27, no. July, pp. 59–64, 1994.
- [20] S. Kawana and R. A. L. Jones, “Character of the glass transition in thin supported polymer films,” *Phys. Rev. E*, vol. 63, no. 2, p. 21501, 2001.
- [21] J. S. Sharp and J. A. Forrest, “Free Surfaces Cause Reductions in the Glass Transition Temperature of Thin Polystyrene Films,” *Phys. Rev. Lett.*, vol. 91, no. 23, p. 235701, Dec. 2003.
- [22] F. L. Pratt, T. Lancaster, M. L. Brooks, S. J. Blundell, T. Prokscha, E. Morenzoni, A. Suter, H. Luetkens, R. Khasanov, R. Scheuermann, U. Zimmermann, K. Shinotsuka, and H. E. Assender, “Surface dynamics of a thin polystyrene film probed by low-energy muons,” *Phys. Rev. B*, vol. 72, no. 12, p. 121401, Sep. 2005.
- [23] T. Koga, N. Jiang, P. Gin, M. K. Endoh, S. Narayanan, L. B. Lurio, and S. K. Sinha, “Impact of an irreversibly adsorbed layer on local viscosity of nanoconfined polymer melts,” *Phys. Rev. Lett.*, vol. 107, no. 22, pp. 1–5, 2011.
- [24] S. Napolitano and M. Wübbenhorst, “The lifetime of the deviations from bulk behaviour in polymers confined at the nanoscale,” *Nat. Commun.*, vol. 2, p. 260, Mar. 2011.
- [25] S. Napolitano, C. Rotella, and M. Wübbenhorst, “Can Thickness and Interfacial Interactions Univocally Determine the Behavior of Polymers Confined at the Nanoscale?,” *ACS Macro Lett.*, vol. 1, no. 10, pp. 1189–1193, Oct. 2012.

- [26] S. Napolitano, A. Pilleri, P. Rolla, and M. Wübbenhorst, “Unusual Deviations from Bulk Behavior in Ultrathin Films of Poly(tert-butylstyrene): Can Dead Layers Induce a Reduction of Tg?,” *ACS Nano*, vol. 4, no. 2, pp. 841–848, Feb. 2010.
- [27] C. E. Porter and F. D. Blum, “Thermal characterization of PMMA thin films using modulated differential scanning calorimetry,” *Macromolecules*, vol. 33, no. 19, pp. 7016–7020, 2000.
- [28] F. D. Blum, W.-Y. Lin, and C. E. Porter, “Dynamics of adsorbed poly(methyl acrylate) and poly(methyl methacrylate) on silica,” *Colloid Polym. Sci.*, vol. 281, no. 3, pp. 197–202, 2003.
- [29] D. Hudzinsky, A. V. Lyulin, A. R. C. Baljon, N. K. Balabaev, and M. A. J. Michels, “Effects of strong confinement on the glass-transition temperature in simulated atactic polystyrene films,” *Macromolecules*, vol. 44, no. 7, pp. 2299–2310, Apr. 2011.
- [30] G. Vignaud, M. S. Chebil, J. K. Bal, N. Delorme, T. Beuvier, Y. Grohens, and A. Gibaud, “Densification and Depression in Glass Transition Temperature in Polystyrene Thin Films,” *Langmuir*, vol. 30, no. 39, pp. 11599–11608, 2014.
- [31] P. Gin, N. Jiang, C. Liang, T. Taniguchi, B. Akgun, S. K. Satija, M. K. Endoh, and T. Koga, “Revealed Architectures of Adsorbed Polymer Chains at Solid-Polymer Melt Interfaces,” *Phys. Rev. Lett.*, vol. 109, no. 26, p. 265501, Dec. 2012.
- [32] M. Asada, N. Jiang, L. Sendogdular, P. Gin, Y. Wang, M. K. Endoh, T. Koga, M. Fukuto, D. Schultz, M. Lee, X. Li, J. Wang, M. Kikuchi, and A. Takahara, “Heterogeneous Lamellar Structures Near the Polymer/Substrate Interface,” *Macromolecules*, vol. 45, no. 17, pp. 7098–7106, Sep. 2012.
- [33] B. Vanroy, M. Wübbenhorst, and S. Napolitano, “Crystallization of thin polymer layers confined between two adsorbing walls,” *ACS Macro Lett.*, vol. 2, no. 2, pp. 168–172, Feb. 2013.

- [34] L. Zhang, R. Elupula, S. M. Grayson, and J. M. Torkelson, “Major Impact of Cyclic Chain Topology on the T_g -Confinement Effect of Supported Thin Films of Polystyrene,” *Macromolecules*, vol. 49, pp. 257–268, 2015.
- [35] C. J. Durning, B. O’Shaughnessy, U. Sawhney, D. Nguyen, J. Majewski, and G. S. Smith, “Adsorption of poly(methyl methacrylate) melts on quartz,” *Macromolecules*, vol. 32, pp. 6772–6781, 1999.
- [36] Y. Fujii, Z. Yang, J. Leach, H. Atarashi, K. Tanaka, and O. K. C. Tsui, “Affinity of Polystyrene Films to Hydrogen-Passivated Silicon and Its Relevance to the T_g of the Films,” *Macromolecules*, vol. 42, no. 19, pp. 7418–7422, Oct. 2009.
- [37] B. O’Shaughnessy and D. Vavylonis, “Non-equilibrium in adsorbed polymer layers,” *J. Phys. Condens. Matter*, vol. 17, no. 2, p. R63, 2005.
- [38] N. Jiang, J. Shang, X. Di, M. K. Endoh, and T. Koga, “Formation Mechanism of High-Density, Flattened Polymer Nanolayers Adsorbed on Planar Solids,” *Macromolecules*, vol. 47, pp. 2682–2689, 2014.
- [39] O. Guiselin, “Irreversible Adsorption of a Concentrated Polymer Solution,” *Europhys. Lett.*, vol. 17, pp. 225–230, 1992.
- [40] A. Beena Unni, G. Vignaud, J. K. Bal, N. Delorme, T. Beuvier, S. Thomas, Y. Grohens, and A. Gibaud, “Solvent Assisted Rinsing: Stability/Instability of Ultrathin Polymer Residual Layer,” *Macromolecules*, vol. 49, no. 5, pp. 1807–1815, Feb. 2016.
- [41] M. Sen, N. Jiang, J. Cheung, M. K. Endoh, T. Koga, D. Kawaguchi, and K. Tanaka, “Flattening Process of Polymer Chains Irreversibly Adsorbed on a Solid,” *ACS Macro Lett.*, vol. 5, no. 4, pp. 504–508, 2016.
- [42] C. Housmans, M. Sferrazza, and S. Napolitano, “Kinetics of irreversible chain adsorption,” *Macromolecules*, vol. 47, pp. 3390–3393, 2014.

- [43] C. Rotella, S. Napolitano, L. De Cremer, G. Koeckelberghs, and M. Wübbenhorst, “Distribution of Segmental Mobility in Ultrathin Polymer Films,” *Macromolecules*, vol. 43, no. 20, pp. 8686–8691, Oct. 2010.
- [44] F. D. Blum, E. N. Young, G. Smith, and O. C. Sitton, “Thermal Analysis of Adsorbed Poly (methyl methacrylate) on Silica,” *Langmuir*, vol. 22, no. 10, pp. 4741–4744, 2006.
- [45] M. J. Burroughs, S. Napolitano, D. Cangialosi, and R. D. Priestley, “Direct Measurement of Glass Transition Temperature in Exposed and Buried Adsorbed Polymer Nanolayers,” *Macromolecules*, vol. 49, no. 12, pp. 4647–4655, 2016.
- [46] C. M. Hansen, *Hansen Solubility Parameters, A User’s Hand book*. Taylor & Francis, 2007.
- [47] D. C. Sherrington, “Preparation, structure and morphology of polymer supports,” *Chem. Commun.*, no. 21, pp. 2275–2286, 1998.
- [48] L. Xu, A. Sharma, and S. W. Joo, “Dewetting of stable thin polymer films induced by a poor solvent: Role of polar interactions,” *Macromolecules*, vol. 45, pp. 6628–6633, 2012.
- [49] R. Mukherjee and A. Sharma, “Instability, Self Organization and Pattern Formation in Thin Soft Films,” *Soft Matter*, vol. 11, pp. 8718–8740, 2015.
- [50] S. H. Lee, P. J. Yoo, S. J. Kwon, and H. H. Lee, “Solvent-driven dewetting and rim instability,” *J. Chem. Phys.*, vol. 121, no. 2004, pp. 4346–4351, 2004.
- [51] L. Xu, A. Sharma, S. W. Joo, H. Liu, and T. Shi, “Unusual Dewetting of Thin Polymer Films in Liquid Media Containing a Poor Solvent and a Nonsolvent,” *Langmuir*, vol. 30, no. 49, pp. 14808–14816, Dec. 2014.
- [52] O. Al-khayat, K. Geraghty, K. Shou, A. Nelson, and C. Neto, “Chain Collapse and Interfacial Slip of Polystyrene Films in Good/ Nonsolvent Vapor Mixtures,” *Macromolecules*, vol. 49, no. 4, pp. 1344–1352, 2016.

- [53] A. Verma and A. Sharma, "Submicrometer pattern fabrication by intensification of instability in ultrathin polymer films under a water-solvent mix," *Macromolecules*, vol. 44, no. 12, pp. 4928–4935, 2011.
- [54] R. Seemann, S. Herminghaus, and K. Jacobs, "Gaining control of pattern formation of dewetting liquid films," *J. Phys. Condens. Matter*, vol. 13, no. 21, p. 4925, 2001.
- [55] A. Sharma and R. Khanna, "Pattern Formation in Unstable Thin Liquid Films," *Phys. Rev. Lett.*, vol. 81, no. 16, pp. 3463–3466, 1998.
- [56] A. Sharma and R. Khanna, "Pattern formation in unstable thin liquid films under the influence of antagonistic short- and long-range forces.," *J. Chem. Phys.*, vol. 110, no. 10, pp. 4929–4936, 1999.
- [57] L. Xue and Y. Han, "Pattern formation by dewetting of polymer thin film," *Prog. Polym. Sci.*, vol. 36, no. 2, pp. 269–293, 2011.
- [58] A. Sharma, "Relationship of Thin Film Stability and Morphology to Macroscopic Parameters of Wetting in the Apolar and Polar Systems," *Langmuir*, vol. 28, no. 23, pp. 861–869, 1993.
- [59] D. R. Lide, *CRC Handbook of Chemistry and Physics*. CRC press, 2003.
- [60] J. H. Kim, J. Jang, and W.-C. Zin, "Thickness Dependence of the Glass Transition Temperature in Thin Polymer Films," *Langmuir*, vol. 17, no. 9, pp. 2703–2710, May 2001.
- [61] A. El Ouakili, G. Vignaud, E. Balnois, J.-F. Bardeau, and Y. Grohens, "Multiple glass transition temperatures of polymer thin films as probed by multi-wavelength ellipsometry," *Thin Solid Films*, vol. 519, no. 6, pp. 2031–2036, Jan. 2011.
- [62] T. Lan and J. M. Torkelson, "Methacrylate-based polymer films useful in lithographic applications exhibit different glass transition temperature-confinement effects at high and low molecular weight," *Polymer.*, vol. 55, no. 5, pp. 1249–1258, Mar. 2014.
- [63] K. F. Mansfield and D. N. Theodorou, "Molecular dynamics simulation of a glassy polymer surface," *Macromolecules*, vol. 24, no. 23, pp. 6283–6294, Nov. 1991.

- [64] J. A. Forrest, K. Dalnoki-Veress, J. R. Stevens, and J. R. Dutcher, “Effect of Free Surfaces on the Glass Transition Temperature of Thin Polymer Films,” *Phys. Rev. Lett.*, vol. 77, no. 10, pp. 2002–2005, Sep. 1996.
- [65] W. E. Wallace, D. A. Fischer, K. Efimenko, W.-L. Wu, and J. Genzer, “Polymer Chain Relaxation: Surface Outpaces Bulk,” *Macromolecules*, vol. 34, no. 15, pp. 5081–5082, Jul. 2001.
- [66] Z. Yang, Y. Fujii, F. K. Lee, C.-H. Lam, and O. K. C. Tsui, “Glass Transition Dynamics and Surface Layer Mobility in Unentangled Polystyrene Films,” *Science*, vol. 328, no. 5986, pp. 1676–1679, Jun. 2010.
- [67] S. Kawana and R. a L. Jones, “Effect of physical ageing in thin glassy polymer films.,” *Eur. Phys. J. E. Soft Matter*, vol. 10, no. 3, pp. 223–30, Mar. 2003.
- [68] R. Inoue, K. Kawashima, K. Matsui, T. Kanaya, K. Nishida, G. Matsuba, and M. Hino, “Distributions of glass-transition temperature and thermal expansivity in multilayered polystyrene thin films studied by neutron reflectivity,” *Phys. Rev. E*, vol. 83, no. 2, p. 21801, Feb. 2011.
- [69] H. Tsuruta, Y. Fujii, N. Kai, H. Kataoka, T. Ishizone, M. Doi, H. Morita, and K. Tanaka, “Local Conformation and Relaxation of Polystyrene at Substrate Interface,” *Macromolecules*, vol. 45, no. 11, pp. 4643–4649, Jun. 2012.
- [70] X. Zheng, M. H. Rafailovich, J. Sokolov, Y. Strzhemechny, S. A. Schwarz, B. B. Sauer, and M. Rubinstein, “Long-Range Effects on Polymer Diffusion Induced by a Bounding Interface,” *Phys. Rev. Lett.*, vol. 79, no. 2, pp. 241–244, 1997.
- [71] M. Asada, N. Jiang, L. Sendogdular, J. Sokolov, M. K. Endoh, T. Koga, M. Fukuto, L. Yang, B. Akgun, M. Dimitriou, and S. Satija, “Melt crystallization/dewetting of ultrathin PEO films via carbon dioxide annealing: the effects of polymer adsorbed layers,” *Soft Matter*, vol. 10, no. 34, pp. 6392–6403, 2014.

- [72] N. Jiang, M. K. Endoh, and T. Koga, “Structures and Dynamics of Adsorbed Polymer Nanolayers on Planar Solids Structures and Dynamics of Adsorbed Polymer Nanolayers on Planar Solids,” in *Non-equilibrium Phenomena in Confined Soft Matter*, S. Napolitano, Ed. Springer, 2015, pp. 129–160.
- [73] J.-M. Y. Carrillo, S. Cheng, R. Kumar, M. Goswami, A. P. Sokolov, and B. G. Sumpter, “Untangling the Effects of Chain Rigidity on the Structure and Dynamics of Strongly Adsorbed Polymer Melts,” *Macromolecules*, vol. 48, no. 12, pp. 4207–4219, Jun. 2015.
- [74] C. B. Roth and J. R. Dutcher, “Glass transition and chain mobility in thin polymer films,” *J. Electroanal. Chem.*, vol. 584, no. 1, pp. 13–22, Oct. 2005.
- [75] J. A. Forrest, K. Dalnoki-Veress, and J. R. Dutcher, “Interface and chain confinement effects on the glass transition temperature of thin polymer films,” *Phys. Rev. E*, vol. 56, no. 5, pp. 5705–5716, 1997.
- [76] E. K. Lin, R. Kolb, S. K. Satija, and W. L. Wu, “Reduced polymer mobility near the polymer/solid interface as measured by neutron reflectivity,” *Macromolecules*, vol. 32, pp. 3753–3757, 1999.

Conclusion and Perspectives

In this thesis, the investigations were done mainly around the deviation in polymer thin film properties when they are confined by their thickness. Even if there exist numerous studies reporting such property deviations, the non-agreement of these reported results lead to controversies that still remain within the scientific community. One of such properties that exhibit anomalous behavior due to film confinement is the density of polymer thin films. Our first mission was to study the density variations in polymer thin films which were achieved by the adsorption of ceria nanoparticles onto the polymer film surface. The usage of ceria nanoparticles for density studies was a novel approach which is devoid of any models which are usually employed in the density studies. As the amount of nanoparticle adsorbed is a monotonic function of the polymer surface refractive index, any increase/decrease in the nanoparticle surface coverage was directly ascribed to an increase/decrease in the thin film refractive index and thereby density. The main outcome of this study is that, the density of Polystyrene thin films on oxide-free Si wafer increases with a reduction of the film, whereas the PMMA films spin-casted on Si wafers with silicon oxide layer shows a reverse trend; i.e. a decrease of the density with the film thickness. This opposing trend observed is explained by the distinct chain conformation resulting from the difference in polymer substrate interaction.

One of the main difficulties we faced during the first study was the dewetting of films when their thickness is reduced. So our second aim was to find an alternative to this dewetting issue. By rinsing the bulk polymer film with good solvent, we were able to prepare flat polystyrene films with a controlled thickness ranging from 1.3 to 7.0 nm. The films are found to be stable, even after the scrutiny of their stability by an annealing procedure above the glass transition temperature. Films were found to be stable on oxide-free silicon irrespective of film thickness. In case of films on 2 nm oxide-covered silicon substrates, they were found to be unstable below a thickness of 2.9 nm and metastable above 2.9 nm. The Lifshitz-van der Waals intermolecular theory, which can predict the domains of stability as a function of the film thickness and of the substrate nature was fully reconciled with our experimental observations. We surmise that this reconciliation is due to the good solvent rinsing procedure that removes the residual stress and the density variation of the polystyrene films inhibiting thermodynamically the dewetting on oxide-free silicon.

As rinsing with a good solvent is found to be a promising method for obtaining ultra-thin polymer films, it was indeed intriguing to see what happens to the characteristics of residual polymer film if we use different solvents for rinsing. Hence the study given in Chapter 3 deals with the significance of choosing solvents for deconstructing polymer thin films. The solvents toluene, chloroform, tetrahydrofuran and acetone were chosen for the study, considering their relative energy difference with the polymer. It was found that smaller the relative energy differences between the polymer and the solvent, faster the dissolution and desorption of the polymer chains. The thickness of the residual layer is thus a function on the solvent quality. It was found that the films undergo spinodal dewetting at different time and thickness, depending on the solvent nature, mainly the polarity. On the theoretical side, the polar acid-base component together with the Lifshitz-van der Waals free energy could perfectly explain the unstable and metastable domains for the four different solvents.

From the previous studies, one could successfully obtain stable films by rinsing with a good solvent. The following question was whether these residual layers possess the same properties like their bulk counter parts or they exhibit some deviations in their properties. The final study reported in the dissertation (Chapter 4) deals with the characteristics and properties of polystyrene residual layers on H-terminated Si wafer. The residual layers of polystyrene on the H-terminated wafers, after rinsing with various solvents were devoid of spinodal dewetting as their thickness above 7 nm. In case of rinsing with a polar solvent like acetone, the residual layer underwent dewetting at a microscopic scale. Unlike the glass transition behavior of bulk polymer, two temperature transitions were observed for the residual polymer layer, one above and one below the bulk glass transition value of polymer. The elevated temperature transition observed is attributed to the chains pinned to the substrate whereas the temperature transition observed below the bulk T_g is found to have its origin from the unadsorbed polymer segments in contact with the free surface.

Altogether, this work contributes towards a better understanding of the density variations observed in polymer thin films upon confinement. It provided a promising way to obtain stable ultra-thin polymer films by the method of solvent rinsing, which is reconciled with the Lifshitz-van der Waals intermolecular theory. It can also help one to understand various characteristics and properties of polymer residual layer.

There are lots of interesting factors which are yet to be investigated in addition to what we have discussed here. For example, as the ceria nanoparticles adsorption is found to be a promising method to characterize the density variations in the polymer thin films, it can be interesting to try this method on polymer residual layers to investigate their properties. Another study which can be interesting is to reconstruct thin films of various thickness range over the polymer residual layer to understand their properties, and then to compare it with the films made by direct spin coating. This can help one to understand whether or not the recoating over the residual layer influence the films properties.

Apart from the various factors that can influence the properties of the polymer residual layer we have already studied, an important factor that should be considered in the future study is the polymer tacticity. The tacticity is found to have influence on the configuration differences in the adsorbed layer,[1] glass transition temperature,[2], [3] dielectric properties [4] etc. Hence it is very intriguing to know whether or not the polymer tacticity affect the properties of the polymer residual layer, which is reported to have its influence on the thin film properties.

Considering the polymer films that dewets on the substrate, the dewetted polymer structures can be more interesting leading to its applications, if one can control the spinodal wavelength by controlling the parameters such as solvent rinsing time, annealing, type of solvent used etc.

REFERENCES

- [1] Y. Grohens, M. Brogly, C. Labbe, and J. Schultz, "Chain flattening of spin-cast PMMMA on aluminum mirrors: Influence of polymer tacticity," *Eur. Polym. J.*, vol. 33, no. 5, pp. 691–697, 1997.
- [2] Y. Grohens, M. Brogly, C. Labbe, M.-O. David, and J. Schultz, "Glass Transition of Stereoregular Poly(methyl methacrylate) at Interfaces," *Langmuir*, vol. 14, no. 11, pp. 2929–2932, May 1998.
- [3] E. V Thompson, "Dependence of the glass transition temperature of poly (methyl methacrylate) on tacticity and molecular weight," *J. Polym. Sci. Part A* \square *2 Polym. Phys.*, vol. 4, no. 2, pp. 199–208, 1966.
- [4] J. H. Park, D. K. Hwang, J. Lee, S. Im, and E. Kim, "Studies on poly (methyl methacrylate) dielectric layer for field effect transistor: Influence of polymer tacticity," *Thin Solid Films*, vol. 515, no. 7, pp. 4041–4044, 2007.

LIST OF FIGURES

| | |
|--|----|
| Figure 0-1. Three forms of polymer thin films: free standing, supported and capped films. _____ | 1 |
| Figure 1-1: Structure of polystyrene. _____ | 20 |
| Figure 1-2: Structure of PMMA _____ | 21 |
| Figure 1-3: Silicon surface before and after the piranha treatment _____ | 23 |
| Figure 1-4: Schematic representation showing the changes of oxidized Si (100) wafer when immersed in HF solution [5], [6] _____ | 24 |
| Figure 1-5: Representation of Hansen solubility sphere. _____ | 26 |
| Figure 1-6: Schematic representation of the spin coating process. The substrate represented by black, solvent: green and the polymer: red respectively. _____ | 28 |
| Figure 1-7: A schematic diagram showing the working principle of ellipsometry (Horiba scientific) _____ | 29 |
| Figure 1-8: A typical geometry of an ellipsometric experiment showing the p- and s-directions. The light is linearly polarized initially and is elliptically polarized after being reflected from the sample. _____ | 30 |
| Figure 1-9: a.) Radiation interacting with a single plane parallel interface between Material 1, with refractive index N_1 , and Material 2, with refractive index N_2 . b.) Diagram of the beam path in a sample comprised of a film, with thickness d and refractive index N_1 , between Material 0, with refractive index N_0 , and Material 2, with refractive index N_2 . _____ | 31 |
| Figure 1-10: The photograph of Jobin-Yvon spectroscopic ellipsometer with labeled parts. _____ | 33 |
| Figure 1-11: Raw ellipsometric curves showing Δ as function of temperature for 100 nm PS film on Si wafer with native oxide. _____ | 35 |
| Figure 1-12: A schematic diagram showing the working principle of AFM. _____ | 36 |
| Figure 1-13: Photograph of Nanoscope IIIa with labeled parts. _____ | 37 |
| Figure 1-14: Inter atomic force vs. distance curve with different modes of operation. _____ | 38 |
| Figure 1-15: A schematic representation of AFM operating in tapping mode _____ | 39 |
| Figure 1-16: The photograph of Empyrean Panalytical reflectometer. _____ | 41 |
| Figure 1-17: Schematic representation for the wettability of surface _____ | 44 |
| Figure 1-18: Photograph showing the solvent rinsing performed with dip coater. _____ | 45 |
| Figure 2-1. a) Zero-frequency (2-3) and b) dispersive (2-4) contributions of the Hamaker constant as a function of the dielectric and the refractive index of the polymer surface for a given CeO_2 NP dispersion (with $n_{\text{NP}}=1.9$, $\epsilon_{\text{NP}}=25$, $n_{\text{sol}}=1.33$ and $\epsilon_{\text{sol}}=80$). _____ | 53 |
| Figure 2-2. Schematic illustration of the ceria NPs adsorption process. The key parameters are the adsorption time, the refractive index of the polymer thin film and the NP dispersion, which allows tuning the surface coverage on samples of any shape and size. _____ | 55 |

| | |
|---|----|
| Figure 2-3. Amount of ceria NPs adsorbed onto various hydrophobic (polymer) thin films as a function of the refractive index. | 56 |
| Figure 2-4. a) Adsorption of CeO ₂ NP onto polystyrene surface as a function of the NP solution concentration monitored by optical reflectometry during 2 hours. b) AFM topographic image (1x1 μm ²) showing the surface of the PS film densely covered with CeO ₂ NP. | 57 |
| Figure 2-5: Refractive index of PS/H-Si as a function of the film thickness calculated at 605 nm by ellipsometry. (dotted line is the guide for eyes) | 58 |
| Figure 2-6: AFM topographic images showing the adsorbed ceria nanoparticles to the PS-H Si surface of PS film thickness, h: (a) 6.7 nm, (b) 13.99 nm, (c) 18.84 nm, (d) 36 nm, (e) 75.26 nm, (f) 143.55 nm. (Scan size 1*1 μm) | 59 |
| Figure 2-7: NP coverage (in percentage %) as a function of PS film thickness h computed from AFM images | 60 |
| Figure 2-8: AFM topographic images showing the adsorbed ceria nanoparticles to the PMMA/SiO _x -Si surface of PMMA film thickness, h: (a) 6.66 nm, (b) 12.43 nm, (c) 32.1 nm, (d) 41.1 nm, (e) 66.74 nm, (f) 95.11 nm. (Scan size 1*1 μm) | 61 |
| Figure 2-9: NP surface coverage (in percentage %) as a function of PMMA film thickness | 62 |
| Figure 2-10: Refractive index of PMMA-SiO _x -Si as a function of the PMMA film thickness. | 63 |
| Figure 2-11. PS film thickness vs. long-range effective interfacial potential as a function of the SiO _x layer thickness | 64 |
| Figure 2-12: AFM topographic images showing the adsorbed ceria nanoparticles on films of PMMA film ~30 nm on Si wafer a) without oxide layer on the substrate b) Oxide thickness of 1.7 nm on the substrate c) oxide thickness of 424 nm on the substrate. Scan area of 1*1 μm. | 65 |
| Figure 2-13: AFM topographic images showing the adsorbed ceria nanoparticles on films of PMMA film ~4 nm on Si wafer a) without oxide layer on the substrate b) oxide thickness of 424 nm on the substrate. Scan area of 1*1 μm. | 66 |
| Figure 2-14: Interfacial potential vs. film thickness of PMMA films as function of SiO _x layer thickness. | 68 |
| Figure 2-15: Schematic representation showing that the critical volume is reached at a lower temperature for the thinner film. | 69 |
| Figure 2-16: The schematic representation of the free volume that evolves with temperature, for PMMA and PS films. v* stands for the critical volume. | 70 |
| Figure 3-1: Sketch of the effective interface potential as a function of film thickness for stable (1), unstable (2), and metastable (3) films. | 81 |
| Figure 3-2: AFM images of PS films spin-coated at 2000 rpm on (a) SiO _x -Si and (b) H-Si surfaces from a 1.5 g/L solution (scan size = 5x5 μm ²) and on (c) SiO _x -Si and (d) H-Si surfaces from a 0.75 g/L solution (scan size = 15x15 μm ²). The thicknesses of the films determined by XRR are ≈ 6.8 nm, 7.1 nm, 3.2 nm and 4.3 nm for the images (a), (b), (c) and (d), respectively. The insets of figures (c) and (d) correspond to the evolution of the height along the drawn line. | 84 |
| Figure 3-3: XRR and EDP profiles showing dewetting of directly spin-coated ultrathin films. XRR data (different symbols) and analyzed curves (solid line) of as-prepared PS films on H-Si and SiO _x -Si substrates by direct spin- | |

coating of 0.75 g/L solution (curves are shifted vertically for clarity). Insets: corresponding EDPs showing very low coverage of the PS films with respect to the bulk electron density $\approx 0.344 \text{ e} \cdot \text{\AA}^{-3}$. _____ 85

Figure 3-4: Structural evolution as a result of solvent rinsing. XRR data (different symbols) and analyzed curves (solid line) of unannealed (a) and pre-annealed (b) 7 nm PS films on SiO_x-Si substrates before and after toluene rinsing during different durations (curves are shifted vertically for clarity). Insets: corresponding EDPs showing different thicknesses of the PS films with different toluene rinsing time. _____ 86

Figure 3-5: Solvent rinsing of a thick ($h_0 \approx 130 \text{ nm}$) PS film. XRR data (different symbols) and analyzed curves (solid line) of a thick PS film on a SiO_x-Si substrates before and after toluene rinsing during different durations as mentioned in the legend. Insets: corresponding EDPs showing different thicknesses of the PS films with different toluene rinsing times. _____ 87

Figure 3-6: Solvent rinsing of a 7 nm preannealed PS film grown on H-Si substrate. XRR data (different symbols) and analyzed curves (solid line) of a preannealed 7 nm PS film on H-Si substrates before and after toluene rinsing during different durations as mentioned in the legend (curves are shifted vertically for clarity). Insets: corresponding EDPs showing different thicknesses of the PS films with different toluene rinsing times. _____ 88

Figure 3-7: Solvent rinsing of a 7 nm preannealed PS film grown on a H-Si substrate. XRR data (different symbols) and analyzed curves (solid line) of a preannealed 7 nm PS film on a H-Si substrates before and after toluene rinsing during different durations as mentioned in the legend (curves are shifted vertically for clarity). Insets: corresponding EDPs showing different thicknesses of the PS films with different toluene rinsing times. _____ 89

Figure 3-8: Residual layer thickness h_{res} as a function of R_g . _____ 90

Figure 3-9: Correlation between the kinetics of dissolution and annealing. (a) Residual thickness (h_{res}) of pre-annealed and unannealed PS film of $h_0 \approx 7 \text{ nm}$ grown on SiO_x-Si and H-Si substrates as a function of rinsing time (t_{rins}). (b) Schematic illustration of the formation of an adsorbed layer h_{ads} . _____ 91

Figure 3-10: AFM topography image of pre-annealed residual films on (a) SiO_x-Si and (b) H-Si substrates obtained after 70 min of toluene rinsing. Inset of (a) and (b) show the 3D AFM images after scratching some regions of residual film by AFM tip in order to confirm that this is polymer rather than Si substrate. (c) Attenuated total reflectance absorbance spectra of a PS ultrathin film before ($h_0 \approx 18.0 \text{ nm}$) and after ($h_{ads} \approx 5.2 \text{ nm}$) a "quick" toluene rinsing (up to 20 min) confirming the existence of PS residual layer on Si substrate. _____ 93

Figure 3-11: AFM topographic images (scan size = $1 \times 1 \mu\text{m}^2$) presented in the top panel (A) show the morphologies of residual films of thickness h_{res} (a) $\approx 1.5 \text{ nm}$, (b) $\approx 2.5 \text{ nm}$, (c) $\approx 4.0 \text{ nm}$, (d) $\approx 4.6 \text{ nm}$, (e) $\approx 5.0 \text{ nm}$ and (f) $\approx 6.0 \text{ nm}$ on H-Si after post-annealing. In the bottom panel (B) are shown similar results for h_{res} (a) $\approx 1.3 \text{ nm}$, (b) $\approx 1.7 \text{ nm}$, (c) $\approx 2.2 \text{ nm}$, (d) $\approx 3.5 \text{ nm}$, (e) $\approx 4.9 \text{ nm}$ and (f) $\approx 6.8 \text{ nm}$ thick films on SiO_x-Si. Inset shows their corresponding 2D FFT image. Morphologies were obtained after post-annealing at 120°C during 24 h. Note that the thicknesses that are mentioned here are the thicknesses of the residual films just before the post-annealing. Z_m represents the maximum height in nm. _____ 96

Figure 3-12: AFM topography images illustrate a 2.3 nm thick PS film (residual) on an oxide-free Si substrate. (a) Scan size = $5 \times 5 \mu\text{m}^2$ (RMS roughness ≈ 0.16 nm) and (b) Scan size = $2 \times 2 \mu\text{m}^2$ (RMS roughness ≈ 0.16 nm). The images were taken after post annealing at 170°C during 24 h. _____ 97

Figure 3-13: Power spectral density (PSD) curves of residual PS films grown on SiO_x-Si substrates having different thicknesses calculated from AFM images presented in Figure 3-11. B. _____ 98

Figure 3-14: (a) Normalized XRR data (symbol) of RCA-cleaned Si and analyzed curves (solid lines. Inset: XPS spectrum of RCA-cleaned Si substrate demonstrating the existence of SiO_x layer on top of Si. (b) Normalized XRR data (symbol) of HF-cleaned Si substrate and fitted curve (solid line) using model 1 without oxide layer. Inset: XPS spectrum confirming the absence of an oxide layer on H-Si substrate after HF-treatment. _____ 99

Figure 3-15: Simulated $\Delta F^{\text{VDW}}(h)$ (solid lines) and $[\Delta F^{\text{VDW}}(h)]'$ (dashed line) curves using Eq.3-4 assuming 2 nm native oxides present on SiO_x-Si substrate. Curve 'A', drawn by choosing $A_{\text{Si/PS/Air}} = -6.0 \times 10^{-20}$ J and $A_{\text{SiOx/PS/Air}} = -0.2 \times 10^{-20}$ J, corresponds to a stable state. Curve 'B', deduced with $A_{\text{Si/PS/Air}} = -4.4 \times 10^{-20}$ J and $A_{\text{SiOx/PS/Air}} = 1.6 \times 10^{-20}$ J, depicts an unstable state. Curve 'C', plotted assuming $A_{\text{Si/PS/Air}} = -5 \times 10^{-20}$ J and $A_{\text{SiOx/PS/Air}} = 0.7 \times 10^{-20}$ J, corresponds to either a metastable state above $h_{\text{trans}} \approx 2.9$ nm and unstable films below h_{trans} . The letters a,b,c,d,e and f are corresponding to the AFM images presented in Figure 3-11. Color of state : stable in pink, unstable in gray, metastable in green. _____ 100

Figure 3-16: Evolution of the free energy as a function of SiO_x thickness. Simulated (a) (b) curves using equation 3-4 considering 4 different thicknesses (dSiO_x) of native oxides in SiO_x-Si substrate. All the curves are plotted with $A_{\text{Si/PS/Air}} = -5.0 \times 10^{-20}$ J and $A_{\text{SiOx/PS/Air}} = 0.7 \times 10^{-20}$ J. The intercept point of curves to the x-axis indicates the value of h_{trans} . (c) Plot of h_{trans} as a function of dSiO_x. Fitted linear curve (dashed line) draws a border line between stable or metastable and unstable regimes. _____ 102

Figure 3-17: AFM topographic images (Scan size = $2 \times 2 \mu\text{m}^2$) show the morphologies of residual films of thicknesses h_{res} (a) ≈ 1.5 nm, (b) ≈ 2.5 nm, (c) ≈ 4.0 nm, (d) ≈ 4.6 nm, (e) ≈ 5.0 nm and (f) ≈ 6.0 nm on H-Si substrates without post annealing. Z_m represents the maximum height in nm. _____ 104

Figure 4-1: Sketch representing the desorption mechanism of PS/SiO_x-Si in contact with a good solvent. The substrate, the polymer and the solvent are shown in black, orange and blue respectively. _____ 113

Figure 4-2: The schematic view of the two different chain conformations after the solvent rising supported PS thin film [14]. _____ 114

Figure 4-3: (a) Optical microscope image of the PS/SiO_x-Si film after spin coating and pre-annealing. (b) The 3D presentation of topographic image of PS/SiO_x-Si film obtained using AFM. (c) The height profile along the drawn red line. _____ 116

Figure 4-4: Residual thickness (h_{res}) of bound PS after rinsing with different solvents. h_{res} is measured by ellipsometry and complemented with XRR. _____ 117

| | |
|---|-----|
| Figure 4-5: AFM topography (scan size = $5 \times 5 \mu\text{m}^2$) of residual film obtained after rinsing with different solvents: a) toluene, b) chloroform, c) THF and d) acetone. The dotted line represents the transition to spinodal dewetting. _ | 119 |
| Figure 4-6: Optical images of PS films rinsed with acetone from 5s to 2h (scale bar $100 \mu\text{m}$). The scan size of AFM image = $5 \times 5 \mu\text{m}^2$ _____ | 120 |
| Figure 4-7: (a) Simulation of the Lifshitz-van der Waals component of the free energy ΔF_{LW} and (b) its second derivative $\Delta F_{LW}''$ as a function of film thickness h for PS films for the four layer system Si/SiO _x /PS/Solvent under different solvent media. The effective Hamaker constants are the ones given in Table 4-3 and the thickness of the SiO _x layer was taken to be equal to 1.7 nm. _____ | 126 |
| Figure 4-8 : The contact angle values between a bulk PS substrate and various solvents measured by contact angle goniometry. Photographs corresponding to the measurements are given above the bars. _____ | 128 |
| Figure 4-9: Simulation of (a) the effective free energy ΔF and (b) its second derivative $\Delta F''$ as a function of PS film thickness h for a four layer Si/SiO _x /PS/Solvent system. In these simulations, 4 solvents are considered: toluene, chloroform, THF and acetone. The effective free energy takes into account the effective contribution of the Lifshitz-van der Waals ΔF_{LW} and of the polar ΔF_p components as well as the steric repulsion energy c/h^α . _____ | 130 |
| Figure 5-1: Schematic representation for the temperature transitions observed in an amorphous material _____ | 140 |
| Figure 5-2. Residual thickness (h_{res}) of PS obtained by ellipsometry after rinsing with various solvents and post annealing (Acetone PS-HF is approximate value) _____ | 143 |
| Figure 5-3. Optical microscope images showing the PS/H-Si after rinsing with acetone and post annealing (Scale bar: $500 \mu\text{m}$) _____ | 144 |
| Figure 5-4. AFM images of PS/H-Si after rinsing with solvents a) toluene, b) chloroform, c) THF and d) acetone and post annealing. Scan size ($5 \times 5 \mu\text{m}$). Inset shows the surface profiles which scales from 0-1.4 nm. _____ | 146 |
| Figure 5-5. Simulation of (a) the effective interfacial potential ΔF and (b) its second derivative $\Delta F''$ as a function of PS film thickness ' h ' for PS/H-Si. The effective free energy takes into account the effective contribution of the Lifshitz-van der Waals ΔF_{LW} and of the polar ΔF_p components as well as the steric repulsion energy c/h^α . _____ | 148 |
| Figure 5-6. Raw ellipsometric curves showing Δ as function of temperature for a) PS/H-Si (100 nm) measured at 2.75 eV b) PS/H-Si (~ 7.9 nm) after chloroform rinsing and post annealing. _____ | 150 |
| Figure 5-7. Glass transition temperature of PS/H-Si after rinsing with various solvents. _____ | 151 |
| Figure 5-8. Schematic representation of the effect of solvent rinsing on the supported thin film and transition temperature _____ | 152 |

LIST OF TABLES

| | |
|--|-----|
| Table 1-1: The Hansen solubility parameter values of PS, PMMA and toluene | 27 |
| Table 2-1. Nanoparticle coverage obtained on ~30 nm PS films with various oxide thicknesses. | 64 |
| Table 2-2. Nanoparticle coverage obtained on ~30 nm PMMA films with various oxide thicknesses. | 65 |
| Table 2-3. Nanoparticle coverage obtained on ~4 nm PMMA films with various oxide thicknesses. | 66 |
| Table 2-4. Shows the increase (\uparrow) or decrease (\downarrow) of Glass transition temperature (T_g), Coefficient of thermal expansion (CTE) and the density(ρ) with decrease in film thickness of PS and PMMA. | 70 |
| Table 3-1: Preparation of the PS rinsed films on Si substrates (6 samples on H-Si and 6 samples on SiO _x -Si). Pre-annealing time t_{an} of the film (before the rinsing procedure) and the duration of toluene rinsing t_{rins} determine the thicknesses of residual layer (h_{res}). | 95 |
| Table 3-2: Correlation between the Hamaker constant values of $A_{Si/Si}$, $A_{PS/PS}$ and $A_{SiOx/SiOx}$ and the resulting effective Hamaker constants $A_{Si/PS/Air}$ and $A_{SiOx/PS/Air}$ from the "mixing rule" of equation 3-3. Curves A, B and C refer to the three different states as shown in Figure 3-15. | 100 |
| Table 4-1: The HSP and relative energy difference values PS and some of its good solvents. | 118 |
| Table 4-2: The Hamaker constants reported in the literature and their average value used in our calculations. | 124 |
| Table 4-3: Correlation between the surface tension of pure solvents and the effective Hamaker constants of the three layer systems. $\gamma_{Solvent}$ is the surface tension of the pure solvents. $A_{Solvent/Solvent}$ is the Hamaker constant of the solvent, $A_{SiO_2/PS/Solvent}$ and $A_{Si/PS/Solvent}$ are the effective Hamaker constants of SiO ₂ /PS/Solvent and Si/PS/Solvent three layer systems, respectively. The values are calculated from the average Hamaker constant values in Table 4-2. | 125 |
| Table 4-4: Correlation between the surface tension $\gamma_{PS/Solvent}$, the total S , the Lifshitz-van der Waals S_{LW} and the polar S_p spreading coefficients. | 129 |
| Table 5-1. Parameters for the simulation of interfacial potential curve. $A_{SiO_2/PS/Solvent}$ and $A_{Si/PS/Solvent}$ are the effective Hamaker constants of SiO ₂ /PS/Solvent and Si/PS/Solvent three layer systems. S_p , the polar spreading coefficient. RED, relative energy difference values PS and some of its good solvents. | 149 |

PUBLICATIONS

- J. K. Bal, T. Beuvier, A. B. Unni, E. A. Chavez Panduro, G. Vignaud, N. Delorme, M. S. Chebil, Y. Grohens, and A. Gibaud, “*Stability of Polymer Ultrathin Films (<7 nm) Made by a Top-Down Approach*,” **ACS Nano**, vol. **9**, no. **8**, pp. **8184–8193**, Aug. 2015.
- A. B. Unni, G. Vignaud, J. K. Bal, N. Delorme, T. Beuvier, S. Thomas, Y. Grohens, and A. Gibaud, “*Solvent Assisted Rinsing: Stability/Instability of Ultrathin Polymer Residual Layer*,” **Macromolecules**, vol. **49**, no. **5**, pp. **1807–1815**, Feb. 2016.
- A. B. Unni, G. Vignaud, J-P Chapel, J. Giermanska, J. K. Bal, N. Delorme, T. Beuvier, S. Thomas, M. S. Chebil, Y. Grohens, and A. Gibaud “*Probing directly the density variation of confined polymer thin films via simple CeO₂ nanoparticle adsorption*” (communicated)
- M. S Chebil, J. K. Bal, G. Vignaud, T. Beuvier, N. Delorme, A. B. Unni, Y. Grohens, A. Gibaud, “*Origin of Depressed T_g in Confined Polystyrene Thin Films: An Approach Using Supercritical Carbon Dioxide*” (communicated)

CONFERENCE PRESENTATION

- Oral communication at the International Conference, Groupe Français d'études et d'applications des Polymères (GFP), November -2015 at Luxembourg Institute of Science and Technology, Luxembourg

Topic: *Stable polymer thin films (<7nm) obtained by means top down solvent rinsing approach*

